ABSTRACT

Title of dissertation: MITOCHONDRIAL VDAC AND BACTERIAL PORA/C1:

ION PERMEATION AND SELECTIVITY

Alexander G. Komarov, Doctor of Philosophy, 2005

Dissertation directed by: Professor Marco Colombini
Department of Biology

VDAC and PorA/C1 are large diameter channels with properties reminiscent of those found in narrow channels. VDAC, located in the mitochondrial outer membrane, shows high selectivity for ATP over comparably sized ions. VDAC is characterized by a single open state with anionic selectivity and multiple cation-selective closed states. PorA/C1 from *Neisseria meningitidis* achieves high cationic selectivity and large conductance.

VDAC has multiple functions in cellular processes and the most important one is the regulation of metabolite flow across the outer membrane. A variety of functions could be achieved by the existence of different isoforms. In this thesis I summarized the electrophysiological properties of VDAC-like proteins from *Drosophila Melanogaster* encoded by genes CG17137, CG17139 and CG17140. The ability of these proteins to form channels was tested on planar membranes and liposomes. Channel activity was

observed with varying degrees of similarity to VDAC. Two of these proteins (CG17137, CG17140) produced channels with anionic selectivity in the open state. Sometimes channels exhibited closure and voltage gating, but for CG17140 this occurred at much higher voltages than is typical for VDAC. CG17139 did not form channels.

The special selectivity of VDAC for large anions was explored using the mutant of the mouse isoform 2. Inserted into planar membranes, mutant channels lack voltage gating, have a lower conductance, demonstrate cationic selectivity and, surprisingly, are still permeable to ATP. The estimated ATP flux through the mutant is comparable to that for the wildtype. Also we determined that the intact outer membrane containing the mutant is permeable to NADH and ADP/ATP. Both experiments support the counterintuitive conclusion that converting a channel from anion to cation preference does not substantially influence the flux of negatively charged metabolites. However, this finding supports the previous proposal that ATP translocation through VDAC is facilitated by a set of specific interactions between ATP and the channel wall.

The third part of my thesis represents experimental data supporting the theoretical model for the PorA/C1 structure. This model explains the almost ideal cationic selectivity of the channel and high level of rectification.   These properties are proposed to arise from a high density of charges in the channel that results in both high selectivity and high ionic flux.

MITOCHONDRIAL VDAC AND BACTERIAL PORA/C1:
ION PERMEATION AND SELECTIVITY

by

Alexander G. Komarov

Dissertation submitted to the Faculty of the Graduate School of the
University of Maryland, College Park in partial fulfillment
of the requirements for the degree of
Doctor of Philosophy
2005

Advisory Committee:

       Professor Marco Colombini, Chair
       Professor Elizabeth Gantt
       Professor Hey-Kyoung Lee
       Professor Sergey Bezrukov
       Professor Sergei Sukharev

PREFACE

This thesis is a summary of my research on large ion channels, VDAC from mitochondria and PorA/C1 from the bacterium *N. meningitidis*. This work was started more than five years ago when I have joined the University of Maryland as a pre-doctoral visiting student. Those two years under UMD/NIH pre-doctoral visiting program became very exciting and productive which resulted in publishing of two papers where I was the second author (Rostovtseva et al., 2002a; Rostovtseva et al., 2002b). My progress in the field of electrophysiology and the wonderful scientific environment were the reasons why I decided to continue my study at UMD and applied to join the Biology program. Now I am happy that my work in the following years has come to fruition.

This dissertation contains six chapters. In the first chapter I introduce the general background on the permeation through ion channels and mechanisms of their selectivity. This chapter also includes a description of the objects of my study. Chapter 2 contains information about methods, which I used in my research. The following three chapters are distinct manuscripts, which represent different aspects of the study of large channels.

The work included in Chapter 3 has been published in the *Biophysical Journal* in 2004. That was done in collaboration with Dr. William Craigen. The results shown in Fig.3.1 were obtained by Dr.Craigen and co-workers. Under that project I characterized VDAC-like proteins from *Drosophila melanogaster* where the only one VDAC isoform was previously identified. Experiments with planar phospholipid membranes and liposomes allowed me to define the channel-forming activity of those proteins as well as their properties such as single channel conductance, molecular weight cut-off, selectivity

and voltage gating. I believe that my experiments will be important in the further investigation of the function of those proteins in the cell.

Chapter 4 is a submitted manuscript summarizing my second project in collaboration with Dr. Craigen. This work contains important information about mechanisms of selectivity and metabolite permeation through VDAC. My results support the previous proposal that ATP translocation through VDAC is facilitated from a set of specific interactions between ATP and the channel wall, rather than the overall charge of the channel.

Chapter 5 represents a manuscript under preparation. This work is a result of collaboration with Dr. Vicente Aguilella (Spain). My contribution began as the experimental testing of a new theoretical model for permeation of ions through the meningococcal channel, PorA/C1. This model explains transport properties of the channel, including how PorA/C1 is capable to achieve both high conductance and high selectivity. My results are presented in Fig. 5.3-5.5. During this study I discovered that the channel has very unusual properties. I found that PorA/C1 shows a preferential direction of insertion into a membrane in the presence of a salt gradient. It also is very sensitive to a reverse gradient resulting in drastic changes in properties.

A short final discussion as well as directions of future research are included in Chapter 6.

During the course of my graduate studies I also participated in one more project (Holmuhamedov et al., 2004). However this work is not related to my main topic of research and therefore is not included in this thesis.

DEDICATION

I would like to dedicate this thesis to my mother, Ella Vasilyeva, for her understanding and support.

ACKNOWLEDGEMENTS

TABLE OF CONTENTS

LIST OF TABLES

LIST OF FIGURES

viii

CHAPTER 1: GENERAL INTRODUCTION

Ion channels: permeation and selectivity

The evolutionary process has generated an enormous variety of ion channels with highly specialized functions. However, despite this diversity the main function of channels remains the same: to generate a water-filled pathway through the membrane and thus provide a means for translocating lipid insoluble molecules through the membrane.

The simplest definition of an ion channel is "a narrow, water-filled tunnel, permeable to the few ions and molecules small enough to fit through the hole" (Hille, 1992). However, this simple definition does not encompass more complex behavior. First of all, for charged molecules steric hindrance is only one factor. Charged molecules also face an electrostatic barrier, which can make the effective diameter of the hole much smaller than for neutral molecules. Secondly, channel closure, or gating, also influences the flux through the channel.

Three types of gating are known: voltage gating, ligand gating and mechanosensitive gating. The first type was initially found in sodium and potassium channels from the squid giant axon (Hodgkin and Huxley, 1952; Hodgkin, Huxley and Katz, 1952). Then voltage-gated calcium channels from muscle fibres of crab legs were discovered (Fatt and Ginsborg, 1958; Hagiwara and Naka, 1964). A different (symmetrical) type of voltage dependence was later shown in the voltage dependent anion channel (VDAC) from mitochondria (Schein, Colombini and Finkelstein, 1976). Another mechanism of channel gating (ligand-dependent) is attributed to a variety of membrane receptors. Nicotinic acetylcholine (ACh) receptor from muscles was the first example demonstrating that binding and unbinding of a specific ligand can control the

opening and closure of the channel (Neher and Sakmann, 1976). Now we know about a large number of receptor channels which are closely related to the second messenger mechanism. The third type of gating is represented by mechanosensitive channels from bacteria. Discovered by Martinac et al. (1987), these channels prevent bacteria from lysis at conditions of low osmotic pressure. An increase in membrane tension due to osmosis results in the opening of large channels allowing the fast efflux of internal osmolytes (Booth and Louis, 1999; Spencer et al., 1999; Blount et al., 1999; Sukharev, 2002).

Selectivity in channels is generally achieved by intimate interactions between traversing ions and the channel's walls. The part of the channel responsible for such interactions is called the selectivity filter. The high-resolution structure of a selectivity filter was revealed when the crystal structure at the KcsA potassium channel from *Streptomyces lividans* was solved (Roux and MacKinnon, 1999; Zhou et al., 2001). This filter catalyses the dehydration, transfer and rehydration of a potassium ion (Morals-Cabral, Zhou and MacKinnon, 2001). The filter contains four potential ion-binding sites, which can be occupied by K^+ in a dehydrated state or a water molecule. In each of these positions a potassium ion is surrounded by eight oxygen atoms from the protein. This structure takes advantage of the electrostatic repulsion of K^+ ions in adjacent sites to achieve both high selectivity and high flux. It was proposed that the maximum conductance rate could be achieved if two ions move in a concerted fashion between two configurations, K^+ - water - K^+ - water (1,3 configuration) and water - K^+ - water - K^+ (2,4 configuration). Such a precise definition of the central structural element in the KscA channel was an extremely important step in the field of ion channels since the

fundamental structure of the KcsA selectivity filter is conserved in all potassium channels (MacKinnon et al., 1998).

A high level of ion selectivity is generally associated with narrow pores. Large channels are traditionally regarded as simple "molecular sieves". Proteins that form large aqueous pores are presumed to allow passage of solutes without sufficient interaction with the protein walls to provide selectivity above general electrostatic effects. Indeed, large pores usually do not demonstrate a pronounced selectivity. A weak selectivity for small ions could be explained by the overall charge on the channel wall. The Large-Channel Theory (LCT) (Zambrowicz and Colombini, 1993) developed from the fixed-charge membrane theory of Teorell (Teorell, 1953) divides the channel into two compartments: a relatively charged cylindrical shell of solution adjacent to the wall and a relatively neutral central cylinder of solution. The ion flow through the outer compartment depends on the partitioning of ions into this charged region and driving forces including Donnan potentials at the ends of the channel and the diffusion potential within the pore. The flux in the inner compartment is dominated by free diffusion. The net ion flow through the channel is the sum of fluxes in the two compartments. At steady state with an externally applied electric field, the currents in these two compartments flow in opposite directions. According to this theory, the central cylinder acts as a shunt whereas the selectivity of the channel is defined by the ion flow in the outer compartment. The predictions of LCT are in good agreement with experiments in a variety of experimental situations where the classical Goldman-Hodgkin-Katz theory fails completely (Peng et al., 1992).

The LCT applies to the flow of small ions through a large pore. However, the reason for the existence of channels with large aqueous pores is to allow the passage of large molecules. As these molecules pass through the pore they may interact with the walls in a way that allows for selectivity. Indeed, there are examples when large pores demonstrate pronounced selectivity for certain substrates (details will be presented later in this introduction and in Chapter 4). This evidence requires new theoretical approaches to describe the transport properties of wide channels. These models might include concepts normally applied only to narrow pores.

Traditionally ionic movement through pores was modeled in two ways: diffusion (electrodiffusion) theory and rate theory (activated barrier crossing). The partitioning-electrodiffusion model was proposed by Goldman (1943) and Hodgkin and Katz (1949). It is also called constant-field theory. This approach describes ionic permeability and selectivity of membranes with some general assumptions. First of all, the membrane is considered to be homogenous. Charged particles enter the membrane instantaneously from the bulk solution. Ions are assumed not to interact with each other (i.e. independent motion). The ion flux is determined by the internal concentration gradient and by the electric field. Finally, the electric field inside the membrane is assumed to be constant. In practice these assumptions are often incorrect.

A recent version of the diffusion theory is a continuum theory (Levitt, 1985) which uses Poisson-Nernst-Planck formalism (will be described in Chapter 5). The model assumes that the ion channel is completely characterized by three factors: its geometric shape, the potential energy interaction between an ion and charge on the channel wall, and the potential energy interaction between two ions at arbitrary positions inside the

channel (Levitt, 1989, 1991). This approach predicts the fluxes of ion species, the maximum number of ions allowed in the channel, the location of the energy wells and the shape of the energy barriers.

Another theory for the ion transport through channels is the two-barrier-one-binding-site model (Schwarz et al., 2003; Benz et al., 1987). This approach considers a channel containing a single binding site for a certain substrate. In order to reach the site, ions should pass an entrance barrier, which could be different on the each side of the membrane (for asymmetrical channels). The binding site itself is viewed as a potential energy well, which increases the residence time of the particle inside the channel. The ion flux in this case is described by rate constants for influx and efflux and by the residence time of the particle in the channel, which is assumed to have a single-exponential distribution.

The recent publication (Berezhkovskii and Bezrukov, 2005) demonstrated that a combination of two different approaches, continuum and rate theories, may provide a better understanding of ion transport through the large pores.

VDAC: general information, properties, functions

VDAC is a 30-32 kDa channel-forming protein found in the mitochondrial outer membrane of all eukaryotes (Colombini et al., 1996). Like many mitochondrial proteins, VDAC is produced by free cytosolic ribosomes. Then it inserts into the mitochondrial outer membrane. The VDAC content in mammals is approximately 5-7% of all outer membrane protein (Wielburski and Nelson, 1983), however in fungi (for example, *Neurospora Crassa*) this content reaches 50%.

The length of the protein ranges between 274 and 295 amino acids. VDAC from disparate eukaryotic species, from different kingdoms, share a form with a highly conserved fundamental structure and *in vitro* electrophysiological properties. When studied in planar membranes, the channels formed by VDAC demonstrate multiple conductance states with different ionic selectivity: a single "open" state with high conductance and anionic selectivity at low voltages (< 30 mV), and multiple "closed" states with low conductance and cationic selectivity. The motion of the voltage-sensitive domain was found to be responsible for channel gating (Song et al., 1998b). The gating of VDAC is symmetrical at both positive and negative voltages. In the open state the positively charged voltage sensor (the filled part in Fig.1.1) is located in the transmembrane region (the central segment in Fig.1.1) which determines the anionic selectivity. An increase in voltage causes a motion of the sensor to the membrane surface (left and right segments in Fig.1.1) resulting in a change of the overall charge on the channel wall, generation of an electrostatic barrier to anionic metabolites and therefore closure of the channel to those substances. This is likely accompanied by a change in the sites that specifically interact with ATP as will be seen in Chapter 4 of this thesis. The numerical values of the functional parameters such as single channel conductance, selectivity and voltage dependence are very similar for VDAC from different species (Colombini, 1989). Analysis of hydrophilic - hydrophobic profiles reveals that VDAC from different species have a highly conserved secondary structure (Fig. 1.2).

Multiple VDAC isoforms have been identified in numerous diverse species including yeast (Blachly-Dyson et al., 1997), human/mouse (Sampson et al., 1996), and
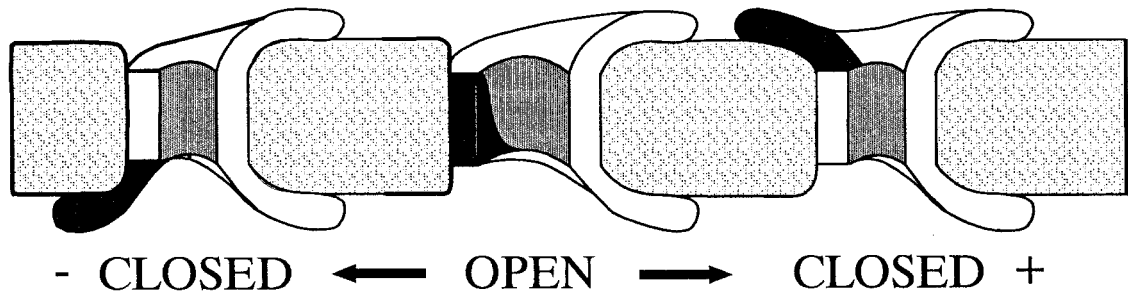
Figure 1.1. VDAC voltage gating is caused by a motion of the mobile domain. In the open state (the central segment) this positively charged domain (the filled part) forms a part of the channel wall which determines anionic selectivity. The closed state is achieved at both negative ("- closed" segment) and positive ("+ closed" segment) voltages.
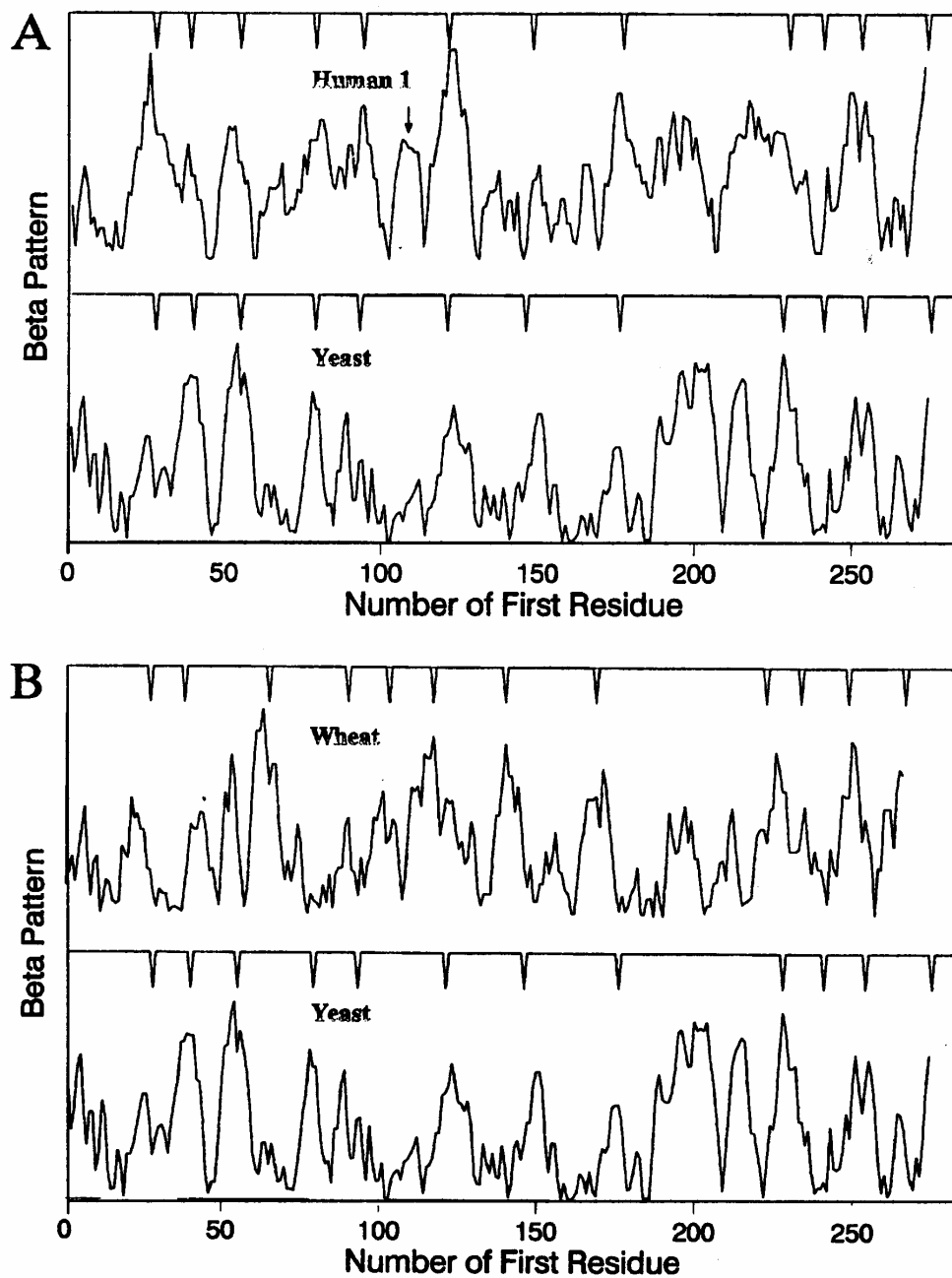
Figur 1.2. Comparisons of the β-patterns (see page 37) of the VDAC sequences of yeast

and human (A) and yeast and wheat (B). The small dips above the patterns point to the

number of the beginning amino acid of each of the β-strands in the proposed folding

patterns (see page 11). *Figure is taken from Song and Colombini (1996).*

8

wheat (Elkeles et al. 1995). Three VDAC-like proteins, which could be classified as isoforms, have been found and studied in *Drosophila Melanogaster* (Oliva et al., 2002; Komarov et al., 2004; Aiello et al., 2004). The electrophysiological characteristics of the prototypic VDAC from different species are highly conserved yet the biophysical properties of individual isoforms from the same species are often quite distinct (Xu et al., 1999).

VDAC plays a role in several fundamental cellular processes. By forming the major pathway for metabolite flux across the mitochondrial outer membrane, VDAC is involved in the regulation of metabolite flow across mitochondria and therefore influences mitochondrial function (Vander Heiden et al., 2000, 2001). For example, deletion of the major VDAC gene in yeast causes a 20-fold reduction in the permeability of the mitochondrial outer membrane to NADH (Lee et al., 1998). VDAC may have an important role in the initiation of apoptosis as indicated by its regulation of Ca^{2+}-uptake (Rapizzi et al, 2002). However its possible participation in the formation of the permeability transition pore complex (Halestrap et al., 2002) is not well established yet. VDAC closure and subsequent interference with ADP/ATP exchange (Vander Heiden et al., 2001) seems to lead to the permeabilization of the outer membrane to proteins resulting in the execution phase of apoptosis. In addition, VDAC has been reported to be a component of the peripheral benzodiazepine receptor complex (McEnery, 1992) and is involved in binding of hexokinase and glycerol kinase to mitochondria (Adams et al. 1991).

Mammalian VDAC isoforms

Three different VDAC isoforms were found in human and mouse genomes. One of the parts of my thesis is focused on the mutant of the second mouse VDAC isoform, mVDAC2. The length of this protein is 295 amino acids, and it is coded by the gene located in the proximal region of mouse chromosome 14 (Blachly-Dyson and Forte, 2001). Compared to the major VDAC isoform (mVDAC1), mVDAC2 has a short N-terminal extension (see Fig. 4.3 on the page 75). Both of these isoforms are expressed in kidney, brain, skeletal muscles, and heart to a higher extent than in other tissues (Sampson et al., 1996). Mouse VDAC2 is also highly expressed in testes while this tissue is deficient for mVDAC1 (Xu et al., 1999). This fact suggests a specialized function for mVDAC2. The electrophysiological properties of mVDAC1 and mVDAC2 are similar however they are quite different from those of the mouse VDAC3. This last isoform is believed to play another role than just a channel former. A traditional way to study mouse VDAC isoforms is their expression and purification from yeast cells. All three isoforms complement the growth deficiency observed when yeast VDAC1 is knocked out but mVDAC3 does so poorly (Xu et al., 1999). Thus all three perform one similar function in yeast cells.

Mouse VDAC2 demonstrates channel-forming activity in both liposomes and planar phospholipid membranes (Xu et al., 1999). The measured non-electrolyte size cut-off for both mVDAC1 and mVDAC2 is estimated between 3400 and 6800 Da. Insertion of mVDAC2 protein into planar membrane results in two populations of channels, each having a different open-state conductance. The channels with a smaller conductance

have lower anion selectivity. Once inserted into the membrane they are unable to interchange between the two forms. Both forms undergo normal VDAC voltage gating.

One of the most important biological roles of mVDAC2 could be its inhibition of apoptosis. Recent observations indicate that mVDAC2 forms a complex with pro-apoptotic protein, BAK (Cheng et al., 2003). BAK is an integral protein of the mitochondrial outer membrane with a molecular mass of ~23 kDa (Mikhailov et al., 2003). It was established that only oligomeric BAK (active form) participates in an increase of mitochondrial outer membrane permeability. Monomeric BAK was shown to interact specifically with mouse VDAC2. Overexpression of mVDAC2 inhibited the process of BAK oligomerization, and a knock-out of mVDAC2 (but not mVDAC1) caused an increase of BAK activation. In addition, 60-kDa BAK complex with mVDAC2 was found in cells containing mVDAC2, but not in cells having only mVDAC1 and mVDAC3 isoforms. These results provide strong evidence that mouse VDAC2 plays an important role in interfering with the BAK-mediated apoptotic pathway. These observations make a study of mVDAC2 quite interesting and important.

VDAC structure: what we know so far

The exact crystal structure of VDAC is not known. However we can glean information from examining its primary structure. A great deal of past experimental work culminated in a transmembrane folding pattern for VDAC that consists of 1 α-helix and 13 β strands which was proposed for VDAC from *Neurospora crassa* (Song et al., 1998a). Authors used an approach that minimized any damage to the native form of protein. Site-directed mutagenesis introduced conservative mutations into yeast VDAC1

11

and identified transmembrane strands and the location of the voltage sensor (Blachly-Dyson et al., 1990; Thomas et al., 1993). Cysteine residues were also introduced at sites throughout *N.crassa* VDAC, which naturally lacks cysteine residues. Prior to incorporation of modified channels into the planar phospholipid membranes cysteine residues were specifically biotinylated. Upon a channel insertion those biotinylated sites served as targets for molecules of streptavidin. The size of streptavidin does not allow it to penetrate through the VDAC channel and so streptavidin can interact only with residues facing the side of its addition. Streptavidin binding resulted in changes in the single channel properties such as conductance and voltage gating and provided critical topological information (Song et al., 1998a). Based on a variety of experiments, especially the mutagenesis approaches, albeit was possible to define the exact location of residues, those in the transmembrane region, outer loops or the voltage sensor. It was clearly established that the α-helix and four β-strands (II, III, IV and XIII) are involved in the formation of the voltage sensor (the mobile domain).

Since the fundamental structure of VDAC sequences from different species is highly conserved we can use the proposed folding pattern as a template for generation of putative folding patterns for VDAC from other sources. In this approach some general criteria should be followed. Choosing the best candidate for the transmembrane β-strands we postulate: 1) A candidate strand should have a good alternating hydrophilic and hydrophobic pattern; 2) Chain-distorting prolines should not be located in the middle of the transmembrane strand but rather at the ends of the strands; 3) There should be no adjacent charged amino acids except at the ends; 4) The strand should have good sequence homology to the corresponding transmembrane β-strand for *N.crassa* VDAC.

This approach allowed me to generate a putative folding pattern for mouse VDAC2 (see Fig. 4.3 on the page 75) which was used to choose the points for mutations described in Chapter 4 of my thesis.

Specific selectivity of VDAC

A few years ago my co-authors and I studied *N.crassa* VDAC using current noise analysis. We found that VDAC channels can distinguish between ATP and UTP (Rostovtseva et al., 2002a). The evidence favors the existence of a binding site inside the VDAC channel that discriminates between purines and pyrimidines. The nucleotide-generated low-frequency noise obeys the following sequence: β-NADPH > β-NADH = α-NADH > ATP > ADP > β-NAD $\geq$ AMP > UTP. The ability to generate current noise spans a forty-fold range for different nucleotides from barely measurable to highly pronounced. In contrast to this wide range, addition of any of these nucleotides reduces the single channel conductance for small ions to a very similar extent, indicating a similar residency time inside the channel. Thus, the selectivity among nucleotides observed based on noise generation likely arises from a process other than ability to penetrate into the channel. If we consider ATP and UTP, molecules with very similar size and charge, the only factor, which can explain 6-7 –fold difference in their ability to generate current noise, is the type of nucleotide base. ATP has a purine base whereas UTP contains a pyrimidine base. We concluded that the source of the current noise is related to the interaction of nucleotides with the channel wall. The more pronounced interaction in the case with purine-containing metabolites might be a result of their binding to the base-specific binding site.

More recently our group established that VDAC can differentiate between natural

metabolites and synthetic molecules of similar charge and size (Rostovtseva et al.,

2002b). Moreover, the effective radius of those molecules (0.4-0.5 nm) is much smaller

than the radius of VDAC in the open conformation (1.2-1.5 nm). In contrast to

nucleotides, the presence of tetraglutamate (T-Glu) and 1-hydroxypyrene-3,6,8-trisulfate

(HPTS) did not reduce the conductance of VDAC channels, as would be expected if these

were capable of penetrating into the lumen of these channels. The results from open-

channel current-noise measurements provided further support for the conclusion that

VDAC is not permeable for those synthetic molecules. T-Glu did not induce excess

current noise, indicating no disturbance of small ion flow through VDAC. HPTS did

produce a low level of noise. However, it is likely that the noise observed was due to a

nonspecific effect, not to HPTS penetration into the channel.

These observations suggest that VDAC achieves selectivity that goes beyond the

size and net charge of the permeating species. So we have concluded that VDAC is

capable of differentiating between similar molecules based on their shape and charge

distribution rather than just size and charge.

PorA/C1: general background

Class 1 porin (PorA/C1) from *Neisseria meningitidis* is a large channel, which has

both large selectivity and large conductance (Jeanteur et al., 1991; Song et al., 1999). In

nature this channel serves as a part of porin channel trimers that consist of one PorA and

two PorB proteins. In contrast to other porins, PorA/C1 does not exhibit voltage gating

however it is highly selective (24 to 1 in favor of Na^+ over Cl^- in a two-fold NaCl

14

gradient). For example, class 2 and class 3 porins are only weakly selective for anions. When incorporated in planar phospholipid membranes in the presence of 200 mM NaCl salt, pure PorA/C1 demonstrates the single trimer conductance of 0.97 nS (Song et al., 1999). Also PorA/C1 shows strong rectification, so that the current through the channel at voltages of opposite signs has a four-fold difference (see Fig. 5.2 on the page 109).

As in the case with VDAC the precise crystal structure of PorA/C1 is not available. The proposed folding pattern consists of 16 β-strands, which form a barrel-like water-filled pore (Ley et al., 1991; Song et al., 1999). High selectivity and pronounced rectification might be attributed to an asymmetrical channel structure with a highly negatively charged selectivity filter (nine negative charges) located on the edge of the channel (see Fig. 5.2 page 109). The diameter of the pore in the region of the selectivity filter was estimated as 1.4 nm whereas it is 2.1 nm on the other side (Song et al., 1999). In vivo the narrow part of the channel faces the extracellular space and the wider – the periplasmic space of bacteria.

CHAPTER 2: METHODS

Planar membrane technique

Most of the experiments for my dissertation work were done using the planar

membrane technique (Montal and Mueller, 1972) as modified (Colombini, 1987). An

experimental chamber consists of two compartments (*cis* and *trans*) with volume 2.5 ml

divided by thin (50 μm) Teflon partition which contains a small hole with diameter of 70-

90 μm. A phospholipid solution in hexane is layered on the surface of the aqueous

solutions in each compartment. Evaporation of hexane results in a lipid monolayer. When

two monolayers are raised above the hole in the partition they form the solvent-free

bilayer which is the simplest example of the general structure of biological membranes.

Insertion of channels into the planar phospholipid membrane is achieved by

adding an aliquot of a detergent-containing solution with purified channel-former protein

to the aqueous phase. The process of insertion has a spontaneous character and, in

general, depends on such factors as a tightness of the membrane, concentration of protein

in the aqueous solution and concentration of a detergent.   Application of a voltage across

the membrane allows the observation of channel insertion as a step-wise increase in the

current (for example, Fig. 3.4A on the page 42).

The general scheme of the experimental set-up is presented in Figure 2.1. Two

silver/silver chloride electrodes with 3.0 M KCl, 15% agarose bridges (Bezrukov and

Vodyanoy, 1993) were used to interface with the aqueous solutions. One electrode was

grounded ("*cis*") and the second ("*trans*") was connected to the amplifier (AXOPATCH

200B) in the voltage clamp mode. This allowed to control the voltage across the planar

membrane and amplified the recorded current, which represents the ion flux through the

channel.
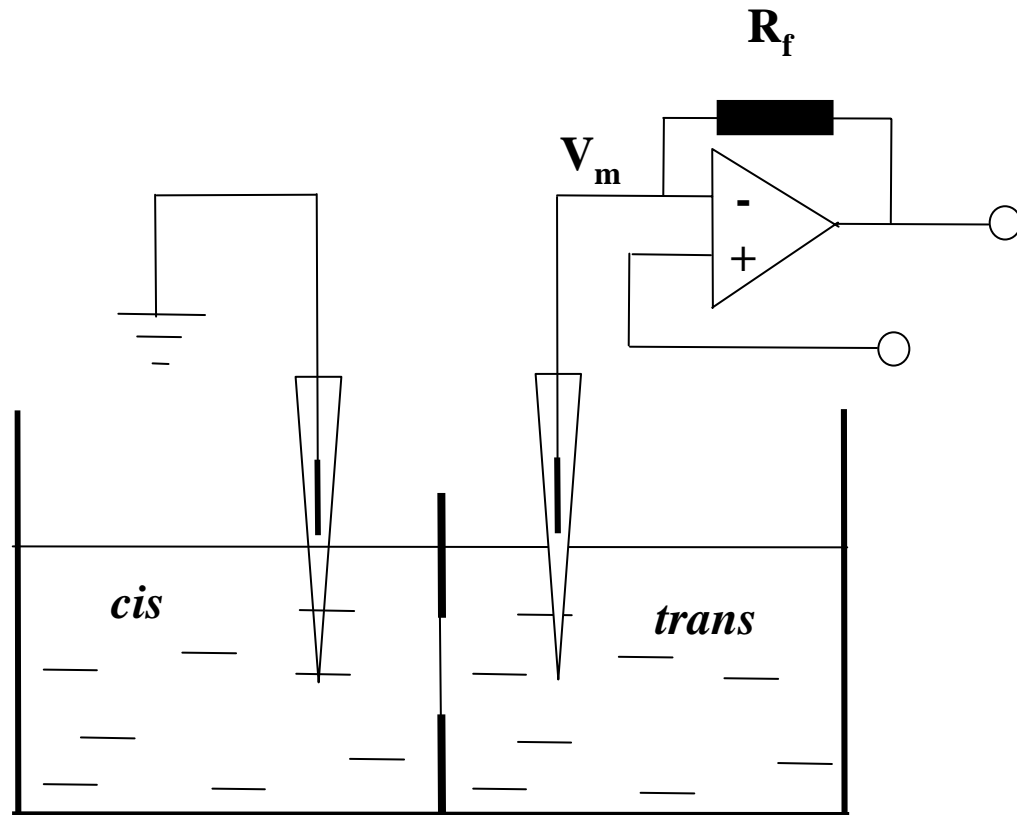
Figure 2.1. The experimental set-up used for planar membrane measurements.

A teflon partition divides the chamber into two compartments ('*cis*' and '*trans*'). The

lipid bilayer is formed across the hole of 70-90 μm diameter. The ion flux across the

membrane is recorded as a current and the voltage (V_m) is controlled by a pair of

silver/silver chloride electrodes connected to the ground and amplifier respectively. The

amplifier is set in the voltage clamp mode with feedback resistor R_f

Liposomal assay

Liposomes with incorporated channels allow one to obtain information from a large population of channels whereas the planar membrane method studies a selected and small number of channels that happen to insert into the membrane. In the planar membrane experiment it is possible that a minor constituent might be responsible for the observed activity. The liposome model also eliminates the need for the protein to insert into the membrane from an aqueous environment.

In this work the liposomal assay was used to determine the size of channels. The liposomes were made as follows (Colombini, 1980): 22.5 mg of egg phosphatidyl-choline (Sigma, St. Louis, MO) and 2.0 mg of egg phosphatidylserine (Avanti Polar Lipids, Inc., Alabaster, AL), both dissolved in chloroform, were mixed together and dried down under N_2. One ml of 1 mM KCl, 1 mM HEPES, pH 7.0 solution was added to the dry lipids and the material was sonicated (at 0 to 5°C). One ml of mitochondrial membranes suspended in 1 mM KCl, 1 mM HEPES, pH 7.0 containing 1.2 mg of protein was mixed into the lipid solution prepared above. The mixture was sonicated again and lyophilized overnight. Liposomes were produced by dispersing the dry material in 1 ml of 20 mM KCl, 1 mM EDTA, pH 7.0. Fifty microliters of this liposome suspension were added to 0.8 ml of 20 mM KCl, 1 mM EDTA, pH 7.0 and the absorbance at 400 nm was monitored. Nonelectrolytes of different molecular weight were dissolved in the same solution and added to the liposomes when the liposomes had stabilized (no change in absorbance with time).

Mixing of liposomes with these solutions induces liposome shrinkage due to the fact that water moves out of the liposomes faster than the solute can move in. In the case

of a permeable solute, reswelling follows the shrinkage of the liposomes. The shrinkage-reswelling process was observed by measuring changes in light scattering at 400 nm over time. A decrease of the liposome size causes an increase in apparent absorbance and a decrease in absorbance indicates reswelling of the liposomes. The rate of reswelling reflects the permeability of the liposome membrane. If the solute is impermeable the liposomes will shrink but not reswell.

Isolation of yeast mitochondria

NADH and ADP/ATP fluxes across the outer membrane of intact yeast mitochondria can be measured to assess the permeability of the outer membrane to these metabolites. Yeast mitochondria were isolated from cells lacking yeast VDAC1 but express VDAC from other sources, in this work, from mice.

Mitochondria were isolated from *S. cerevisiae* essentially as published by Daum et al. (1982) but modified as previously described (Lee et al., 1998). After harvesting, the yeast cells were washed with distilled water once. Then they were suspended in medium consisting of 0.1 M Tris.SO$_4$, 10 mM DTT, pH 9.4 at the proportion of 0.5 g wet weigh cells per 1 ml of solution and incubated at 30°C for 10 min. After washing with 1.2 M sorbitol solution the yeast cells were resuspended in 1.2 M sorbitol, 20 mM KH$_2$PO$_4$, pH 7.2. To remove the cell wall, yeast cells were treated with zymolyase (20,000 U/g)(Seikagaku Corporation, Ijamsville, MD) and incubated at 30°C for 25 min. The enzyme concentration of 10 mg per gram of cells was used. Addition of 10% N-lauroylsarcosine to a drop of cell suspension allowed a check of spheroplast formation by phase contrast microscopy. The spheroplast fraction was sedimented at 6000 rpm for 5

min (GSA rotor) and washed twice with 1.2 M sorbitol, 20 mM KH_2PO_4, pH 7.2 solution. Intermediate steps did not involve the resuspension of spheroplasts in the fresh buffer, instead of that the bottle with the pellet was rotated by 180° (around its long axis) between centrifugations. The final pellet with spheroplasts was suspended in 0.6 M mannitol, 10 mM Tris.Cl, 0.6 % PVP, 0.1 mM EGTA and 0.1 % BSA, pH 7.2 (H-medium) by using a Pipetman P5000 with approximately 1 cm cut-off the disposable tip. In order to obtain a high level of mitochondria intactness (above 80%) homogenization was not used. Resuspension was sufficient to lyse most of the cells. The suspension of lysed spheroplasts was centrifuged at 3000 rpm for 5 min (SS-34 rotor) and the supernatant-containing mitochondria were stored on ice. The pellet was resuspended and sedimented again and a second portion of supernatant was collected. Both tubes with supernatant were centrifuged at 9000 rpm for 10 min (SS-34 rotor). To keep pellets with the mitochondrial fraction loose, two ml of 10 % Percoll was layered at the bottom of each tube before centrifugation. The pellets were resuspended in H-medium as was described above, pooled and the procedure with low and high speed centrifugations was repeated. The final pellet was suspended in 4-6 ml of H-medium. To separate intact mitochondria from damaged, centrifugation in a Percoll gradient was used. The mitochondrial suspension was layered on the top of 45% (14ml)-18%(8 ml)-5%(6 ml) Percoll gradient and sedimented at 10,500 rpm for 30 min. Then the major (lower) band was collected, washed once with H-medium and suspended in a small volume of H-medium (1-2 ml). Care was taken to minimize carry over of Percoll into the mitochondrial pellet.

A measurement of the protein concentration of the mitochondrial fraction was

done by using 100 mM Tris.SO$_4$, 0.4% SDS, pH 8.0 solution. Equal aliquots of this

buffer and H-medium containing mitochondria were mixed and an absorbance of the

sample (A$_x$) was detected at two different wavelengths, 280 and 310 nm. Then the

concentration of protein was calculated by using formula: C (mg/ml)=(A$_{280}$ – A$_{310}$)/1.05

(Clarke, 1976). In our experiments the total protein concentration in mitochondrial

suspension was 10-15 mg/ml.

The intactness of isolated mitochondria was determined based on the rate of

cytochrome c-dependent oxygen consumption (Douce at al., 1987). Exogenously added

cytochrome c should reach the mitochondrial inner membrane to be oxidized by cyt c

oxidase. In this case the outer membrane serves as a barrier for the reaction. The rates of

oxygen consumption for intact (υ_{intact}) and osmotically shocked mitochondria ($\upsilon_{disrupted}$)

were compared and the percentage intactness was calculated as follows:

$$\textit{\% intactness = (1 - }\upsilon_{intact}/\upsilon_{disrupted})\textit{*100.}$$

Osmotic shock was applied by mixing of 40 µl of mitochondrial suspension with 1.5 ml

of water, incubating for 3 min on ice, and then adding double concentrated respiration

buffer (1.3 M sucrose, 20 mM HEPES, 20 mM KH$_2$PO$_4$, 10 mM KCl, 10 mM MgCl$_2$, pH

7.2) to restore the initial osmotic pressure.

Oxygen consumption was measured by using a Clark oxygen electrode. An

aliquot of ascorbate (50 µl of 0.48 M) was added to a 3 ml volume of R-medium (0.65 M

sucrose, 10 mM HEPES, 10 mM KH$_2$PO$_4$, 5 mM KCl, 5 mM MgCl$_2$, pH 7.2) containing

either intact or disrupted mitochondria to maintain the cytochrome c in the reduced form.

Addition of 180 µg of cytochrome c induced oxygen consumption. Finally, an aliquot of

KCN (0.2 mM final) was used to block cytochrome c oxidase and detect the level of

KCN-dependent respiration. I used 10 minutes intervals between additions. The final rate of oxygen consumption for both intact and damaged mitochondria was calculated as a difference in slopes before and after KCN addition.

Intactness of mitochondria varied in the range 78-86%.

Isolated mitochondria were used for metabolite transport measurements. More details on the methods used in experiments with intact mitochondria can be found in Chapter 4.

CHAPTER 3

The Physiological Properties of a Novel Family of VDAC-Like Proteins from *Drosophila Melanogaster*

Alexander G. Komarov[1,3], Brett H. Graham[2], William J. Craigen[2], and Marco Colombini[1]

[1]Department of Biology, University of Maryland, College Park, MD 20742;

[2]Departments of Molecular and Human Genetics and Pediatrics, Baylor College of Medicine, Houston, TX 77030;

[3]St.Petersburg Nuclear Physics Institute, Gatchina, Russia, 188350.

Running Title: *VDAC-like proteins from Drosophila*

KEYWORDS:

VDAC, isoforms, channel formation, planar membranes, liposomes

ABSTRACT

VDAC, a major protein of the mitochondrial outer membrane, forms voltage-dependent, anion-selective channels permeable to most metabolites. Although multiple isoforms of VDAC have been found in different organisms, only one isoform (*porin/*DVDAC) has been previously reported for *D. melanogaster*. We have examined the physiological properties of three other *Drosophila* proteins (CG17137, CG17139, CG17140) whose primary sequences have significant homology to DVDAC. A comparison of their hydropathy profiles (beta pattern) with known VDAC sequences indicates the same fundamental folding pattern but with major insertions and deletions. The ability of these proteins to form channels was tested on planar membranes and liposomes. Channel activity was observed with varying degrees of similarity to VDAC. Two of these proteins (CG17137, CG17140) produced channels with anionic selectivity in the open state. Sometimes channels exhibited closure and voltage gating, but for CG17140 this occurred at much higher voltages than is typical for VDAC. CG17139 was not able to form channels. DVDAC and CG17137 were able to rescue the temperature-sensitive conditional-lethal phenotype of VDAC-deficient yeast, whereas CG17139 and CG17140 demonstrated no complementation. Similar structure and channel formation indicate that VDAC-like proteins are part of the larger VDAC family but the modifications are indicative of specialized functions.

INTRODUCTION

VDAC, also known as mitochondrial porin, is a 30-32 kDa channel-forming protein found in the mitochondrial outer membrane of all eucaryotes (Colombini et al., 1996). It forms an aqueous pore with a diameter of about 3 nm in the open state and 1.8 nm in the closed state. This closed state is still conductive to small ions but effectively impermeant to anionic metabolites (Rostovtseva and Colombini, 1996; Rostovtseva et al., 2002a). In the open state VDAC is permeable to non-electrolytes up to 5000 Da. A model of the secondary structure of VDAC, consisting of 1 α-helix and 13 β-strands, has been proposed based on a variety of experiments (Song et al., 1998a). These 14 elements form a barrel-like structure that spans the membrane. Other theoretical models have been proposed with a larger number of transmembrane strands (Mannella, 1996). Spectroscopic studies have shown that transmembrane strands are tilted at a 45° angle (Abrecht et al., 2000).

VDAC from disparate eukaryotic species, from different kingdoms, share a form of VDAC with a highly conserved fundamental structure and *in vitro* electrophysiological properties. The length of the protein ranges between 274 and 295 amino acids. When studied in planar membranes, the channels formed by VDAC demonstrate multiple conductance states with different ionic selectivity: a single "open" state with high conductance and anionic selectivity, and multiple "closed" states with low conductance and cationic selectivity. The motion of the voltage-sensitive domain is responsible for channel gating (Song et al., 1998b). In the open state the positively charged voltage sensor is located in the transmembrane region. An increase in voltage causes the movement of the sensor toward the membrane surface resulting in an electrostatic barrier

to anionic metabolites and therefore closure of the channel. The numerical values of the functional parameters such as single channel conductance, selectivity and voltage dependence are very similar for VDAC from different species (Colombini, 1989).

VDAC plays a role in several fundamental cellular processes. By forming the major pathway for metabolite flux across the mitochondrial outer membrane, VDAC is involved in the regulation of metabolite flow across mitochondria and therefore influences mitochondrial function (Vander Heiden et al., 2000, 2001). VDAC may have an important role in the initiation of apoptosis as indicated by its regulation of Ca^{2+}-uptake (Rapizzi et al, 2002) and possible participation in the formation of the permeability transition pore complex (Halestrap et al., 2002). VDAC closure and subsequent interference with ADP/ATP exchange (Vander Heiden et al., 2001) seem to lead to the permeabilization of the outer membrane to proteins resulting in the execution phase of apoptosis. In addition, VDAC has been reported to be a component of the peripheral benzodiazepine receptor complex (McEnery, 1992) and may be involved in binding hexokinase and glycerol kinase to mitochondria (Adams et al. 1991). Such a wide variety of functions may require the presence of specialized proteins in the form of isoforms and VDAC-like proteins.

Multiple VDAC isoforms have been identified in numerous diverse species including yeast (Blachly-Dyson et al., 1997), human/mouse (Sampson et al., 1996), and wheat (Elkeles et al. 1995). The electrophysiological characteristics of the prototypic VDAC from different species are highly conserved yet the biophysical properties of individual isoforms from the same species are often quite distinct (Xu et al., 1999). While the specific functions of individual VDAC isoforms remain to be elucidated,

studies with *in vivo* model systems have given some insights. For example, while VDAC has been implicated in the initiation of apoptosis, one isoform, mammalian VDAC2, interacts with pro-apoptotic BAK to inhibit apoptosis (Cheng et al., 2003). Moreover when overexpressed, yeast VDAC2 (POR2) was shown to restore normal cell growth in the absence of yeast VDAC1 (POR1) but did not form channels in reconstituted systems (Blachly-Dyson et al., 1997). This implies that a VDAC isoform can be involved in cell survival yet does not necessarily require channel-forming activity. Mice deficient for VDAC isoforms exhibit distinct phenotypes. VDAC1 deficient mice demonstrate altered mitochondrial permeability in skeletal muscle (Anflous et al., 2001), while VDAC3 deficient mice are infertile with structural sperm axonemal defects, in addition to respiratory chain abnormalities in muscle (Sampson et al., 2001). Finally, VDAC1, VDAC3, and VDAC1/VDAC3 deficient mice exhibit isoform-specific defects in learning and synaptic plasticity (Weeber et al., 2002).

The recent annotation of the *Drosophila melanogaster* genome (The-FlyBase-Consortium 2003) revealed three putative VDAC isoforms whose genes are tightly clustered in tandem with the original *Drosophila* VDAC (DVDAC or *porin*) (Oliva et al., 2002). In this report, we describe our studies to characterize the physiological properties of these putative VDAC isoforms.

MATERIALS AND METHODS

Yeast Strains and Media

M3 (*MATα lys2 his4 trp1 ade2 leu2 ura3*) is the parental wild-type (with respect to POR1) strain. M22-2 (Δ*por1*) contains a deletion of *POR1* by insertion of yeast *LEU2*

at the POR1 locus (Blachly-Dyson et al., 1990). The yeast media YPD/SMM (2% dextrose as the carbon source/ supplemented with essential nutrients except uracil) and YPG/SMM (3% glycerol as the carbon source/ supplemented with essential nutrients except uracil) were prepared as described (Kaiser et al., 1994).

Generation of Yeast Expression Constructs

For *Drosophila* VDAC, DVDAC, oligonucleotide-directed mutagenesis was used to generate a *NcoI* site at the start codon, and a *NsiI* site in the 3' UTR. This allowed for the complete open reading frame of the DVDAC cDNA to precisely replace the yeast VDAC1 gene previously subcloned into a single-copy yeast shuttle vector as previously described (Sampson et al., 1997). For *CG17137*, *CG17139*, and *CG17140*, oligonucleotide-directed mutagenesis was used to generate a blunt restriction enzyme site (*EheI* for CG17137, *MlyI* for *CG17139,* and *PmeI* for CG17140) at the first codon downstream of the start codon such that when ligated to the *NcoI*-digested and blunted single-copy yeast shuttle vector, the open reading frame of the yeast VDAC1 is precisely replaced by the corresponding *Drosophila* cDNA. As with DVDAC, either a *NsiI* (*CG17137* and *CG17139*) or a *Sse 8387I* (*CG17140*) (*Sse 8387I* generates ends compatible with *NsiI*) site was generated in the 3'UTR to facilitate cloning. To generate the multiple-copy yeast expression constructs for each *Drosophila* VDAC-like gene, the expression cassette (including the yeast VDAC1 promoter, 5' and 3' UTRs) was excised from the corresponding single-copy shuttle construct as a *BamH1/HindIII* fragment and cloned into the 2μm yeast shuttle vector YEplac195 (Gietz and Sugino, 1988). The sequences of the oligonucleotides are as follows: DVDAC 5'=

GGCAACCATGGCTCCTCCATCATACAG; DVDAC 3'=

CCGCGATGCATTCACGACTAGCGGAAAACC; *CG17137* 5'=

GCGAAGGCGCCGCCAAACACCGACATA; *CG17137* 3'=

CCGCGATGCATCGTTAAGTGATTGGCAGT; *CG17139* 5'=

GCGAAGAGTCCCATGAGAGAACGGATA; *CG17139* 3'=

GCGACCTGCAGGCTACATATTGAAGTACCAT; *CG17140* 5'=

GCGAGTTTAAACAACGGCTGCGCAACTT (note this oligonucleotide also generates

a silent G->A mutation in the third position of the first codon downstream of the start

codon); *CG17140* 3'= GCGAATGCATCAACAGTGAAAACCCCAGGAA. The cDNA

templates utilized are as follows: *porin*=BDGP (Berkley *Drosophila* Genome Project)

Clone ID GM13853 (GenBank AI518978); *CG17137* =BDGP Clone ID AT15574

(GenBank BF500588), *CG17139* =BDGP Clone ID AT07302 (GenBank BF505131), and

CG17140=AT08366 (GenBank BF506017) (Rubin et al. 2000).

Yeast Complementation Analysis

Each expression construct was introduced into the Δ*por1 Saccharomyces*

cerevisiae strain M22-2 by lithium acetate transformation (Gietz et al., 1992). As

controls, wild-type (M3) and Δ*por1* yeast were transformed by the original single- or

multiple-copy shuttle vectors. The yeast strains were then grown in 5 ml YPD/SMM

liquid cultures at 30°C for 72 hr. Each culture was normalized to the M3 cultures based

on OD_{600nm} and spotted onto 2 YPG/SMM plates as six-serial five-fold dilutions. The

plates were incubated at 30°C or 37°C respectively for 6 days.

Preparation of yeast cells

To facilitate cell growth and harvesting, stock cultures were prepared. A colony of yeast cells, containing one of the VDAC-like genes, was inoculated into 50 ml of medium consisting of 95 mg of yeast nitrogen base (#0335-15-9, DIFCO LABORATORIES, Detroit, MI), 250 mg of ammonium sulfate, 1 g of dextrose, and 38.5 mg of CSM-URA (#4511-222, Complete Supplement Mixture minus Uracil; Q-BIOgene, Carlsbad, CA). When the cells reached an O.D. of between 0.6 and 0.8 (at 600 nm) they were stored at 4°C for later use. For mitochondrial isolation, 9 ml of yeast stock solution was inoculated into each of two flasks containing one liter of the same medium and grown with shaking at 30°C. An O.D. between 0.7 and 0.8 was reached at 41 hours after inoculation. Typically, 5-8 grams of cells were obtained. Five grams of cells were used for the isolation of mitochondria.

Isolation of VDAC-like proteins

Mitochondria were isolated from *S. cerevisiae* essentially as published by Daum et al. (1982) but modified as previously described (Lee et al., 1998). The final mitochondrial suspension was hypotonically shocked in 1 mM KCl, 1 mM HEPES, pH 7.5 to break the mitochondrial membranes and release soluble proteins. The membranes were sedimented at 24,000 g for 20 min.

VDAC-like proteins were isolated from mitochondrial membranes and purified according to standard methods (Mannella, 1982; Freitag et al., 1983). The last step was a 1 to 1 hydroxyapatite/celite column that, at low ionic strength, binds most proteins but allows VDAC to flow through. This also is a property of VDAC-like proteins.

Channel conductance measurements

Planar membranes were formed from monolayers made from a solution containing 0.5% of diphytanoylphosphatidylcholine, 0.5% of asolectin - soybean phospholipid (both were from Avanti Polar Lipids, Inc., Alabaster, AL) and 0.1% cholesterol (Sigma, St. Louis, MO) in hexane. The two monolayers formed a bilayer membrane across a 70-90 μm diameter aperture in a 15-μm thick Teflon partition that separated two chambers (modified Montal and Mueller technique, 1972). The total capacitance was 70-80 pF and the film capacitance was 30-35 pF. Aqueous solutions of 1.0 M or 0.10 M NaCl and 1 mM $MgCl_2$ (in some experiments additional 1 mM $CaCl_2$ was present) were buffered by 5 mM HEPES at pH 7.0. All measurements were made at room temperature.

Channel insertion(s) was achieved by adding 0.2-2.0 μl of a 1% Triton X100 solution of purified VDAC-like protein to the 2.5 ml aqueous phase in the *"cis"* compartment while stirring.

The membrane potential was maintained using Ag/AgCl electrodes with 3.0 M KCl, 15% agarose bridges assembled within standard 200 μl pipette tips (Bezrukov and Vodyanoy, 1993). Potential is defined as positive when it is greater at the side of protein addition (*cis*). The current was amplified by an Axopatch 200B amplifier (Axon Instruments, Inc., Foster City, CA) in the voltage clamp mode.

Reversal potential measurements

The reversal or zero-current potential was measured to assess the selectivity in single or multi-channel membranes. A positive reversal potential on the high salt side

31

slows down the flux of anions down their gradient and increases the flux of cations. If a

positive potential brings the current to zero then the channel must pass anions more

readily than cations (i.e. has anionic selectivity). A negative potential would indicate

cation selectivity. We used a 10-fold gradient of NaCl, 1.0 M *cis* and 0.10 M *trans*, plus

Mg^{2+} and HEPES as above. An aliquot of solution containing VDAC-like protein was

added to the side with higher concentration. As the channels can exist in different

conformations each with different selectivity, triangular voltage waves were applied and

the reversal potential of each state obtained by extrapolating the current record to zero

current (see Fig. 3.6 on the page 44).

Liposome permeability measurements

The liposomes were made as follows (Colombini, 1980): 22.5 mg of egg

phosphatidyl-choline (Sigma, St. Louis, MO) and 2.0 mg of egg phosphatidylserine

(Avanti Polar Lipids, Inc., Alabaster, AL), both dissolved in chloroform, were mixed

together and dried down under N_2. One ml of 1 mM KCl, 1 mM HEPES, pH 7.0 solution

was added to the dry lipids and the material was sonicated (at 0 to 5°C). One ml of

mitochondrial membranes suspended in 1 mM KCl, 1 mM HEPES, pH 7.0 containing 1.2

mg of protein was mixed into the lipid solution prepared above. The mixture was

sonicated again and lyophilized overnight. Liposomes were produced by dispersing the

dry material in 1 ml of 20 mM KCl, 1 mM EDTA, pH 7.0.

Fifty microliters of this liposome suspension were added to 0.8 ml of 20 mM KCl,

1 mM EDTA, pH 7.0 and the absorbance at 400 nm was monitored. Nonelectrolytes of

different molecular weight were dissolved in the same solution and added to the

liposomes when the liposomes had stabilized (no change in absorbance with time).   One

might expect that upon shrinkage, the KCl concentration in the liposomes would increase

resulting in extended shrinkage as the KCl redistributes with time. In fact, in these

liposomes K^+ and Cl^- flux is so fast that these redistribute almost as rapidly as water.

Indeed, if hypertonic KCl is used to attempt to shrink the liposomes, there is almost no

shrinkage.

SDS-PAGE electrophoresis

To determine, whether we have VDAC-like proteins in the final fraction of the

purification procedure, we used standard SDS-page electrophoresis procedure (Laemmli,

1970). Equal aliquots of solutions containing VDAC or VDAC-like proteins were mixed

with concentrated sample buffer. Samples were separated on a 12% acrylamide gel

supplemented with 4M urea and the bands stained with GelCode Blue stain (Pierce,

Rockford, IL).

RESULTS

In addition to VDAC, *D. melanogaster* expresses three proteins whose primary

sequences resemble that of VDAC, the VDAC-like proteins. The question to be

addressed is how similar are these proteins to VDAC in terms of structure and function.

DVDAC and CG17137 rescue the conditional lethal phenotype of yeast cells deficient for

VDAC1

Our initial approach for analyzing the function of the VDAC-like genes in

Drosophila melanogaster was to individually express them in a yeast strain that is

deficient for the endogenous VDAC1 gene (*Δpor1*). The *Δpor1* strain is characterized by

a temperature-dependent growth-restrictive phenotype when cultured on a non-

fermentable carbon source such as glycerol: cells are able to grow at 30°C, but not 37°C

(Blachly-Dyson et al., 1990). It has been previously demonstrated that mammalian

VDACs expressed in the *Δpor1* background rescue this conditional phenotype, allowing

growth on glycerol at 37°C (Blachly-Dyson et al., 1993; Sampson et al., 1997). Ryerse *et*

al. previously reported that DVDAC failed to complement *Δpor1* yeast (Ryerse et al.,

1997). However, we observed that DVDAC does indeed complement *POR1* function in

Δpor1 yeast when expressed from the *POR1* promoter on either a single-copy (CEN) or a

multiple-copy (2μm) yeast shuttle vector (Fig. 3.1). Additionally, we observed that

CG17137 rescued the *Δpor1* conditionally growth-restrictive phenotype when expressed

from the single-copy vector. *CG17139* and *CG17140* both failed to complement *Δpor1*

yeast whether expressed from single-copy or multiple-copy vector (Fig. 3.1).

Sequence analysis indicates a VDAC-like secondary structure

The alignment of the amino acid sequences for *D.melanogaster* VDAC and

CG17137 shows extensive sequence identity between these two polypeptides (Fig. 3.2).

CG17139 and CG17140, while far more similar to each other (including the N-terminal
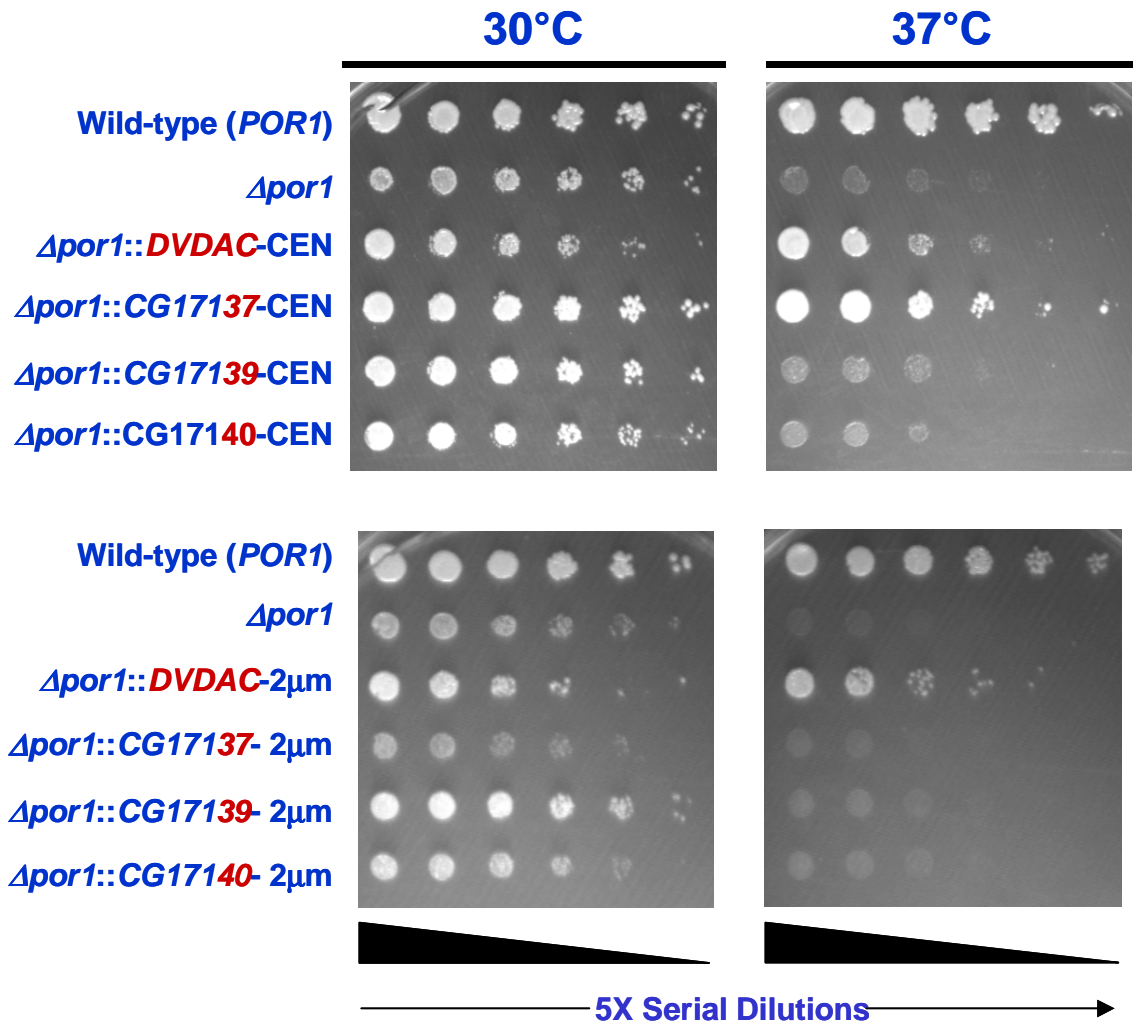
Figure 3.1. Complementation Analysis of DVDAC and VDAC-like Genes in Yeast.
Wild-type (*POR1*), *Δpor1*, or *Δpor1* yeast transformed with the indicated expression constructs plated on 3% glycerol and grown at the indicated temperatures are shown. In each panel, each row represents six serial five-fold dilutions of each strain as indicated.

```
DVDAC      ---------- ---------- ---------- ---------- ----------
CG17137    ---------- ---------- ---------- ---------- ----------
CG17139    MRERIRNLFR RNKRKR---- AASDYLEPHD EGGGNV---- ----QDNRSA      38
CG17140    MKQRLRNLFR RNKMRARPTT VASDANKEQP EPPKQEPSKQ KKTKQDASKQ      50

DVDAC      ---------- ---------- ----
CG17137    ---------- ---------- ----
CG17139    EEDKEEN--- -----KVEML PPPP                                 54
CG17140    EPPKQEEPEK PPKEVEVEII PSPT                                 74

DVDAC      MA--PPSYSD LGKQARDIFS KGYNFGLWKL DLKTKTSSGI EFNTAGHSNQ      48
CG17137    MAAKTPTYPD LGKLARDLFK RGYHPGIWQI DCKTLTNSGI EFFTTGFASQ      50
CG17139    MEGEMPSYFH VGLLAKMCLI HGYTIGRWKL QCTSKTEKDF YLSSFGEGYP     104
CG17140    SEGEMPTYFH VGALAKDCLI NGFKIGAWQM HCSTRTDNDF YLNTFGEGYP     124

DVDAC      ESGKVFGSLE TKYKVKDYGL TLTEKWNTDN TLFTEVAVQD QLLEGLKLSL      98
CG17137    DNSKVTGSLQ SKYKIEDQGL TLTERWNTEN WLFGEIMHRD KLAQGLMLAV     100
CG17139    TWNTVYGGLE AYKESGNFHA SLA--WLSDG DLLSDLGVHG DGLGGTWSTV     152
CG17140    TMKNVFGGME VFKEVGNYST SLG--WFTNN DLLSEIAVRG MNFGSRYGLL     172

DVDAC      EGNFA--PQS GNKNGKFKVA YGHENVKADS DVNIDLKGPL INASAVLGYQ     146
CG17137    EAKFQ--PGS NEADGKFKMG YAQDNFNFLA DIGLNSE-PI LNCSLVVGHK     147
CG17139    LKSMVSYPEG RKFQCKLKCG FDRNPGKVEM YIPIYKEPLL MGYIMMQPVK     202
CG17140    LKSTIGTKDE VSFQTKLKCG LERDPVKVEL VVPLYNEPLF LGYVLVAPVE     222

DVDAC      GWLAGYQTAF DTQQSKLTTN NFALGYTTKD FVLHTAVNDG QEFSGSIFQR     196
CG17137    EFLGGVGTEF DVGNTELKGW KVALGWTNET ATLHGELKNG DTWLASLFYK     197
CG17139    NYLLGYRTVF NVEDRDFNMH AFCGGYSNDV TEVGLKFENF KALRGSIFQR     252
CG17140    NWVLGYRTEY NFDEKGFDKH ALCLGYNNGR TEVGLKLENF EDLRGSIFQR     272

DVDAC      TSDKLDVGVQ LSWASG---- ------TSNT KFAIGAKYQL DDDARVRAKV     236
CG17137    ASEKIDAGIE VTKGAGGGEA AEGEQQGGDV VVNLGMIYHL EEDALVRAKV     247
CG17139    IGEKWAVALK ANLYGN---- ------VSAK SVSIGGQYEW EPGSMLKAKV     292
CG17140    IGEAWAFAIK TNLYSS---- ------ENVK QFAIGVQYDF QNGTMVKAKL     312

DVDAC      NNASQVGLGY QQKLRTGVTL TLSTLVDGKN FNAGGHKIGV GLELEA        282
CG17137    NNLVELGLGY EQKLRDGITA SISAVLDCNN FKDGNHRFGV GIALQC        293
CG17139    RGDSRIGLIF QKKLREDIEV LFHVGFEGSD PINGKHKFGS SWYFNM        338
CG17140    REDSRMGFVY QSKIGENIDV GYHLAFDGVD PIGGAHRIGV SWGFHC        358
```

Figure 3.2. The amino acid sequence of the *D.melanogaster* VDAC was aligned with VDAC-like sequences CG17137, CG17139, CG17140. Colored boxes show matches between VDAC and any of the other sequences: yellow – for uncharged amino acids, red – for negative charged amino acids, and blue – for positive charged amino acids. For the case of N-terminus extensions of CG17139 (1-54 amino acids) and CG17140 (1-74 amino acids) colored boxes indicate matches between the two sequences as well as all charged amino acid residues.

extension) also exhibit significant sequence similarity with VDAC, especially near the N

and C termini. In agreement with Oliva et al. (2002), pairwise alignment of these

polypeptides reveal 42% identity and 65% similarity with DVDAC for CG17137, 23%

identity and 42% similarity for CG17139, and 26% identity and 44% similarity for

CG17140. These values are much lower than those previously reported for VDAC

isoforms from the same species (yeast, mouse, and wheat) however, they are in the same

range as the values obtained from comparisons of VDAC sequences from diverse

organisms. For example, human and yeast VDAC have less than 30% sequence identity

(Blachly-Dyson and Forte, 2001). In fact, pairwise alignment of these *Drosophila*

polypeptides with mouse VDAC1 reveal 58% identity and 75% similarity for DVDAC,

34% identity and 56% similarity for CG17137, 24% identity and 39% similarity for

CG17139, and 21% identity and 38% similarity for CG17140. However, even sequences

with low primary sequence identity form channels with very similar conductance and ion

selectivity. This means that despite divergence in the primary sequence, these proteins

should have a very similar secondary structure.

Our analysis of CG17137, CG17139 and CG17140 for secondary structure

homology with VDAC is based on looking for patterns of alternating hydrophobic and

hydrophilic residues that are required to form transmembrane β-strands lining the wall of

a β-barrel channel. For this purpose we generated the β-pattern profile as described by

Blachly-Dyson et al. (1989). A β-pattern parameter (β) was calculated for each group of

10 adjacent amino acids by combining the hydropathy value (Kyte and Doolittle, 1982)

of each as follows:

$$\beta = \left| \sum_{i=1}^{10} (-1)^{i+1} v(i) \right| \qquad (1)$$

where $v(i)$ is the hydropathy value of the ith amino acid. This yields large numbers for a fragment that has alternating polar-nonpolar pattern. The β-pattern parameters were plotted against the number of the first amino acid in the group. Analysis of *Drosophila* peptide sequences reveals peaks for the location of putative transmembrane strands (Fig. 3.3). These peaks correlate rather well with each other. The overall correlation coefficients are shown in Table 3.1. These are all highly statistically significant (>99%), but clearly there is stronger similarity between DVDAC and CG17137, and between CG17139 and CG17140. These results indicate that all compared sequences might share a similar secondary structure and a similar number of putative transmembrane strands.

In order to test the possibility that the three VDAC-like sequences are in fact channel-forming isoforms of *D. melanogaster* VDAC, the gene products for *CG17137*, *CG17139*, and *CG17140* were purified from mitochondrial outer membranes isolated from Δ*por1* yeast expressing these genes and utilized for electrophysiological studies in reconstituted systems *in vitro*.

CG17137 forms typical VDAC channels

We examined the ability of CG17137 to increase the conductance of planar phospholipid membranes formed under standard conditions (see Materials and Methods). The detergent-solubilized protein was added to the aqueous phase on one side of the membrane and, after some time, conductance increments were observed. Fig. 3.4A shows the insertion of a 0.31 nS conductance. This conductance responded to the application of

38
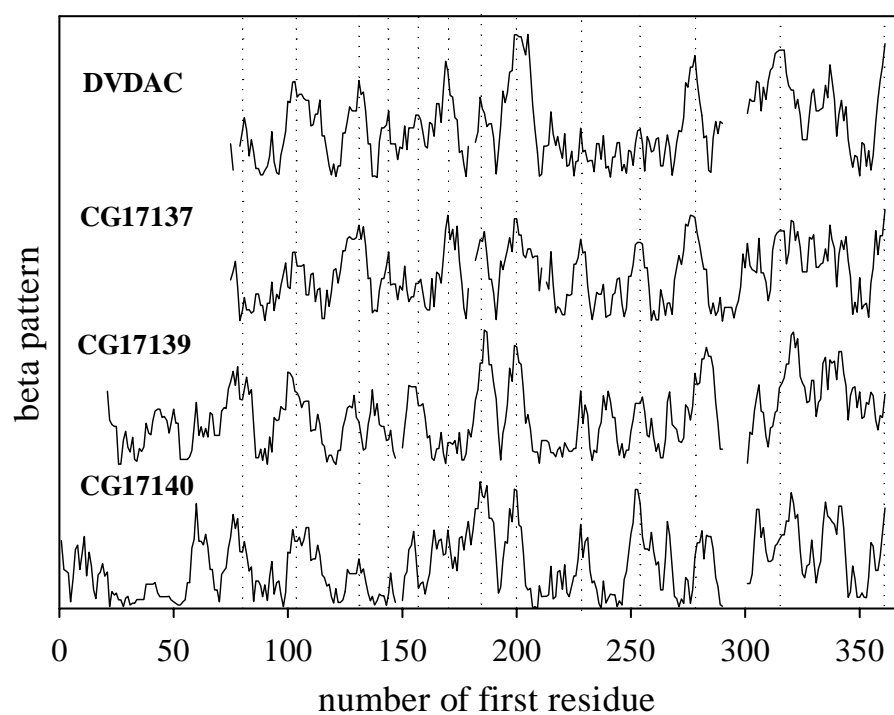
Figure 3.3. A comparison of the β-patterns (see text) of *D.melanogaster* VDAC, CG17137, CG17139 and CG17140. The dotted lines show similarity in location of the peaks. The gaps were generated based on the results of the primary structure alignment.

Table 3.1. Correlation coefficients of β-patterns

	DVDAC	CG17137	CG17139
CG17137	0.70		
CG17139	0.39	0.34	
CG17140	0.46	0.39	0.63

elevated voltages by closing transitions reminiscent of VDAC. However, this was not always the case. In fact, results obtained with this protein were rather variable. CG17137 forms discrete conducting events but we were not able to identify, with confidence, a conductance characteristic of a single channel. The data suggest conducting pathways in the range of 0.5 – 8 nS in the presence of 1.0 M NaCl and 0.13 - 0.46 nS at the presence of 0.10 M NaCl. Based on the known properties of VDAC, one might propose that this range corresponds to a variety of different conductance states of a channel. The voltage dependent gating illustrated in Fig. 3.4B and upon application of a triangular voltage wave (Fig. 3.5) is reminiscent of classical VDAC behavior. However, attempts at further confirmation by looking at selectivity changes associated with gating revealed a complex pattern. We assessed the selectivity by making measurements in the presence of a salt concentration gradient and extrapolating linear segments to determine the zero-current potential. As expected, conductance changes were associated with changes in the selectivity of the channel(s) (Fig. 3.6A). Negative voltages correspond to multiple conductive states with cationic selectivity and positive voltages to the single state with anionic selectivity. A single VDAC channel demonstrates anionic selectivity in the open state and cationic selectivity in the lower conducting closed states. In the case of conductance formed by CG17137 we observed that sometimes the closure of the channel(s) did result in a change toward a preference for cations but at other times the opposite was true. This inconsistency might be explained by a mixture of channel gating and channel insertion or disappearance but variability in the observed conductances also made it difficult to distinguish between these possibilities.

- 8.1 mV

I = 0

1 pA

5 min

+50 mV

0 mV

10 pA

30 s

-50 mV
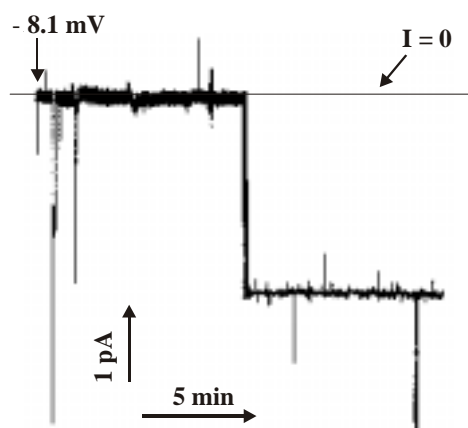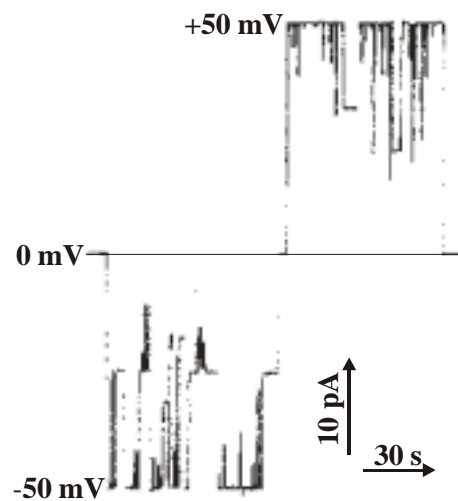
A   B

Figure 3.4. Changes in ionic current through a planar membrane in the presence of CG17137. Both compartments contained 0.10 M NaCl. (A) Insertion of the channel. (B) Gating of the channel at high voltages
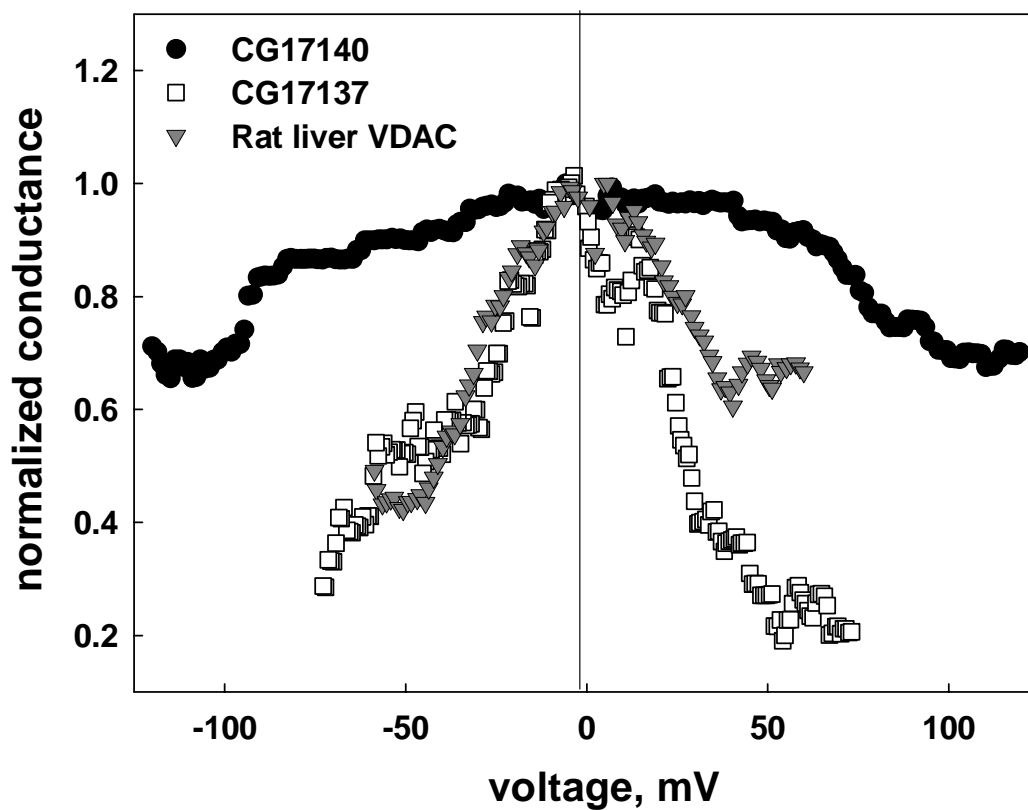
Figure 3.5. Voltage dependence of the conductance of the channels formed by CG17137, CG 17140, and by rat liver VDAC. The voltage was applied in the form of triangular waves (3 mHz, ±73 mV for CG17137 and ±120 mV for CG17140). The membranes contained 2-4 channels.

A

- 7 mV   - 7 mV

I = 0

50 pA

+10 mV

-73   0   73   0   -73

voltage (mV)

B

+ 18 mV

- 23 mV

I = 0

- 18 mV

50 pA

73   0   - 73   0   73
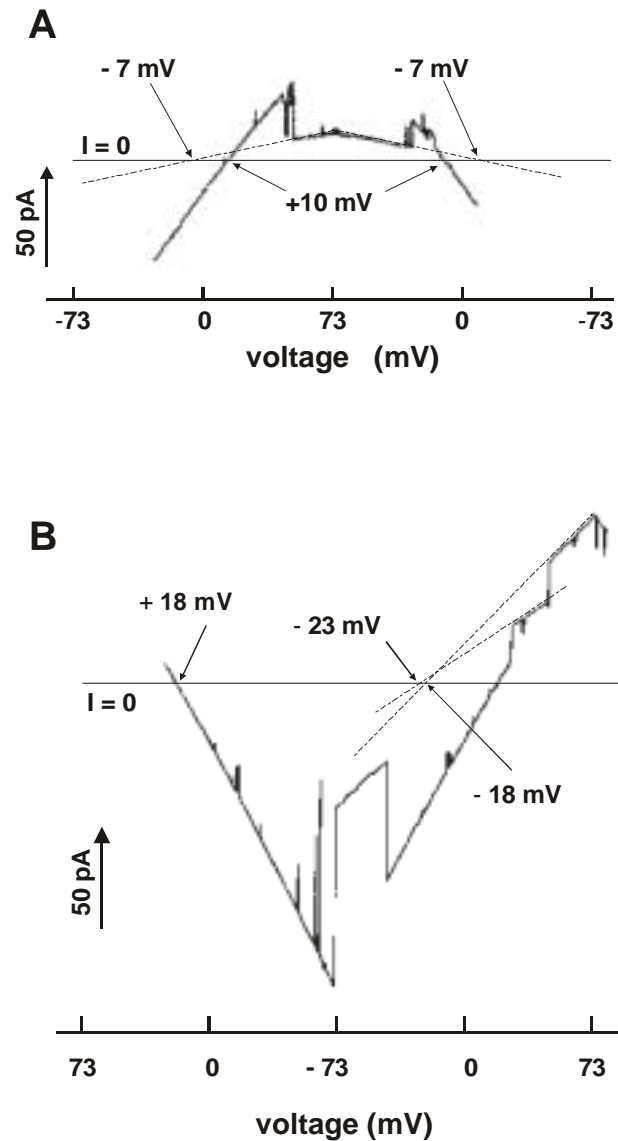
voltage (mV)

Figure 3.6. Selectivity of the channel(s) formed by CG17137 (A) and CG17140 (B) in the presence of a salt gradient. In the case with CG17140 both compartments also contained 1mM $CaCl_2$. The indicated voltage refers to the *cis* side. The voltage was applied in the form of slow triangular waves (3 mHz, ±73 mV). The dotted lines are extrapolations used to determine the reversal potential of each selected conductance level. The numbers associated with the zero-current intercepts show the value of the reversal potential.

44

CG17139 does not demonstrate channel formation

In experiments with planar membranes we were not able to get an increase in membrane conductance after addition of CG17139. Our observations were conducted under varied conditions: different salt concentrations (0.1 M or 1M), salts of sodium or potassium, pH 6.0 – 8.0, presence of different divalent ions (Ca^{2+} or Mg^{2+}). In all cases we observed a lack of channel formation.

CG17140 also forms channels

Fig. 3.7A shows discrete increases in the conductance of planar membranes after addition of detergent-solubilized CG17140. The observed single-channel conductance was 1.38 ± 0.12 nS (mean ± SD) in 1.0 M NaCl. The channels gate (Fig. 3.7B) but only at very high applied voltages (110 mV and higher; Fig. 3.7B). Closure of a normal VDAC channel is observed at 30 mV and higher. Fig.3.5 shows voltage-dependent closure at both positive and negative voltages but closure is incomplete in the voltage range tested. In the presence of a 10-fold salt gradient, CG17140 demonstrated a conductance of 0.61 ± 0.02 nS and a reversal potential of $+ 22.6\pm2.4$ mV, corresponding to anionic selectivity. Closure of these channels resulted in a switch to cationic selectivity with varying values of the reversal potential (Fig. 3.6B). This is in agreement with typical VDAC behavior.
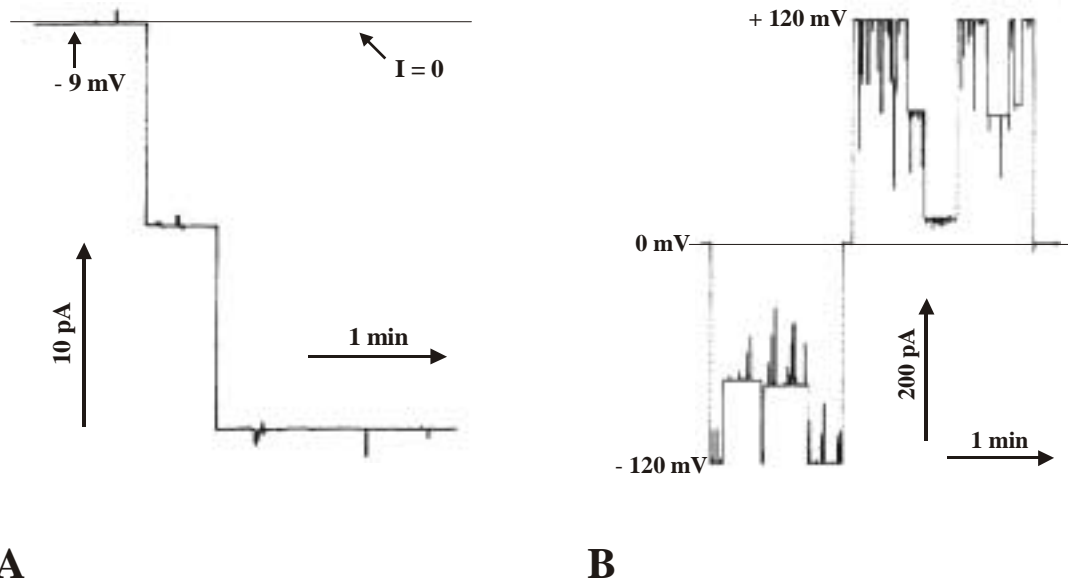
Figure 3.7. Changes in ionic current through a planar membrane in the presence of CG17140. Both compartments contained 1.0 M NaCl. (A) Insertion of two channels. (B) Gating of the channels at high voltage

CG17137, CG17139, CG17140 cause differential permeabilization of liposomes

The use of planar membranes to assess the ability of the VDAC-like proteins to form channels has the drawback that one is selecting for proteins that insert into the membranes. It is possible that a minor constituent might be responsible for the observed activity. The use of liposomes allows one to assess the ability of the population to permeabilize membranes. It also eliminates the need for the protein to insert into the membrane from an aqueous environment.

We incorporated CG17137, CG17139 and CG17140 into liposomes and measured the permeability of the liposomes, using hyperosmotic solutions of non-electrolytes of different sizes. Mixing of liposomes with these solutions induces liposome shrinkage due to the fact that water moves out of the liposomes faster than the solute can move in. In the case of a permeable solute, reswelling follows the shrinkage of the liposomes. The shrinkage-reswelling process was observed by measuring changes in light scattering at 400 nm over time. A decrease of the liposome size causes an increase in apparent absorbance and a decrease of absorbance indicates reswelling of the liposomes. The rate of reswelling reflects the permeability of the liposome membrane. If the solute is impermeable it will demonstrate a lack of reswelling. Using this method we can also estimate the molecular weight cut-off of the permeability pathway.

Fig.3.8 shows the absorbance traces for liposomes containing the VDAC-like proteins. The initial absorbance is due to rapid shrinkage resulting from the hypertonic stress of the indicated non-electrolyte. This was followed by various rates of absorbance reduction due to permeation of non-electrolyte into the liposomes. In CG17137-containing liposomes (top panel), reswelling occurred with all except the highest

molecular weight of non-electrolyte (PEG 6800). This molecular weight cut-off is the same as that reported for VDAC (Colombini, 1980). For CG17140-containing liposomes, the molecular weight cut-off was somewhat lower. The results show no significant reswelling in the presence of γ - cyclodextrin (1300 Da). The liposomes containing CG 17139 did not show significant reswelling with PEG 1500 (the slight decline was not different from control). The CG17139-containing liposomes did show permeability to PEG 1000, but this was also observed when liposomes were formed using mitochondrial membranes isolated from yeast lacking VDAC1 (Fig. 8, panel E, in Xu et al., 1999). Thus there is no detectable permeability increase by the presence of CG17139.

Figure 3.8. The responses of liposomes containing one of the proteins CG17137, CG17139, CG17140 to osmotic pressure changes caused by non-electrolytes. The liposomes were made as described in Material and Methods. The absorbance at 400 nm was recorded. When the liposomes had stabilized (no significant change in absorbance, approximately 1 h after dilution) 67 µl of 50 mM PEG6800, 67 µl of 100 mM PEG3400, 67 µl of 100 mM PEG1500, 220 µl of 20 mM γ-cyclodextrin, 67 µl of 225 mM PEG1000, or 67 µl of 278 mM melezitose was added and quickly mixed at the point shown by the vertical arrows. All tracings in each panel were performed on the same set of liposomes so these can be readily compared. The tilted arrow indicates the brief mixing of the sample during recording showing no significant sedimentation of the liposomes.
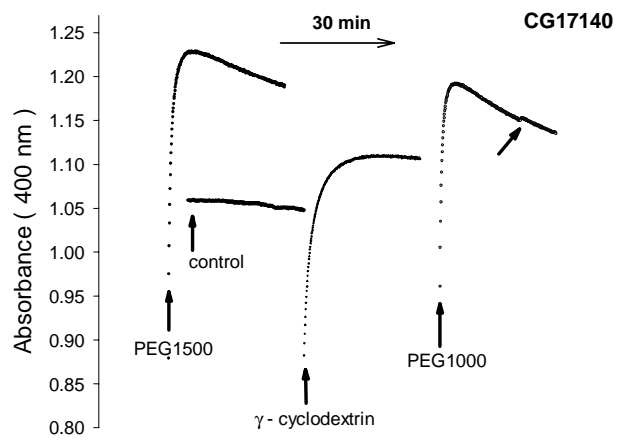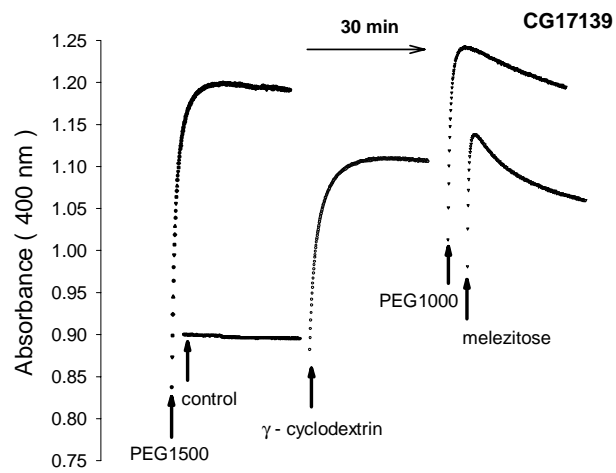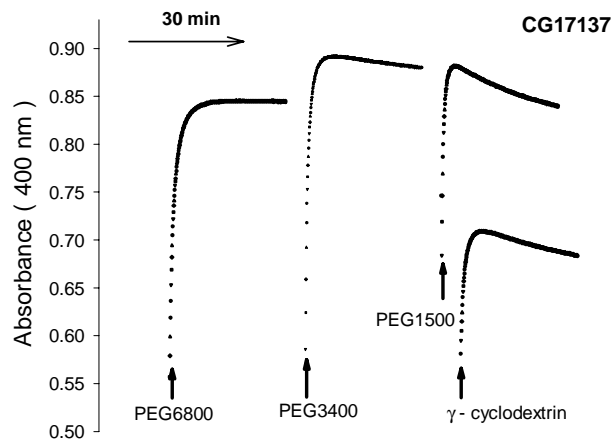
DISCUSSION

The study of the physiological properties of VDAC-like proteins in reconstituted systems (planar membranes and liposomes) is a step in understanding their specialized cellular functions. We used both theoretical and experimental methods for characterization of these proteins. Insights gained from previous publications have allowed us to predict and explain the behavior of the recently discovered VDAC-like proteins. Their similar properties to those of classical VDAC may indicate that some of these proteins are actually VDAC isoforms.

The VDAC-like proteins from *Drosophila melanogaster* were tested for the major VDAC property – the ability to form voltage-dependent channels with characteristic channel size and ion selectivity. CG17137 and CG17140 clearly demonstrate channel-forming activity in both planar phospholipid membranes and in liposomes, CG17139 does not. The voltage dependence and selectivity are also reminiscent of classical VDAC behavior.

Insight into the physiological properties of these proteins was obtained by determining their ability to rescue the conditional lethal phenotype of yeast deficient for VDAC1 (POR1). We demonstrated that DVDAC and *CG17137* can rescue VDAC-deficient yeast, while *CG17139* and *CG17140* cannot. It is unclear why Ryerse et al. could not demonstrate complementation with DVDAC (Ryerse et al., 1997). This complementation pattern roughly correlates to the observed biophysical characteristics of these proteins, with DVDAC demonstrating classical VDAC properties as previously reported (De Pinto et al., 1989). We have demonstrated that CG17137 also exhibits properties similar to those of classical VDAC in planar membranes and liposomes in

51

terms of voltage gating and liposomal permeability. On the other hand, channels formed

by CG17140 demonstrate conductance that is approximately 40% of DVDAC or other

classical VDACs and a smaller aqueous pore as indicated by the impermeability to γ-

cyclodextrin (MW 1300), whereas CG17139 fails to form channels in either planar

membranes or liposomes. The reduced size of the aqueous pore formed by CG17140 may

restrict the flow of some critical metabolite resulting in failure of cells to grow at 37°C.

In any case, of the three VDAC-like proteins, only CG17137 has properties similar

enough to VDAC to functionally substitute for VDAC and thus could be an isoform of

Drosophila VDAC.

The high degree of similarity between the beta pattern of *D.melanogaster* VDAC

and CG17137 indicates that they might share similar folding patterns. To view our results

in the context of predicted secondary structures, we generated the folding patterns (Fig.

3.9) for all studied proteins by analogy with *Neurospora crassa* VDAC (Song et al.,

1998a). The choice of candidate transmembrane β-strands was based on the following

criteria: 1) A candidate strand should have a good alternating hydrophilic and

hydrophobic pattern; 2) Chain-distorting prolines should not be located in the middle of

the transmembrane strand but rather at the ends of the strands; 3) There should be no

adjacent charged amino acids except at the ends; 4) The strand should have good

sequence homology to the corresponding transmembrane β-strand for *N.crassa* VDAC.

When comparing the secondary structure of CG17137 to the *Drosophila* VDAC

folding pattern, the major difference is a 10 amino acid insertion in the long loop region

on the cytosolic face of CG17137 (Fig. 3.9A). This insertion adds 3 negative charges to

the long loop region, which is already rich in charged residues. In fungi, this region

Figure 3.9. The folding patterns for CG17137 (A), CG17139 (B), CG17140(C). The long loop region for CG17137 and the membrane regions have been highlighted: green circles – prolines, blue boxes – positively charged amino acid residues, red boxes – negatively charged amino acid residues. IMS – intermembrane space

between position 184 and 228 is not involved in either voltage gating or selectivity (Thomas et al., 1993; Blachly-Dyson et al., 1994) and may serve as a binding site a for a cytosolic factor. Indeed, the major difference between human VDAC1 (HVDAC1) and human VDAC2 (HVDAC2) is a change from KK to ED at position 199-200 on HVDAC1 and perhaps this explains why HVDAC1 binds hexokinase and HVDAC2 does not (Blachly-Dyson et al., 1993). This change may be sufficient to favor interaction with a specific cytosolic factor. There are other differences between CG17137 and *Drosophila* VDAC and some of these are likely responsible for the differences in the properties of the single channels that were observed. Additionally, the variability of the observed channels formed by CG17137 may indicate the absence of a factor or factors that act to limit the number of structural states. The limiting of variable behavior by VDAC when interacting with controlling factors has been observed on a number of occasions (for example, Holden and Colombini, 1988).

The sequences of CG17139 and CG17140 differ from both CG17137 and *D.melanogaster* VDAC in having long, highly charged N-terminus extensions (Fig.3.9). The role of this feature is unclear. The mouse VDAC2 isoform has such an extension, albeit considerably shorter, but forms channels with canonical VDAC properties. Perhaps, the highly charged N-terminus extensions could serve as a binding site for agents stimulating unknown activities of VDAC-like proteins.

Protein CG17139 differs from the other VDAC-like proteins in its inability to form channels either in planar membranes or in liposomes. Lack of channel formation in planar membranes could be attributed to inability to insert from the aqueous phase. However, the liposomes were formed from a protein-lipid mixture and thus the protein

must have been present in the liposomal membrane. To test the possibility that insufficient protein was present SDS-PAGE of the purified VDAC fractions from the expression yeast strains was performed (Fig. 3.10). Clearly the yield of CG17139 purified from the same amount of yeast cells was even larger than that obtained for CG17137 or CG17140.

The folding pattern generated for CG17139 (Fig. 3.9B) may explain its inability to form channels. Colored squares indicate the presence of consecutive charged residues in the 1st and 11th β-transmembrane strands, which conflicts with the restrictions mentioned above and should inhibit formation of the channel. CG17140 does not have this feature (Fig. 3.9C) and its folding pattern is consistent with the fact that channels were observed.

In conclusion, our results indicate that despite the low degree of primary sequence identity with *Drosophila* VDAC, VDAC-like proteins have retained aspects of VDAC structure and function. The differential ability to complement VDAC-deficient yeast, and varied *in vitro* biophysical properties suggest that the members of this gene family in *Drosophila* play distinct physiological roles that need to be elucidated with future *in vivo* studies.
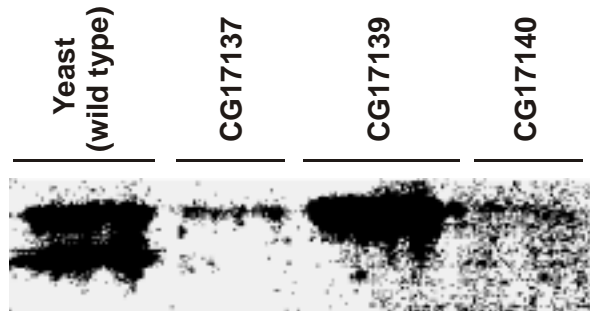
Figure 3.10. SDS-PAGE electrophoresis image of yeast VDAC and VDAC-like proteins.

The proteins were purified from mitochondrial membranes, run on 12% acrylamide gel

and the bands were stained with Coomassie Blue stain. The upper band shown for each

sample ran at approximately 36 kDa.

CHAPTER 4

New Insights into the Mechanism of Permeation through Large Channels

Alexander G. Komarov[1,3], Defeng Deng[2], William J. Craigen[2], and Marco Colombini[1]

[1]*Department of Biology, University of Maryland, College Park, MD 20742;* [2]*Departments of Molecular and Human Genetics and Pediatrics, Baylor College of Medicine, Houston, TX 77030;* [3]*St.Petersburg Nuclear Physics Institute, Gatchina, Russia, 188350.*

Running Title: *Insights into ion permeation*

ABSTRACT

The mitochondrial channel, VDAC, regulates metabolite flux across the outer membrane. The open conformation has a higher conductance and anionic selectivity, while closed states prefer cations and exclude metabolites. In this study 5 mutations were introduced into mouse VDAC2 to neutralize the voltage sensor. Inserted into planar membranes, mutant channels lack voltage gating, have a lower conductance, demonstrate cationic selectivity and, surprisingly, are still permeable to ATP. The estimated ATP flux through the mutant is comparable to that for wild-type VDAC2. The outer membranes of mitochondria containing the mutant are permeable to NADH and ADP/ATP. Both experiments support the counterintuitive conclusion that converting a channel from an anionic to a cationic preference does not substantially influence the flux of negatively charged metabolites. This finding supports our previous proposal that ATP translocation through VDAC is facilitated by a set of specific interactions between ATP and the channel wall.

INTRODUCTION

VDAC is known as the major pathway for metabolite flux across the mitochondrial outer membrane (MOM) (Colombini, 1979; Mannella and Colombini, 1984; Mannella, Forte and Colombini, 1992; Lee et al., 1998; Xu et al., 1999). This 30-32 kDa protein forms large channels with a molecular weight cut-off of up to 5000 for nonelectrolytes in the fully open state (Colombini, 1980). VDAC has a single open and multiple low-conducting closed states. The diameter of the pore is about 3 nm in the open and 1.8 nm in the closed state (Colombini et al., 1987; Mannella, 1989; Mannella, Forte and Colombini, 1992). One proposed secondary structure model includes one α-helix and 13 β-strands (Song et al., 1998a). These 14 elements form a barrel-like transmembrane structure that is tilted at a 45° angle (Abrecht et al., 2000).

VDAC from different eukaryotic species share highly conserved electrophysiological properties in vitro (Colombini, 1989), including single channel conductance, voltage gating and ionic selectivity. The open state is characterized by higher conductance (about 4 nS in 1 M KCl) and weak anionic selectivity (2:1 in favor of Cl^- over K^+ in a 10-fold KCl gradient). Closed states of VDAC have lower conductance (about 50-60% reduction compared to the open state) and cationic selectivity. Transition between the open and closed states is voltage dependent and is the result of the motion of the positively charged voltage sensor (Song et al., 1998b). At low voltages (less than 30 mV) this mobile domain forms part of the channel wall, which contributes to the anionic selectivity of the open state. At high voltages the voltage sensor moves out of the lumen of the channel causing channel closure and a switch to cationic selectivity. The voltage

dependence has a symmetrical character referring to the sign of the applied voltage (Schein et al., 1976; Colombini, 1979).

Whereas VDAC demonstrates only slight ionic preference in the presence of small ions, the permeability of the open and closed states to metabolites or large anions is dramatically different. Direct measurements of ATP flux have determined that ATP can penetrate through VDAC in the open state, however it becomes virtually impermeant upon closure of the channel (Rostovtseva and Colombini, 1997). Although the effective diameter of the ATP molecule is only 0.96 nm (calculated from the diffusion coefficient from Rostovtseva et al., 2002a), this metabolite cannot pass through the closed state (1.8 nm in diameter). Simple electrostatic repulsion from the channel wall is thought to account for this impermeability.

In previous work we found that the open state of VDAC demonstrates another type of selectivity (Rostovtseva and Bezrukov, 1998; Rostovtseva et al., 2002a; Rostovtseva et al., 2002b). The penetration of large negatively charged molecules through VDAC was monitored by measuring the interference of those substrates to the flow of small ions. This interference can result in two observables: an increase in the current noise and a reduction of the single channel conductance. Among nucleotides (NADPH, NADH, NAD, ATP, ADP, AMP, UTP) the ability to reduce the single channel conductance was very similar, however the ability to generate current noise exhibited a strong dependence on the nucleotide base. These observations led us to propose the existence of a nucleotide-binding site within the channel lumen that recognizes purine-containing nucleotides.

The same experimental approach revealed the ability of VDAC to differentiate between metabolites and synthetic molecules. Synthetic anions such as tetraglutamate and 1-hydropyrene-3,6,8-trisulfate, which have an effective size and charge comparable to ATP, did not interfere with the flux of small ions, indicating that these ions could not permeate through VDAC. Noise analysis also did not provide any evidence for the penetration of these molecules into the channel. This set of experiments showed that VDAC has a special type of selectivity for large anions. This selectivity is based on the shape of the molecule and charge distribution rather than just charge and effective size.

In the current work we demonstrate that the permeability of VDAC to metabolites is defined by a specific interaction between metabolites and the channel wall rather than by the overall charge of the channel lumen.

MATERIALS AND METHODS

Preparation of yeast cells

M3 (*MATα lys2 his4 trp1 ade2 leu2 ura3*) is the parental wild-type strain (with respect to POR1). M22-2 (*Δpor1*) lacks *POR1* due to the insertion of the yeast *LEU2* gene at the *POR1* locus (Blachly-Dyson et al., 1990). To generate a wild-type mouse VDAC2 (mVDAC2) yeast shuttle vector, oligonucleotide-directed mutagenesis was used to create a *Nco*I site at the start codon and a *Nsi*I site within the 3' untranslated region. This allowed for the complete open reading frame of the mVDAC2 cDNA to precisely replace the yeast VDAC1 gene previously subcloned into a single-copy yeast shuttle vector (pSEYC58), as described (Sampson et al., 1997), placing expression of the engineered gene under the control on the endogenous transcriptional control elements.

For site-directed mutagenesis of individual amino acids, oligonucleotide primers were designed according to the desired amino acid substitution. The sequences of the oligonucleotides are listed in Table 4.1. PCR-based mutagenesis was performed using a commercial kit following the manufacturer's protocol (QuickChange XL Site-directed mutagenesis, Stratagene). Each substitution was created sequentially and confirmed by DNA sequencing. The relevant mutant mVDAC2 (K19E-K31E-K60E-K95E-D227K) was introduced into M22-2 using a shuttle vector, as previously described (Sampson et al., 1997).

To facilitate cell growth and harvesting, stock cultures were prepared (following Lee et al., 1998) by inoculating a single colony into 50 ml of medium consisting of 335 mg of Difco™ Yeast Nitrogen Base w/o Amino Acids (#291940, Becton, Dickinson and Company, Sparks, MD), 50 mg of KH_2PO_4, 38.5 mg of CSM-URA (#4511-222, Complete Supplement Mixture minus Uracil; Q-BIOgene, Carlsbad, CA), and 1 ml of 85% lactic acid. The medium was adjusted to pH 5.5 by adding of solid KOH. Autoclaving time and temperature were reduced (110°C, 15 minutes) to minimize pH drop and achieve good growth characteristics. When the cells reached an O.D. of between 0.7 and 0.9 (at 600 nm) they were stored at 4°C for later use. For mitochondrial isolation, 9 ml of yeast stock solution were inoculated into each of two flasks containing one liter of the same medium and grown with orbital shaking at 30°C. A final O.D. between 0.7 and 0.9 gave approximately 4-5 grams of cells.

Table 4. 1. Oligonucleotides used to generate the amino acid substitutions

Primer name	Sequence
K19E For	cagagacattttcaac***gaa***ggatttggctttgg
K19E Rev	ccaaagccaaatcc***ttc***gttgaaaatgtctctg
K31E For	gctggatgtg***gaa***acgaagtcatgcagcggtgtgg
K31E Rev	caccgctgcatgacttcgt***ttc***cacatccagc
K60E For	gcgggaccttggagacc***gaa***tacaaatggtgtg
K60E Rev	cacaccatttgta***ttc***ggtctccaaggtcccgctaa
K95E For	tgtcaaggtttg***gaa***ctgacttttgacaccacc
K95E Rev	ggtggtgtcaaaagtcag***ttc***caaaccttgac
D99K For	actgactttt***aaa***accaccttttcaccgaacacagg
D99K Rev	cctgtgttcggtgaaaaggtggt***ttt***aaaagtcag
D127K For	cctcggctgt***aaa***gttgactttgattttgc
D127K Rev	ccagcaaaatcaaagtcaac***ttt***acagccgagg
D227K For	ctaaataccagttg***aaa***cctactgcttctatctctgc
D227K Rev	gcagagatagaagcagtagg***ttt***caactggtatttagc

Isolation of intact yeast mitochondria.

Mitochondria were isolated from *S. cerevisiae* essentially as published by Daum et al. (1982), but modified as previously described (Lee et al., 1998) in order to obtain highly intact mitochondria. The final mitochondrial pellet was suspended in approximately 1 ml of medium containing 0.6 M mannitol, 10 mM Tris•Cl, 0.6% PVP. 0.1 mM EGTA and 0.1% BSA, pH 7.2. Mitochondrial protein was measured by the method of Clark (1976). The protein concentration in mitochondrial suspension was 10-15 mg/ml.

Assessing MOM integrity

The integrity of the MOM of purified mitochondria was determined based on the rate of cytochrome c-dependent oxygen consumption (Douce at al., 1987). Exogenously added cytochrome c should reach the mitochondrial inner membrane to be oxidized by cytochrome c oxidase. In this case, the outer membrane serves as a barrier for the reaction. The rates of oxygen consumption for intact (υ_{intact}) and osmotically shocked mitochondria ($\upsilon_{disrupted}$) were compared and the percentage of intact mitochondrial was calculated as follows:

$$\% \ intact = (1 - \upsilon_{intact}/\upsilon_{disrupted})*100.$$

Osmotic shock was applied by mixing of 40 µl of mitochondrial suspension with 1.5 ml of water, incubating for 3 min, and further addition of the double concentrated respiration buffer (1.3 M sucrose, 20 mM HEPES, 20 mM KH_2PO_4, 10 mM KCl, 10 mM $MgCl_2$, pH 7.2) to restore the initial osmotic pressure.

Oxygen consumption was measured by using a Clark oxygen electrode. An

aliquot of ascorbate (50 µl of 0.48 M) was added to the 3 ml volume of R-medium (0.65 M sucrose, 10 mM HEPES, 10 mM KH_2PO_4, 5 mM KCl, 5 mM $MgCl_2$, pH 7.2) containing either intact or disrupted mitochondria to maintain the cytochrome c in the reduced form. The addition of 180 µg of cytochrome c was used to induce oxygen consumption. Finally, an aliquot of KCN (0.2 mM final) was used to block cytochrome c oxidase and determine the level of KCN-independent respiration.

Integrity of mitochondria varied from 78-86%.

Measurements of outer membrane permeability

a) Permeability to NADH

To determine MOM permeability we used the method previously reported by Lee et al. (1998) for yeast mitochondria. NADH added to isolated yeast mitochondria is oxidized primarily by an NADH dehydrogenase located on the outer surface of the inner membrane (Ohnishi, Kawaguchi and Hagihara, 1966). The rate of NADH oxidation can be limited by the flux of NADH through the MOM (Fig. 4.1).

The permeability of the MOM to NADH was determined by assuming that the rate of NADH oxidation for intact mitochondria is identical to the net flux of NADH through the membrane and dividing this rate by the concentration difference of NADH across the membrane. The medium NADH concentration was monitored directly by measuring the absorbance at 340 nm. The intermembrane space NADH concentration was estimated from the oxidation rate of shocked mitochondria. We assumed that (i) in the disrupted mitochondria the NADH concentration in the intermembrane space is the same as in the medium and (ii) the same local NADH concentration in the vicinity of the
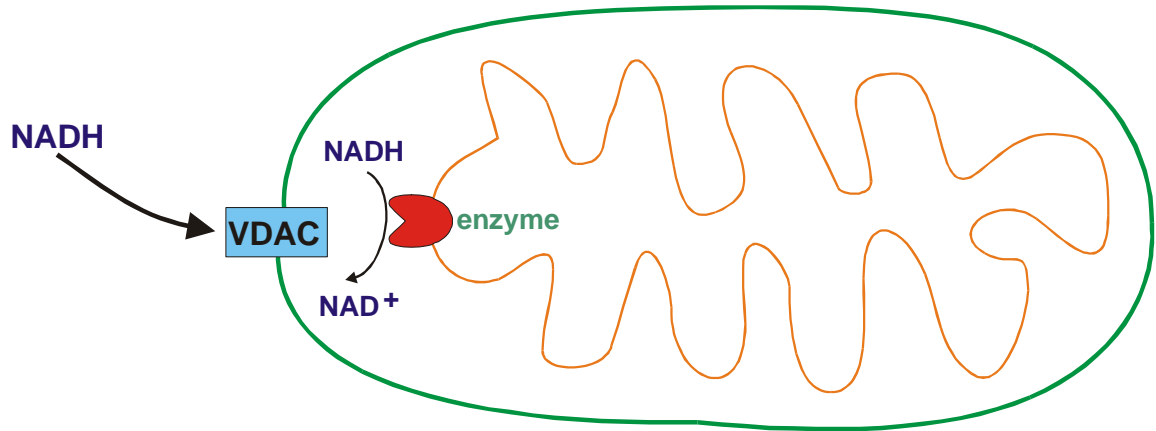
Figure 4.1. Measurements of the MOM permeability to NADH. The enzyme is NADH dehydrogenase.

dehydrogenase results in the same oxidation rate. Thus, the NADH concentration in the intermembrane space is the same as the concentration needed to achieve the same oxidation rate in disrupted mitochondria. At low NADH concentrations the calculated permeability values are not meaningful because the concentration differences are insignificant when compared to the noise.

Samples of intact mitochondria were prepared by 10-fold dilution of the mitochondrial suspension (0.7-3.0 mg/ml of total protein) with R-medium. Disrupted mitochondria were obtained by using a mild osmotic shock as previously described (Lee et al., 1998). One volume of mitochondrial suspension was mixed with 2 volumes of distilled water and incubated in ice for 10 min. Then, 5 volumes of R-medium and 2 volumes of double concentrated R-medium were added to restore the initial osmotic pressure. The uncoupler, FCCP (3 µM final concentration) was added to both intact and shocked mitochondrial samples to ensure that the membrane potential would not inhibit the rate of NADH oxidation. An aliquot of NADH (30 µM final concentration) was added to start the reaction.

b) Permeability to ADP/ATP

In order to estimate the permeability of the intact MOM to ADP/ATP we used a method similar to that described for NADH. The flux of ADP/ATP across MOM was determined by comparing the activity of adenylate kinase in suspensions of intact and osmotically shocked mitochondria. The intermembrane space enzyme adenylate kinase was assayed by a standard method (Sottocasa, 1967), using a coupled enzyme system (hexokinase and glucose-6-phosphate dehydrogenase) and detecting the rate of $NADP^+$ reduction (Fig. 4.2).
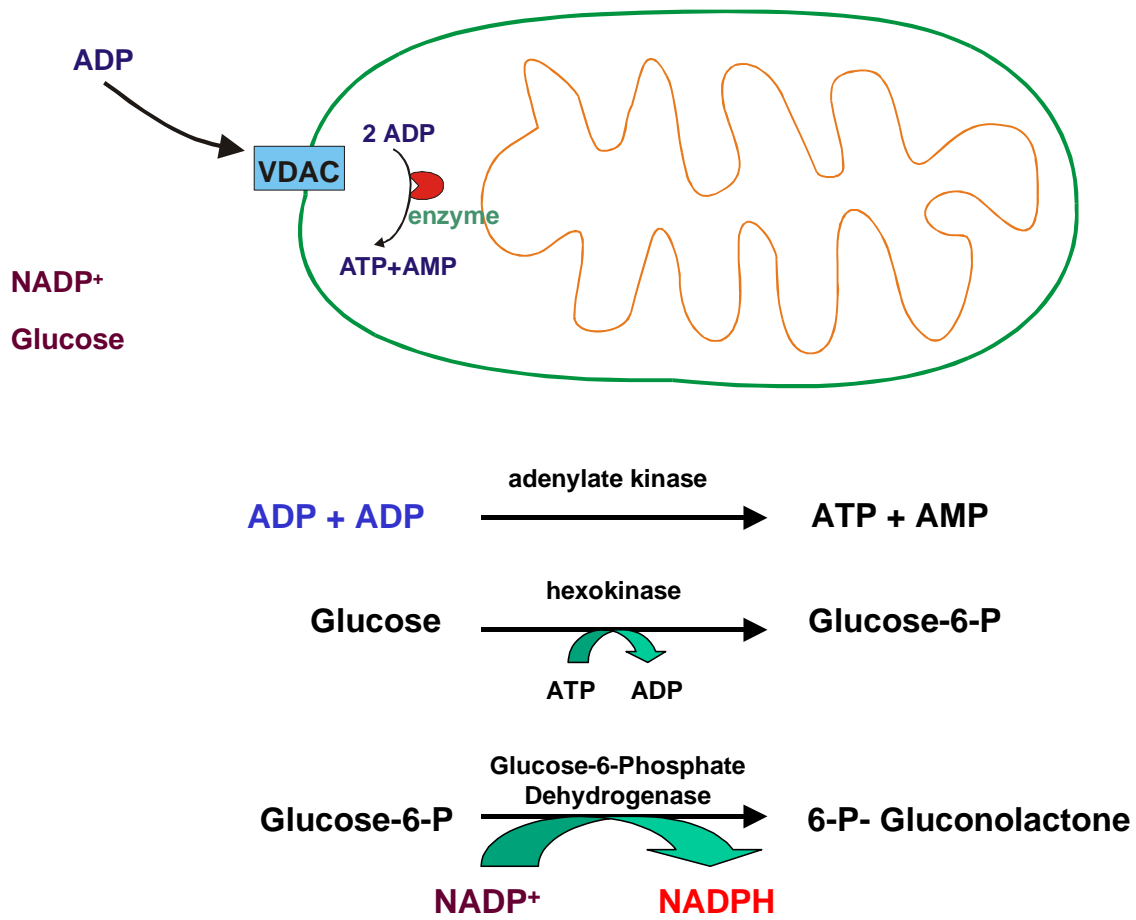
Figure 4.2. Measurements of the MOM permeability to ADP/ATP. The enzyme is adenylate kinase.

Like NADH, access of externally added ADP to the intermembrane space may be limited by the permeability of the MOM. The consumption of ADP can be indirectly determined by the rate of the reduction of externally added $NADP^+$. Two molecules of ADP enter the intermembrane space through the outer membrane and are transformed by adenylate kinase to ATP and AMP. ATP must cross the outer membrane to be consumed by the coupled enzyme system (hexokinase and glucose-6-phosphate dehydrogenase) and glucose to produce NADPH (monitored at 340 nm). ATP cannot move to the matrix because the adenine nucleotide translocator (ANT) was blocked by atractyloside (20 µg/ml final concentration). Oxidation of NADPH was blocked by the use of CN^- (0.2 mM).

A similar approach to that used for NADH was used to calculate the permeability of the MOM to ADP/ATP. However, the situation is more complex because adenylate kinase is located in the intermembrane space and the added enzymes are in the medium. Thus, at steady state the overall rate of NADPH production must be equal to net efflux of ATP from the mitochondrion to the medium and equal to one half the net flux of ADP into the mitochondrion (reflecting the stoichiometry of adenylate kinase). The [ADP] is known because it must be the initial concentration minus the [NADPH] that is measured continuously. The [ADP] in the intermembrane space required to maintain the correct ADP flux is not known. The medium [ATP] should be very low because of the action of hexokinase. Again, the [ATP] in the intermembrane space needed to achieve the correct flux of ATP is not known. However, the rate of adenylate kinase activity, which must be the same as the rate of NADPH production, will be reduced by the presence of ATP in the intermembrane space, as dictated by the known kinetics of the enzyme. We

determined the [ATP] in the intermembrane space by measuring the reduction of the rate of NADPH production when the MOM is intact. We assumed that when the MOM is disrupted hexokinase maintains the [ATP] near zero.

Kinetic studies of yeast adenylate kinase (Su and Russell, 1966) have shown that the reaction is limited by the rate of conversion of the enzyme from E-ADP$_2$ to E-AMP-ATP. Thus, we were able to assume that the binding steps in the adenylate kinase reaction were at equilibrium. We established a spreadsheet to model the adenylate kinase reaction and constrained it using the published V_{max} and K_m values for the forward and reverse reactions ($K_{ADP} = 2.7 \bullet 10^{-4}$ M, $K_{AMP} = 5.8 \bullet 10^{-5}$ M, and $K_{ATP} = 5.4 \bullet 10^{-5}$ M; $V_{reverse} = 2.14 \bullet V_{forward}$). We further assumed independence of the binding constants of all substrates. The model yielded the following binding constants: $k_{ADP} = 6.0 \bullet 10^{3}$ M, $k_{AMP} = 4.5 \bullet 10^{4}$ M, and $k_{ATP} = 4.5 \bullet 10^{4}$ M. The model then was used to determine the [ATP] that would cause the observed reduction in the adenylate kinase reaction rate.

Samples of intact mitochondria were prepared by 40-fold dilution of the mitochondrial suspension (10-14 mg/ml of total protein) with A-medium (0.6 M sucrose, 50 mM Tris-Cl, 5mM MgSO$_4$, 10 mM Glucose, 0.2 mM NADP$^+$, 20 µg/ml atractylosides, 0.2 mM KCN, pH 7.5). Disrupted mitochondria were obtained by using a mild osmotic shock. One volume of mitochondrial suspension was mixed with 9 volumes of distilled water and incubated in ice for 5 min. Ten volumes of double concentrated A-medium and 20 volumes of A-medium were then added to restore the initial osmotic pressure. An aliquot containing ADP (250 µM final concentration), hexokinase and glucose-6-phosphate dehydrogenase (10 units each) was added to start the reaction.

Purification of the mVDAC2 mutant

The mVDAC2 mutant was isolated from mitochondrial membranes and purified according to standard methods (Mannella, 1982; Freitag et al., 1983). The final mitochondrial suspension was hypotonically shocked in 1 mM KCl, 1 mM HEPES, pH 7.5 to disrupt the mitochondrial membranes and release soluble proteins. The membranes were sedimented at 24,000 g for 20 min. The pellet was resuspended in a buffer consisting of 15% DMSO, 2.5% Triton X-100, 50 mM KCl, 10 mM Tris•Cl, 1mM EDTA, pH 7.0 and sedimented in a microcentrifuge at 14,000 rpm for 30 min. The supernatant was passed through a column containing a one to one mixture of hydroxyapatite/celite that, at low ionic strength, binds most proteins but allows VDAC to flow through. Samples of mutant VDAC were stored at -85°C for the future use.

Channel conductance measurements

Planar membranes were formed from monolayers made from a solution containing 0.5% of diphytanoylphosphatidylcholine, 0.5% of asolectin - soybean phospholipid (both from Avanti Polar Lipids, Inc., Alabaster, AL) and 0.1% cholesterol (Sigma, St. Louis, MO) in hexane. The two monolayers form a bilayer membrane across a 70-90 μm diameter aperture in a 15-μm thick Teflon partition that separates two chambers (modified Montal and Mueller technique, 1972). The total capacitance is typically 70-80 pF and the film capacitance is 30-35 pF. Aqueous solutions of 1.0 M or 0.10 M NaCl or KCl, 1 mM $MgCl_2$, 1 mM $CaCl_2$ were buffered with 5 mM HEPES at pH 7.0. All measurements were made at room temperature.

Channel insertion was achieved by adding of 0.2-2.0 μl of a 2.5% Triton X-100

solution of purified mVDAC2 mutant protein to the 2.5 ml aqueous phase in the "*cis*" compartment while stirring.

The membrane potential was maintained using Ag/AgCl electrodes with 3.0 M KCl, 15% agarose bridges assembled within standard 200 µl pipette tips (Bezrukov and Vodyanoy, 1993). The potential is defined as positive when it is greater on the side of protein addition (*cis*). The current was amplified by an Axopatch 200B amplifier (Axon Instruments, Inc., Foster City, CA) set to the voltage clamp mode.

The change in the conductance of mVDAC2 mutant protein upon addition of ATP was studied as previously described (Rostovtseva et al., 2002a). After single channel parameters were recorded, membrane-bathing solutions in both compartments were replaced by the same solutions containing ATP. The fresh, denser solution was added to the bottom of the chamber and the old solution was removed from the top. This procedure allows for the detection of the effect of nucleotide on the same channel.

Reversal potential measurements

The reversal or zero-current potential was measured to assess the selectivity in single or multi-channel membranes. The reversal potential of an ideally cation-selective membrane was found by measuring the reversal potential of a synthetic ion exchange membrane under identical conditions. Since the same electrodes and the same solutions were used to record reversal potentials for ideally cation-selective membranes and the VDAC-doped membranes, electrode asymmetries and liquid junction potentials influence both sets of measurements identically.

We used a 10-fold gradient of KCl, 1.0 M *cis* and 0.10 M *trans*, plus HEPES as

above, and a 4-fold gradient of disodium ATP salt (SigmaUltra; Sigma-Aldrich, St.Louis, MO) adjusted to pH 7.0 with NaOH. An aliquot of a solution containing the mVDAC2 mutant protein was added to the side with the higher concentration. Results are expressed as mean $\pm$ S.D.

Quantifying purified mVDAC2 protein

To compare the levels of expression of wild-type and mutant mVDAC2 we used standard SDS-page electrophoresis procedure (Laemmli, 1970). Both wild-type and mutant proteins were purified from the equal amounts of mitochondria (measured by total protein concentration). Following the addition of concentrated sample buffer, samples were separated on a 10% acrylamide gel supplemented with 4M urea and the bands stained with GelCode Blue stain (Pierce, Rockford, IL). Molecular weight standards were purchased from Invitrogen (BenchMark™ Protein Ladder, #10747-012, Carlsbad, CA). Densitometry was performed using the AlphaImager™2000 Documents&Analysis System and AlphaImager 3.2 software (both from Alpha Innotech Corporation, San Leandro, CA).

RESULTS

The initial purpose of this study was to obtain a voltage-independent mutant form of the mVDAC2 isoform that is constitutively impermeable to anionic metabolites. Five amino acid substitutions were engineered into mVDAC2: K19E, K31E, K60E, K95E, D227K (Fig.4.3, the folding pattern was generated by analogy with *Neurospora crassa*
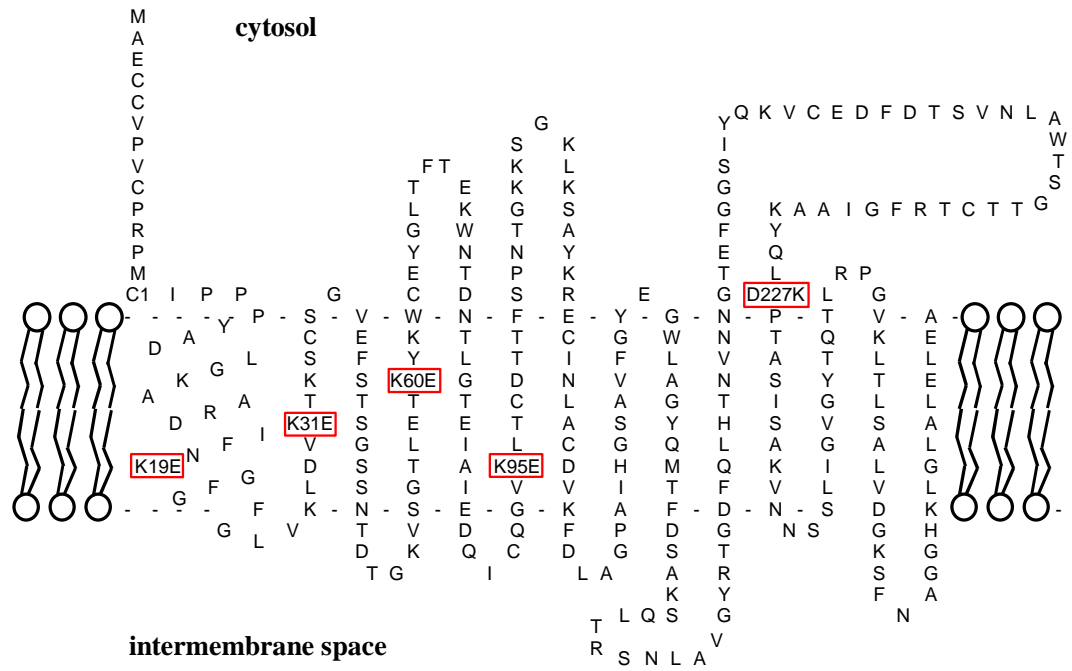
Figure 4.3. The folding pattern for mouse VDAC2 isoform. Boxes indicate points and type of mutation.

VDAC (Song et al., 1998a)). The rationale for choosing these residues is as follows. The first three mutations were designed to neutralize the voltage sensor that is responsible for VDAC's voltage gating. This should keep the channel in the open conformation but reduce the net positive charge in the channel responsible to favoring the flux of anions. This mutant molecule was expressed in a yeast strain lacking the endogenous VDAC1 gene *(Δpor1)*. The *Δpor1* strain is characterized by a temperature-dependent growth-restrictive phenotype when cultured on a nonfermentable carbon source such as glycerol; cells are able to grow at 30°C, but not 37°C (Blachly-Dyson et al., 1990). It has previously been observed that mouse VDACs expressed in the *Δpor1* background rescue this conditional phenotype, allowing for growth on glycerol at 37°C (Blacly-Dyson et al., 1993; Sampson et al., 1997). However, this mutated mVDAC2, when expressed in the *Δpor1* strain, failed to rescue the conditionally growth-restrictive phenotype at 37°C, although it demonstrated normal growth at 30°C (results not shown).

The properties of the mutant mVDAC2 protein resemble those of the closed state of VDAC

After isolation from yeast cells, the mouse VDAC2 mutant was tested for its ability to form channels in planar phospholipid membranes. Upon insertion, the mutant demonstrated a lower conductance (2.1 ± 0.1 (n=7) nS in 1 M KCl) than wild type mVDAC2 (3.8 nS; Xu et al., 1999) and was able to gate in that the channel could close to a very low conducting state but this closure did not depend on voltage (Fig. 4.2, panel A). Lack of voltage-dependent gating was clearly demonstrated by applying triangular voltage waves (Fig.4.4, panel B). The current-voltage relation showed rectification,
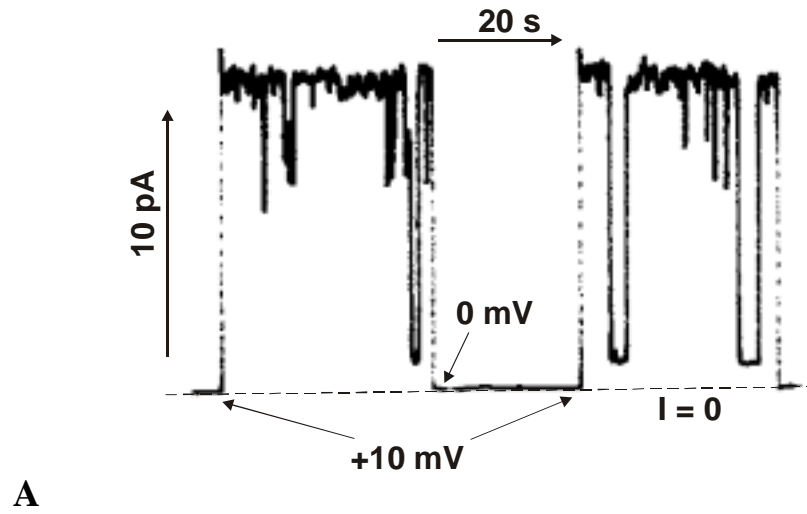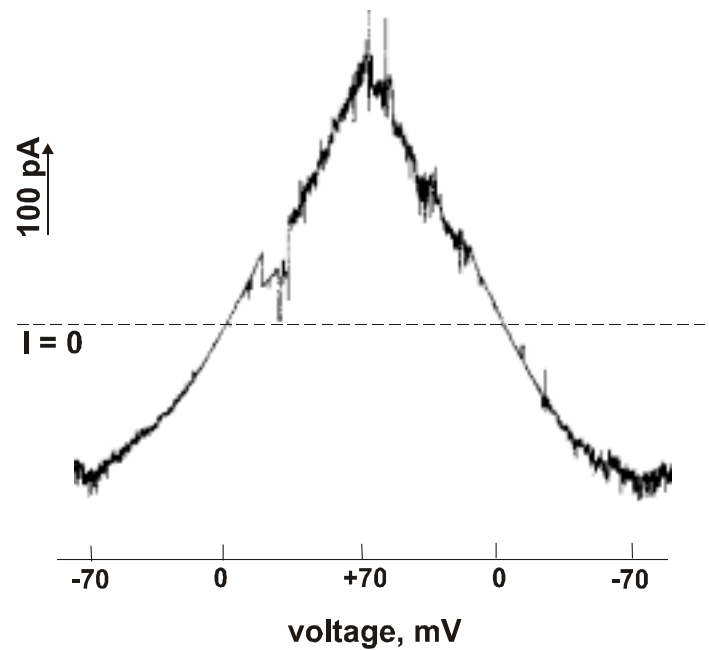
Figure 4.4. Changes in ionic current through a planar membrane in the presence of mouse VDAC2 mutant. (A) Insertion and gating of a single channel in 1.0 M NaCl. (B) Current through a few channels as a function of voltage in 1.0 M KCl (voltage was applied in the form of a triangular wave (3 mHz)). (C) Fast gating at low voltage in 1.0 M NaCl

+10 mV

-10 mV

I =0

0 mV

10 pA

1 min
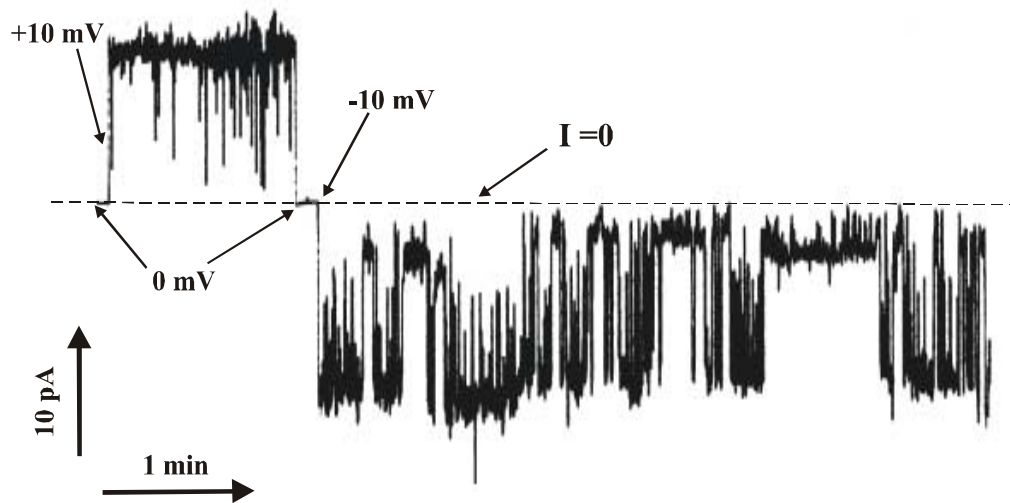
C

which would be expected if the charges introduced were not arranged symmetrically along the length of the channel. In addition, the mutant channel showed selectivity for small cations (K^+) over small anions (Cl^-). The reversal potential of $–24.3\pm 1.4$ (n=7) mV (on the high salt side) for a 10-fold salt gradient yields a permeability ratio, based on Goldman-Hodgkin-Katz theory, of 4.1:1 in favor of K^+. Also the mutant occasionally demonstrated fast gating at low voltage (Fig. 4.4, panel C). Most of these properties resemble the closed state of wild-type mVDAC.

The mutant mVDAC2 protein is permeable to ATP

Figure 4.5 shows a time course of the perfusion of the *cis* side with an ATP solution (81 mM final), followed by a drop in the channel conductance. The perfusion increases the conductivity of the medium. This change in the conductivity was best compensated for in experiments where ATP was added symmetrically. In these experiments the channel conductance dropped by about 20% relative to the medium conductivity (from 2.1 nS to 1.7 nS). This indicates that ATP interferes with the flow of small ions and thus enters the channel lumen. Interestingly, the addition of the same concentration of HPTS (1-hydroxypyrene –3,6,8-trisulfate), which is a synthetic molecule with similar size and charge as ATP that does not permeate through VDAC (Rostovtseva et al., 2002b), did not have any effect on the single channel conductance (data not shown).

Measurements of the channel selectivity in the presence of a sodium ATP salt gradient (200 mM vs 50 mM) supported our conclusion that the mutant is permeable to ATP. Membranes containing the mutant channel had a reversal potential of -20 ± 1 (n=4)
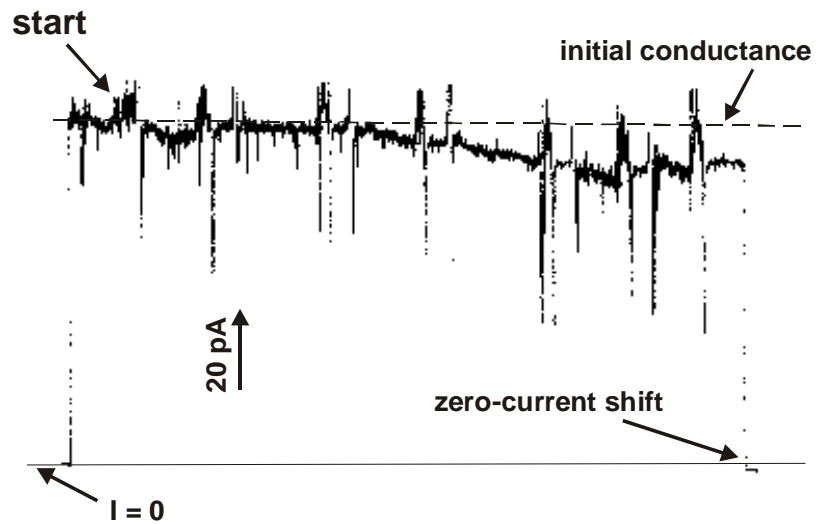
**Figure 4.5.** ATP addition (81 mM final) to one side of the membrane reduced the current flow through four mutant channels (in 1.0 M KCl). The noise was caused by six steps of manual perfusion. The imposed asymmetry causes a small shift of zero-current.
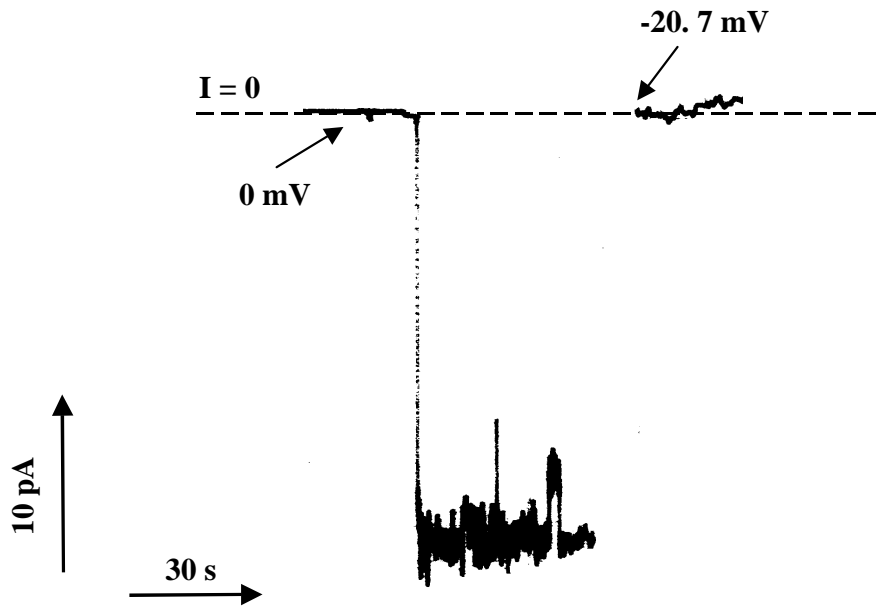
Figure 4. 6. In the presence of a 4-fold gradient of sodium ATP (200 mM vs 50 mM) mVDAC2 mutant demonstrated cationic selectivity. The voltage was applied to the high salt side.

mV (Fig. 4.6), but control experiments with a cation-selective membrane yielded a reversal potential of -26 ± 1 (n=4) mV. Combining these values with the current at zero voltage, we estimated the flux of ATP through the mutant channel as 3.3 x 10^6 ions/sec (see APPENDIX), and this is comparable with the value for the wild-type VDAC (Rostovtseva and Colombini, 1996).

Expression of mutant mVDAC2 permeabilizes the MOM to ATP and NADH

Figure 4.7 illustrates the rate of NADH oxidation by intact and osmotically shocked mitochondria when either mouse VDAC2 (panel A), the mutant (panel B) or no VDAC (ΔPOR1) (panel C) were expressed. In all cases the rate of NADH oxidation was higher when the outer membrane was damaged (Fig.4.7, insets), thus removing the barrier to flow. However, the difference in the rate of NADH oxidation varies, reflecting differences in permeability. Mitochondria containing wild-type mVDAC2 showed the smallest difference, indicating the highest permeability to NADH. The calculated permeability of mitochondria containing mutant mVDAC2 is almost 10-fold smaller than for those containing wild-type mVDAC2, but is still larger than the permeability of mitochondria lacking VDAC (Fig. 4.8). This relationship may reflect different expression levels for the mutant and wild-type mVDAC2.

In order to address this possibility we performed electrophoresis analysis after loading equal amounts of each protein. For correct normalization both the mutant and wild-type mVDAC2 proteins were purified from mitochondrial preparations containing an equal amount of total protein. Figure 4.9 demonstrates that the expression level of the mutant was almost half that of the wild-type mVDAC2. Densitometric quantitation of the

82

Figure 4.7. NADH oxidation by mitochondria isolated from yeast (lacking the yeast VDAC1 gene) expressing mouse VDAC2 (A), the mutant (B), or no VDAC (C). Oxidation by intact mitochondria is shown by open circles, oxidation by osmotically shocked mitochondria - by filled circles. The oxidation rate (inset) was calculated as described in methods. Concentrations of mitochondrial protein were 110 µg/ml (A), 70 µg/ml (B), and 300 µg/ml (C).

A. mouse VDAC2

B. mutant

C. ΔPOR1

NADH concentration, μM (y-axis)

time, min (x-axis)

Inset:
NADH oxidation rate (nmoles/min · mg protein) (y-axis)
NADH concentration, μM (x-axis)

85
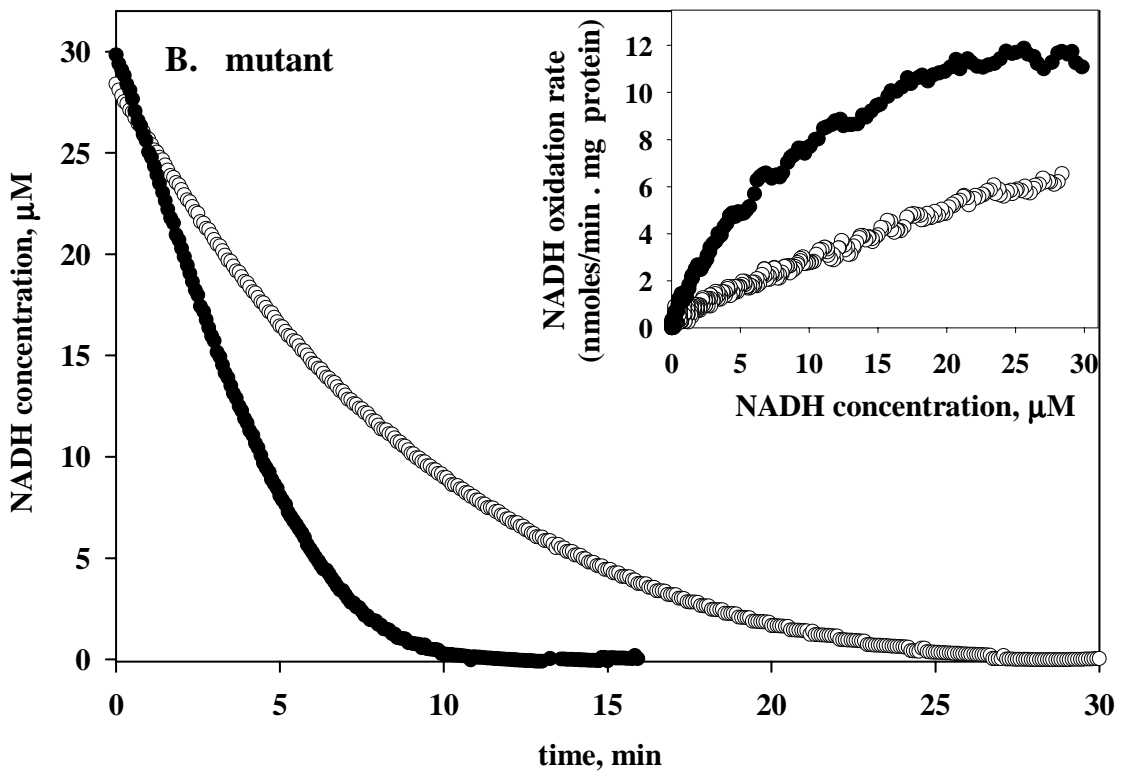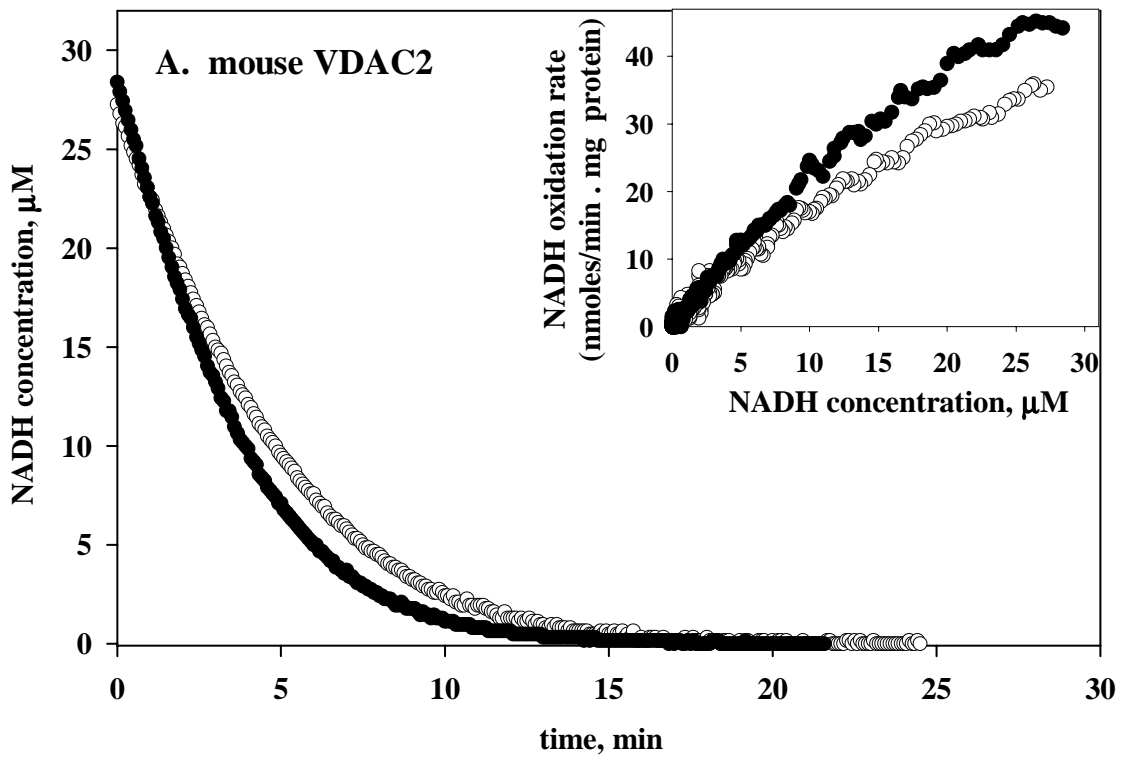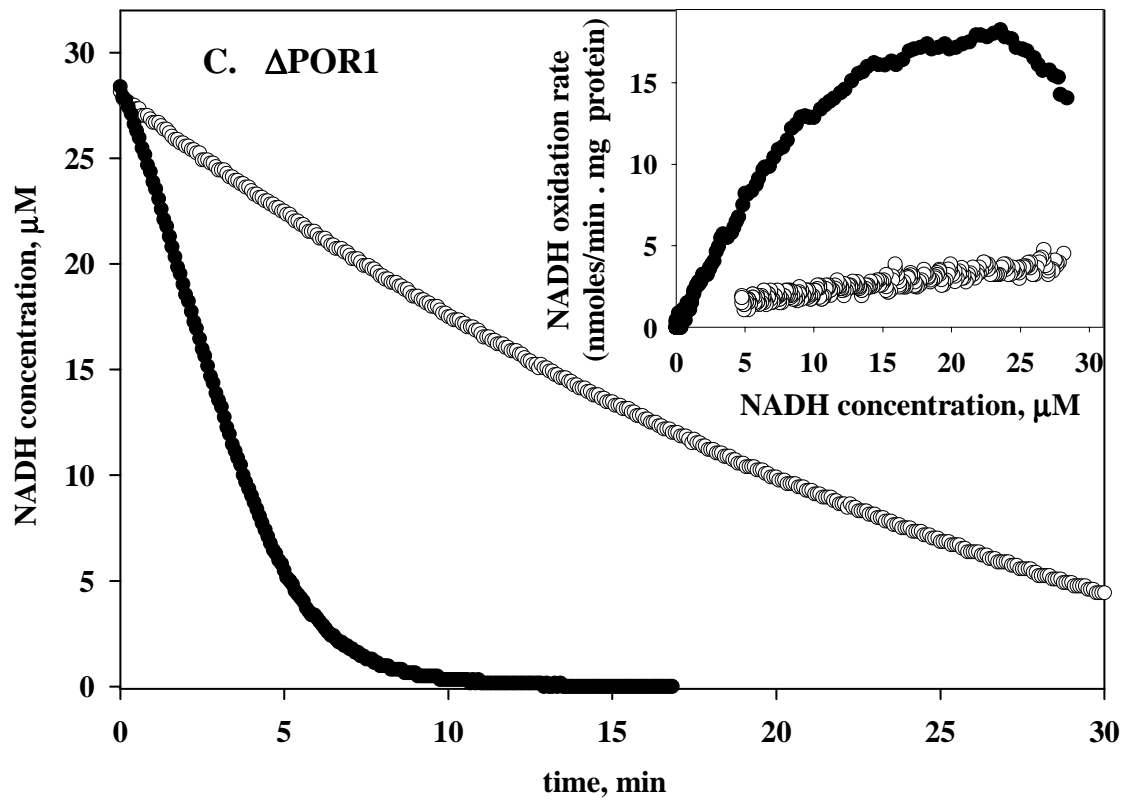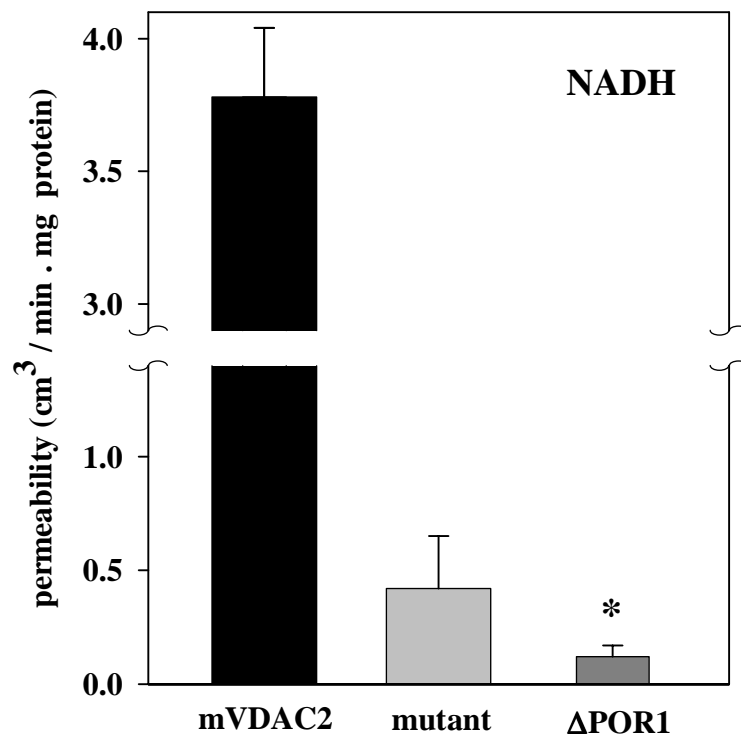
Figure 4.8. A comparison of the average permeability of the MOM to NADH in the
presence of mouse VDAC2, the mutant, or in the absence of VDAC (ΔPOR1). The
average and the standard deviation were calculated based on the results for different
batches of mitochondria (three for mouse VDAC2, five for the mutant and two for
ΔPOR1. The average permeability for each batch was obtained from three independent
measurements of NADH oxidation rate. Since the intactness of mitochondria was in the
range 78-86% the permeability was recalculated for 100% intactness.
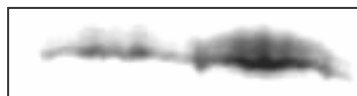
mutant   mVDAC2

Figure 4. 9. SDS-PAGE electrophoresis image of the mutant and mouse VDAC2. The proteins were run in 10% acrylamide gel and the bands were stained with Coomassie Blue stain. The proteins ran at 33 kDa.

bands and comparison with the known amount of protein standards revealed 2.3 μg of the mutant and 4.3 μg of wild-type mVDAC2 per band. Thus, yeast mitochondria with a total protein amount of 15 mg contain approximately 0.09 μg of the mutant or 0.17 μg of wild-type mVDAC2. Hence, after compensating for the protein content, the permeability of the mutant mVDAC2 to NADH is only 5 times smaller than that for wild-type mVDAC2.

The permeability to ADP/ATP was determined by measuring adenylate kinase activity. When wild-type mVDAC2 was expressed the difference in adenylate kinase activity between intact and shocked mitochondria was small (Fig. 4.10, panel A). This is consistent with almost free diffusion of ADP/ATP across the MOM of intact mitochondria. The difference was larger in the presence of the mutant mVDAC2 (Fig. 4.10, panel B), and much larger when no VDAC was expressed (Fig.4.10, panel C). High initial rates were due to an estimated 1% contamination of ATP in the ADP powder used for the preparation of solutions.

Figure 4.11 summarizes permeability values for all three samples. The permeability of the mutant mVDAC2 protein to ADP/ATP was half the permeability of wild-type mVDAC2. This could be explained simply by the difference in protein expression, as discussed above. Thus, we can conclude that the mutations reduced only the permeability to NADH whereas the permeability to ADP/ATP essentially does not change. This is in agreement with our estimation of ATP flux through the mutant mVDAC2 protein based upon planar membrane experiments.
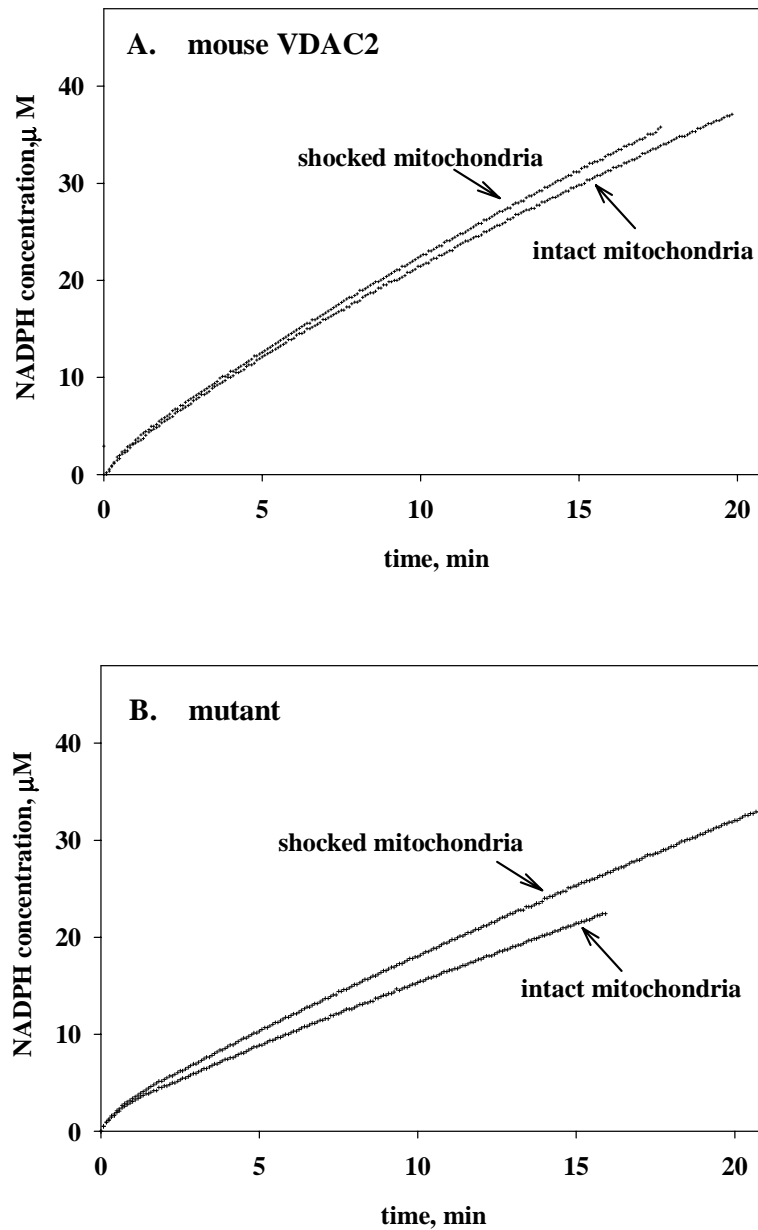
Figure 4.10. Adenylate kinase activity of mitochondria expressing mouse VDAC2 (A), the mutant (B), or no VDAC (C). Reaction was started with addition of 0.25 mM ADP and the NADPH concentration was measured (absorbance at 340 nm). Added enzymes were *Glucose-6-Phosphate Dehydrogenase* and *Hexokinase*. Concentrations of mitochondrial protein were 280 μg/ml (A), 288 μg/ml (B), and 250 μg/ml (C).

89

C. ΔPOR1

shocked mitochondria

intact mitochondria
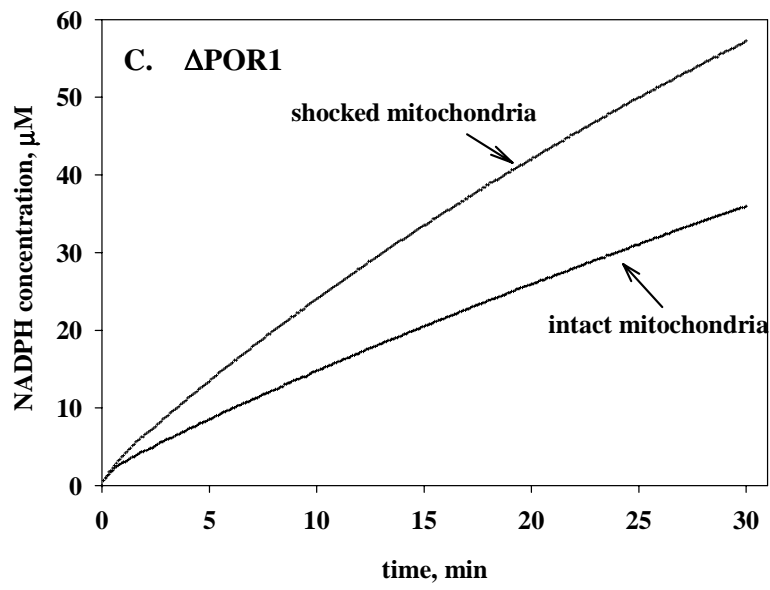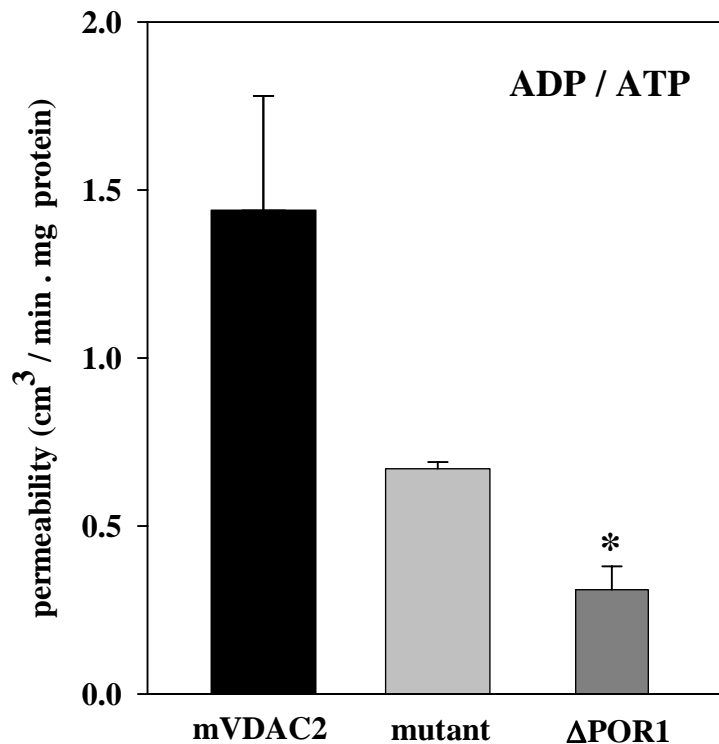
Figure 4.11. A comparison of the average permeability of the MOM to ADP/ATP in the presence of mouse VDAC2, the mutant, or in the absence of VDAC (ΔPOR1). The average and the standard deviation were calculated based on the results for different batches of mitochondria (two for each type of mitochondria). The average permeability for each batch was obtained from three independent measurements of NADPH reduction rate. Since the intactness of mitochondria was in the range 78-86% the permeability was recalculated for 100% intactness.

91

DISCUSSION

Large channels are traditionally considered as "molecular sieves" that differentiate between molecules based only on their size and charge. Typically they exhibit weak ionic selectivity that is presumed to be the result of general electrostatic interactions between a charged permeant and the channel wall. However, there are examples of high levels of selectivity in channels with a large pore diameter that is similar to the selectivity displayed by Na^+, K^+ or Cl^- channels. These examples include maltoporin (also referred as LamB), OmpF and VDAC. Maltoporin, which is involved in the transport of maltose (Szmelcman and Hofnung, 1975), was shown to favor maltooligosaccharide flux over the flux of other oligosaccharides (Luckey and Nikaido, 1980). This selectivity was found to be the result of a specific interaction between maltodextrins and the channel wall (Kullman et al., 2002). OmpF exhibits preferential flux for certain antibiotics like ampicillin and several other penicillins used to kill *E.coli*. However, it is not effective at transporting other "non-specific" antibiotics (Nestorovich et al., 2002). The specificity shown by VDAC for the permeation of large anions, as described in the introduction, provides an example of large, highly selective channels in eukaryotes.

The affinity of VDAC for metabolites might be closely related to its function as a regulator of metabolite flux between mitochondrial spaces and the cytosol. The existence of a specific binding site may play a crucial role in providing sufficient nucleotide translocation under conditions of high energy demand, when the rate of flux through VDAC becomes limiting (Gellerich and Kunz, 1987; Gellerich et al., 1993) and may have

an impact on cell survival. In this case, the binding site might accelerate the flow of crucial metabolites, particularly adenine nucleotides.

Physically, the role of the binding site on the channel wall can be understood by the model of Berezhkovskii and Bezrukov (2005). According to this model the binding site provides the potential well in which an optimal depth increases the probability of substrate translocation through the channel, while at the same time does not lead to significant occlusion of the pore. In other words, a capturing of the molecule entering the lumen of the channel by the potential well (i.e., binding site) allows it to "forget" which entrance it came from and hence the probability of successful translocation is increased.

Results of the current work support the existence of a VDAC binding site for ATP and other nucleotides. We were able to generate a mouse VDAC2 mutant for which the conductance properties resemble the closed state of the wild-type channel. Introduced mutations inactivated the voltage sensor (which resulted in the lack of the voltage-dependent gating) and changed the net charge of the channel lumen, i.e., the selectivity of the channel became cationic without regard for the applied voltage. In this situation we expected that the mutant channel would be permanently closed to metabolites, as has previously been shown for the closed state of VDAC. However, our observations indicate the opposite result. ATP flux through the channel is not influenced by the overall charge of the channel wall. This conclusion is clearly supported by experiments using VDAC incorporated into planar phospholipid membranes and, additionally, by measurements of metabolite flux across the intact MOM. These observations indicate that general electrostatic interactions between the permeant and the channel do not play a crucial role in the transport of ATP through VDAC. There must be additional interactions that

facilitate ATP translocation despite an unfavorable electrostatic environment. The binding site for purine-containing nucleotides is the best candidate for this role.

Interestingly, despite the low primary sequence homology between VDAC isoforms from different species there is remarkable conservation of charged residues at specific positions (Song and Colombini, 1996). It would appear that substitution of these with amino acids of similar charge (e.g., lysine for arginine) is not well tolerated. Thus, the distribution of key charged and polar residues has been selected during evolution to provide a better mechanism for metabolite translocation.

Identification of the VDAC binding site requires further investigation. However, our current work clearly demonstrates that ATP flux through VDAC is not determined by overall charge within the pore but by specific, localized interactive sites where the interaction with VDAC overrides net charge density within the channel. Yet to achieve fast translocation the strength of the overall interaction must be tuned to a precise level. Clearly, large channels are not "general diffusion pores" but show a specificity that is dependent on an intimate interaction between the permeant and the channel wall.

APPENDIX

We estimated ATP flux using the current at zero voltage (V=0) and the permeability ratio

(P_{ATP} / P_{Na}). The permeability ratio was determined using the Nernst-Planck flux

equation. This theory assumes electrical neutrality in the permeability pathway.

The formulas for the total current and for individual ion fluxes are:

$$I = z_+ F \, \phi_+ + z_- F \, \phi_- \qquad\qquad (1)$$

$$\phi_- = -P_- a_- \left(RT \frac{1}{a_-} \frac{da}{dx} + z_- F \frac{dV}{dx}\right) \qquad (2)$$

$$\phi_+ = -P_+ a_+ \left(RT \frac{1}{a_+} \frac{da}{dx} + z_+ F \frac{dV}{dx}\right) \qquad (3)$$

where ϕ is the flux, P is the permeability, a is the ion activity, z is the valence.

Using these formulas we obtain the flux of ATP at zero voltage:

$$\phi_{ATP} = \frac{I_{(V=0)}}{|z| F (P_{Na} / P_{ATP} - 1)} \qquad (4)$$

where z is the effective valence of ATP in the solution.

In order to get the permeability ratio from the measured reversal potential we used an

equation from *Gincel et al. (2001):*

$$\sum_i z_i^2 P_i \frac{\{[a]_{cis} - [a]_{trans} B^{z_i}\}}{1 - B^{z_i}} = 0 \qquad (5)$$

where a is the ion activity and $B = e^{(F/RT)Vrev}$.

In the case of sodium ATP salt equation (5) gives us:

$$\frac{P_{ATP}}{P_{Na}} = \frac{1 - B^z}{z^2(B-1)} \quad \{\frac{[Na]_{cis} - [Na]_{trans} B}{[ATP]_{cis} - [ATP]_{trans} B^z}\} \quad (6)$$

The effective valence of ATP (z) was taken from *Rostovtseva et al. (2002b),* and is equal to -1.4.

Activity ratios for ATP and Na were calculated using the Nernst equation. For this purpose the values of reversal potential were measured separately in the presence of ideally selective cation and anion membranes.

The final values are: $P_{Na} / P_{ATP} = 17$

$$\phi_{ATP} = 3.3 \times 10^6 \text{ ions/sec.}$$

CHAPTER 5

Asymmetry in Meningococcal PorA/C1 Channel: Direction-Dependent Insertion and Reversal Potential

Javier Cervera[1], Alexander G. Komarov[2], Vicente M. Aguilella [1],

and Marco Colombini[2]

[1]Universitat Jaume I, Dept. Ciencias Experimentales, Castellón, Spain;

[2]University of Maryland, Department of Biology, College Park, MD

Running title: ***Reversal potential in PorA/C1 channel***

ABSTRACT

Class 1 porins (PorA/C1) from *Neisseria meningitidis* combine high selectivity and high conductance. The porin has an estimated length of 5 nm, with a negatively charged narrow filter near one of the pore entrances. The results of our theoretical calculations based on a continuum PNP model agree with a previously proposed structure. The measured reversal potential values depend strongly on the orientation of the channel relative to the ion gradient. The rate at which ions enter the filter becomes the limiting step for ionic transport through the channel. The asymmetry can then be explained if the amount of ions entering the filter in the direction of low current is limited by the neutral part of the pore (a structure spanning 4 nm in length and 2 nm in diameter). We also found that the orientation of channel insertion is biased by the direction of an applied salt gradient. The selectivity filter side preferentially ends up facing the low concentration side. Attempts to insert channel in the opposite direction eventually caused a large conformational change of the channel.

INTRODUCTION

Class 1 porin (PorA/C1) from *Neisseria meningitidis* is a large channel, which has both high selectivity and high conductance (Jeanteur et al., 1991; Song et al., 1999). In contrast to other porins, PorA/C1 does not exhibit voltage gating. However it is highly selective (24:1 Na^+ over Cl^- in a two-fold NaCl gradient). When incorporated in planar phospholipid membranes in the presence of 200 mM NaCl salt, pure PorA/C1 demonstrates a single trimer conductance of 0.97 nS (Song et al., 1999). Also, PorA/C1 shows strong rectification, so that reversing the voltage polarity causes a four-fold difference in ion current.

These observations could be explained by the existence of an asymmetrical structure with a highly charged selectivity filter on one end of the channel. The model, proposed by the extrapolation from the known structure of homologous porins (Song et al., 1999), suggests approximately nine negative charges in the narrow constricted region (~1.4 nm in diameter) close to the entrance of the channel. The length of the selectivity filter is supposed to be close to 1 nm (compared to 5 nm of the total channel length). According to this model a high selectivity and high conductance are achieved at the same time by maintaining a high concentration of mobile counterions in the highly negatively-charged constricted region. The consequence of the high concentration of mobile counterions is that if the channel conductance is limited not by the filter itself but by the ability of ions to reach the filter, i.e., the access resistance.

In this paper we confirm the proposed model by theoretical considerations based on applying the Poisson-Nernst-Planck (PNP) formalism to the inferred geometry of the channel.

MATERIALS AND METHODS

Channel reconstitution and reversal potential measurements

The reversal potential or zero-current potential was measured to assess the selectivity in single or multi-channel membranes using different concentrations of NaCl aqueous solutions. Usually it was 0.10 M on one side of the membrane and varying concentrations on the other side (0.050, 0.20, 0.30, 0.40M, etc.) Planar membranes were formed from monolayers made from a solution containing 1% of diphytanoylphosphatidylcholine (Avanti Polar Lipids, Inc., Alabaster, AL) in hexane. The two monolayers form a bilayer membrane across a 70-90 µm diameter aperture in a 15-µm thick Teflon partition that separates two chambers (modified Montal and Mueller technique, 1972). The meningococcal PorA/C1 protein was provided by Dr.Milan Blake. Channel insertion was achieved by adding of 0.1 µl aliquot a 1% Triton X-100 solution of purified PorA/C1 to the 2.5 ml aqueous phase in one of the compartments while stirring.

The membrane potential was maintained using Ag/AgCl electrodes with 3.0 M KCl, 15% agarose bridges assembled within standard 200 µl pipette tips (Bezrukov and Vodyanoy, 1993). Potential is defined as positive when it is greater in the side of protein addition (*cis*). The current was amplified by an Axopatch 200B amplifier (Axon Instruments, Inc., Foster City, CA) in the voltage clamp mode.

All measurements were made at room temperature.

THEORETICAL MODEL

The theoretical model is aimed at describing the transport properties of Meningococcal PorA/C1 of *Neisseria meningitidis.* It is based on the Poisson-Nernst-Planck (PNP) formalism and on the porin *inferred* geometry and charge residues distribution (Song et al., 1999).

The PNP formalism is a so-called continuum approach (Schuss et al., 2001). It models the ionic species by their concentration c, which is a continuum function defined at every point $\vec{r}$ of the system. The solvent is treated as a structureless dielectric medium where the ions move. Often its effect on the ionic transport is reduced to the dielectric permittivity ε which controls the strength of the electrostatic coupling (see Poisson equation below). The PNP formalism was first used to model the properties of macroscopic electrolyte solutions (Onsager, 1926; Onsager, 1927). Its use to model the properties of ion channels is controversial due to the size of these systems. For instance, the formalism is found to overestimate the screening of the fixed and induced charges (Corry et al., 2000). Despite its drawbacks, however, it has proved reliable in wide pores (radius 1 nm) whose properties are mainly determined by long-range electrostatic interactions (Kurnikova et al., 1999; Cardenas et al., 2000; Hollerbach et al., 2000,2002; Hille, 2001; Im and Roux, 2002; Koumanov et al., 2003; Mamonov et al., 2003).

In the PNP approach, the flux density of ionic species i is described by the Nernst-Planck equation (NPE) (Hille, 2001)

$$\vec{j}_i = -\frac{D_i c_i}{RT} \nabla \left(RT \ln a_i + z_i F \phi \right), \qquad i = \pm \tag{1}$$

where D_i, c_i, a_i, z_i are the diffusion coefficient, concentration, activity and charge of species i, respectively, ϕ is the electric potential, R is the gas constant, T is the temperature and F is the Faraday constant. The NPE has two terms. The first one accounts for the flux due to the gradient of the chemical potential of the species $\mu_i = \mu_i^o + RT \ln a_i$. Ions move toward the regions of lower chemical potential . This is more clearly seen in the ideal case, where the activity equals the ionic concentration. In this case ions tend to move down the concentration gradient. In other words, an ion flux arises to equilibrate the system. The second term of the NPE is the migration term, due to the electrostatic force exerted on the ions. It depends on the gradient of the electric potential $\nabla \phi$ and on the charge number of the ionic species z_i. Cationic species ($z_i > 0$) tend to go toward regions of lower electric potential whereas anionic species ($z_i < 0$) go to regions of higher electric potential.

We consider that the system has reached the steady-state regime. In this condition, the continuity equation implies that

$$\nabla \vec{j}_i = 0, \ i = \pm \qquad (2)$$

Eq. 2 imposes that the flux of every ionic species i through any cross section of the ion channel is constant and also that the system no longer depends on time.

The behavior of the system is controlled by the long-range electrostatic interactions. This is described by the Poisson equation (Hille, 2001)

$$\nabla^2 \phi = -\frac{F}{\varepsilon}(c_+ - c_-) \qquad (3)$$

where ε is the dielectric permittivity of the solution, assumed to be constant throughout the system. Eqs. 1-3 are coupled. They need to be solved simultaneously for the electric potential and ionic concentrations in a self-consistent way.

We further assume that the whole system is held at constant temperature T. Also, that the aqueous boundaries outside the porin are perfectly stirred and that no convection process is relevant.

A possible structure of the class 1 porin PorA/C1 from *Neisseria meningitidis* has already been proposed (Song et al., 1999). The authors inferred the geometry and charged residues distribution from homologous porins. The porin has a total length $L = 5$ nm and a radius $R = 1$ nm. The filter is on one of its sides and has a length $L_f = 1.25$ nm and a radius $R_f = 0.7$ nm. It contains nine *negatively* charged residues. From the point of view of the theoretical model, the porin structure and charged residues distribution sets the calculation domain and boundary conditions for the system, which are shown in Fig. 5.1. In the calculation we take into account the area of the porin inaccessible to the ions due to their size (Koumanov et al., 2003). This is done by modifying the structure by the exclusion of the Na$^+$ radius. The experiments were done with NaCl as electrolyte. The Na$^+$ ion has a charge of opposite sign to that of the negative residues and it is likely to be close to the porin walls. The charge residues themselves are modeled as a (negative) surface charge density σ smeared on the filter walls.

The boundary conditions of Eqs. 1 and 3 are determined by the porin structure and fixed charge distribution. In the bulk region, far from the porin entrances, the electrolyte concentration and electric potential are those of the external solutions (see Fig.5.1)
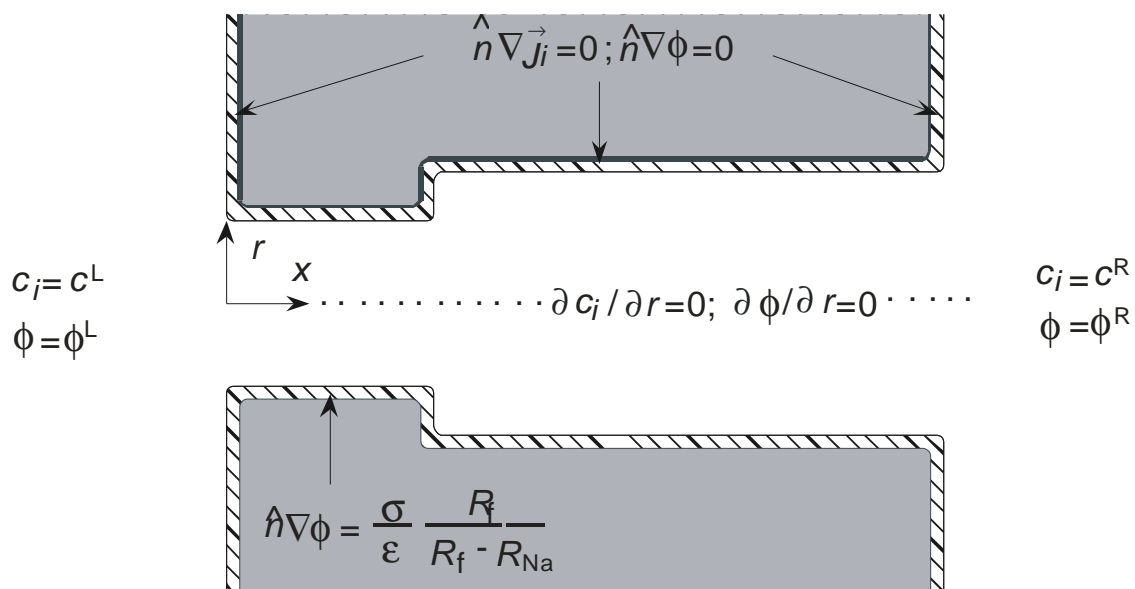
Figure 5.1. Channel geometry used in the calculations. The inferred geometry (Song et al., 1999) is modified by the exclusion of the Na^+ radius (hatched region). The coordinate axis and the boundary conditions are shown.

$$c_i = c_i^{\text{L}}, \phi = \phi^{\text{L}}, \text{ left external solution} \tag{4a}$$

$$c_i = c_i^{\text{R}}, \phi = \phi^{\text{R}}, \text{ right external solution} \tag{4b}$$

The domain remains the same in all calculations. Depending on the porin orientation, the "left" solution corresponds to the *cis* compartment and the "right" solution to the *trans* compartment, or the other way around.

The porin walls are impenetrable to the ions. Therefore, the ion flux directed toward the walls must be zero

$$\hat{n}\nabla\vec{j}_i = 0, \text{ porin walls} \tag{4c}$$

where $\hat{n}$ is the normal vector of the surface porin wall.

No electric field is allowed in the lipid region. This implies that a low dielectric permittivity is assumed in this region. The boundary conditions for the electric potential are then

$$\hat{n}\nabla\phi = 0, \text{ porin walls} \tag{4d}$$

except for the filter walls where Gauss law implies that

$$\hat{n}\nabla\phi = \frac{\sigma}{\varepsilon}\left(\frac{R_{\text{f}}}{R_{\text{f}} - R_{\text{Na}}}\right), \text{ filter walls} \tag{4e}$$

Note that the Gauss law is modified by a factor $R_{\text{f}}/(R_{\text{f}} - R_{\text{Na}})$, where R_{Na} is the Na$^+$ radius, to preserve electroneutrality in the porin cross section (Sims et al., 1993).

Finally, the system is supposed to have cylindrical symmetry, which gives two more boundary conditions

$$\frac{\partial c_i}{\partial r} = 0 \text{, symmetry axis } (r = 0) \tag{4f}$$

$$\frac{\partial \phi}{\partial r} = 0 \text{, symmetry axis } (r = 0) \tag{4g}$$

Eqs. 1-3, subject to the boundary conditions (Eqs. 4), form the system of transport equations we need to solve. To compare with the experiment, the electric current that crosses the porin is calculated

$$I = F(J_+ - J_-) \tag{5}$$

where J_+ and J_- correspond to the fluxes of Na^+ and Cl^- that go through the channel. The latter can be calculated from

$$J_i = 2\pi \int_0^R j_{i,x} r \, dr, \ i = \pm \tag{6}$$

where $j_{i,x}$ is the axial component of the flux density of species i. We have chosen as the integration surface the cross section at the neutral part of the porin but the integration can be done in every cross section.

RESULTS AND DISCUSSION

In the following calculations, the temperature of the system is chosen to be $T = 293 \text{ K}$ and the dielectric permittivity $\varepsilon = 80\varepsilon_0$, where ε_0 is the permittivity of the vacuum. The value of σ is set such that the total charge on the filter equals to nine deprotonated charge residues

$$\sigma = -\frac{9e}{2\pi R_f L_f} \tag{7}$$

where e is the proton charge. For the ionic activity, the mean activity coefficient has been used for both types of ions, $a_+ = a_- = \sqrt{a_+ a_-}$. For the sake of simplicity, a linear fit of the experimental NaCl activity

$$\ln a_i = B \ln c_i + C \tag{8}$$

where $B = 0.9613$ and $C = -0.3114\,\mathrm{M}$, has been used. The error in the fitting is around 10% for high concentration values $c \sim 2\,\mathrm{M}$ (less than 3% for $c < 0.1\,\mathrm{M}$). These values should be compared with the error when it is assumed $a_i = c_i$ (30% for $c \sim 0.1\,\mathrm{M}$ and 50% when $c \sim 2\,\mathrm{M}$). Using Eq. 8, the NPE can be written as

$$\vec{j}_i = -D_i \left(B\nabla c_i + \frac{z_i c_i F}{RT} \nabla\phi \right), \ i = \pm \tag{9}$$

The diffusion coefficients have been used as fitting parameters. In the fitting process we have started with their values at infinite dilution:

$$D_+^0 = 1.33\times10^{-5}\,\mathrm{cm^2/s} \text{ and } D_-^0 = 2.03\times10^{-5}\,\mathrm{cm^2/s}$$

and we have modified them to fit the experimental results.

The system of equations is solved numerically using the Finite Element Method (Lucquin and Pironneau, 1998). To facilitate the calculation, all variables are cast into dimensionless variables:

$$\rho \equiv \frac{r}{L_0} \qquad \chi \equiv \frac{x}{L_0} \qquad C_i \equiv \frac{c_i}{c_0} \qquad \psi \equiv \frac{F\phi}{RT}$$

$$L_D \equiv \sqrt{\frac{\varepsilon RT}{F^2 c_0}} \quad \vec{\zeta}_i \equiv \frac{L_0}{D_+^0 c_0}\vec{j} \quad \sigma^* \equiv \frac{FL_0\sigma}{\varepsilon RT}\left(\frac{R_f}{R_f - R_{Na}}\right) \tag{10}$$

where L_0 is the length scaling factor (of the order of the porin radius) and L_D is the

Debye length. The transport equations in these variables are

$$\frac{1}{\rho}\frac{\partial}{\partial\rho}\left[\rho\left(B\frac{\partial C_i}{\partial\rho}+z_iC_i\frac{\partial\psi}{\partial\rho}\right)\right]+\frac{\partial}{\partial\chi}\left(B\frac{\partial C_i}{\partial\chi}+z_iC_i\frac{\partial\psi}{\partial\chi}\right)=0; i=\pm \tag{11a}$$

$$\frac{1}{\rho}\frac{\partial}{\partial\rho}\left(\rho\frac{\partial\psi}{\partial\rho}\right)+\frac{\partial^2\psi}{\partial\chi^2}=-\left(\frac{L_0}{L_D}\right)^2(C_+ - C_-) \tag{11b}$$

subject to the boundary conditions

$$C_i = C_i^{\mathrm{L}}, \psi = \psi^{\mathrm{L}}, \text{ left external solution} \tag{12a}$$

$$C_i = C_i^{\mathrm{R}}, \psi = \psi^{\mathrm{R}}, \text{ right external solution} \tag{12b}$$

$$\hat{n}\nabla\vec{\zeta}_i = 0; \hat{n}\nabla\psi = 0, \text{ porin walls (not filter)} \tag{12c}$$

$$\hat{n}\nabla\vec{\zeta}_i = 0; \hat{n}\nabla\psi = \sigma^*, \text{ filter walls} \tag{12d}$$

$$\frac{\partial C_i}{\partial\rho} = 0; \frac{\partial\psi}{\partial\rho} = 0, \text{ symmetry axis } (\rho = 0) \tag{12e}$$

Current-voltage curve

Fig.5.2 shows the one monomer current-voltage curve for a symmetric saline

concentration of 0.2 M in *cis* and *trans* compartments. The symbols represent the

experimental values (Song et al., 1999) while the solid line is the fitting using the

theoretical model. A very good agreement between the experiment and the theoretical

model is found. The diffusion coefficients take the values $D_+ = 0.5D_+^0$ and $D_- = 0.5D_-^0$,
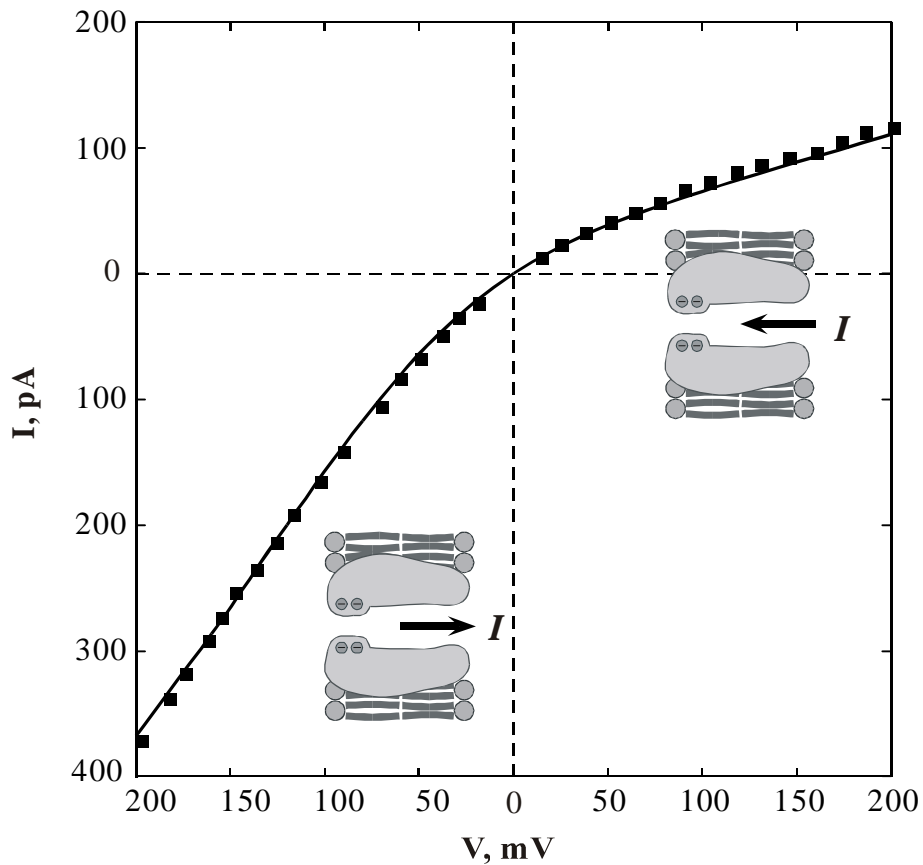
Figure 5.2. Monomer current-voltage curve for a symmetric electrolyte concentrations of 0.20 M. The symbols represent the experimental values (Song et al., 1999) and the solid line the prediction of the theoretical model . The only fitting parameters are the diffusion coefficients which take the values of half the infinite dilution values.

which represents a decrease in the current of the 50 %. This is consistent with previous studies on the OmpF and α-hemolysin channels (Im et al., 2002; Noskov et al., 2004), which show that the PNP approach overstimates the current by 30%-50% when compared to the experimental values and to those obtained using a combination of Grand Canonical Montecarlo and Brownian Dynamics (GCMC/BD) algorithm. It is attributed to the lack of ion-ion interaction in the PNP approach, which reduces the effective diffusion coefficient. In our case this is partially accounted for by using the mean activity instead of the concentration in the chemical potential. The discrepancy should be ascribed to ion-ion interaction not accounted for by the mean activity as well as to the decrease of the diffusion coefficients due to the ion confinement in the porin structure. Since both diffusion coefficients are modified by the same amount, this means that the channel selectivity can be described considering only the long-range electrostatic forces exerted by the charged residues on the ions.

The porin is very asymmetric. This is clearly observed in the rectification the current-voltage curve exhibits. The charge residues at the filter walls lead to an increase of the average electrolyte concentration in the vicinity of the filter to preserve electroneutrality. The current-voltage rectification curve can be explained by the accumulation of the cations near the filter. In the low conducting polarity (negative transmembrane potential), the Na^+ ions, responsible for most of the current since the channel is cation selective, need to cross the neutral part of the porin before they reach the filter (see Fig. 5.2). This limits the supply of Na^+ ions that arrive at the filter compared to the high conducting polarity, where the filter faces the solution directly. The

cationic accumulation near the filter is therefore higher in the second case, which leads to a higher current.

Another feature that can be observed in the current-voltage curve is the qualitatively different shape of the curve in the high and low conductance polarities. While in the high conductance polarity the curve is superlinear (the current increases faster than the applied potential), in the low conductance polarity the curve is sublinear. An explanation can be attempted if we consider the effect the electric field has on the ions in the vicinity of the filter. In both cases, the applied electric field acts accumulating cations in the region close to the filter with a higher potential and depleting them in the opposite side. In the low conductance polarity, this means accumulating cations in the neutral part of the pore and depleting them in the solution facing the filter. Therefore, the depletion is more effective than the accumulation since the latter is restricted by the neutral part of the porin. As a result, the increase in the number of mobile charges near the filter, and then of the current, is sublinear with the applied electric potential difference. However, in the high conductance polarity, the direction of the current is reversed. The cation accumulation occurs in the solution facing the filter and its depletion in the neutral part of the pore. In this case what is more effective is the accumulation of cations. As a consequence, the increase in the number of charged carriers is superlinear with the electric potential difference.

Reversal potential

The fitted values of the diffusion coefficients are reasonable. However, the use of the diffusion coefficients as fitting parameters makes the model quite flexible to fit the

111

experimental current-voltage curve. This means that this fitting as per se is not enough to indicate that the model correctly describes the transport properties of the system. For this reason, the theoretical model was applied to calculate the reversal potential $\Delta\phi_{rev}$ values of the porin. Table 5.1 shows the comparison between the experimental reversal potential values (Song et al., 1999) and those given by the theoretical model. As can be seen, there is a good agreement between the theoretical and experimental values. We have used the diffusion coefficients obtained when fitting the current-voltage curve, although the result would be the same with the infinite dilution values. The model also predicts adequately the change of reversal potential with the absolute values of the electrolyte concentrations for the same *cis | trans* ratio.

Upon considering the agreement obtained between the model and the experimental values up to this point, the model is used to calculate the reversal potential for other combinations of the *cis | trans* concentrations.

Figure 5.3 shows the reversal potential as a function of the concentration ratio c_{cis}/c_{trans} for a fixed low electrolyte concentration of 0.10 M. The solid lines are the model prediction and the symbols are the experimental measurements. Since the porin exhibits a large asymmetry, the reversal potential is calculated for the two possible orientations of the porin in the lipid bilayer: with the filter facing the *trans* side (upper curve) and with the filter facing the *cis* side (lower curve). The figure shows how the asymmetry in the charge distribution of the porin induces an asymmetry in the reversal potential. This type of asymmetry has also been observed in the OmpF porin (Alcaraz et al., 2004). As can be seen, the theoretical upper curve fits the experimental values. As for the lower curve, it agrees with the values obtained so far. Collecting the experimental

112

Table 5.1. Experimental (Song et al., 1999) and theoretical values of the reversal

potential of PorA/C1 for two different gradients of NaCl

| *cis | trans*	Experimental	Theoretical Model
0.1 M | 0.2 M	-15.1 ± 0.3 mV (n=11)	-15.2 mV
0.5 M | 1.0 M	-11.6 ± 0.3 mV (n=3)	-10.2 mV
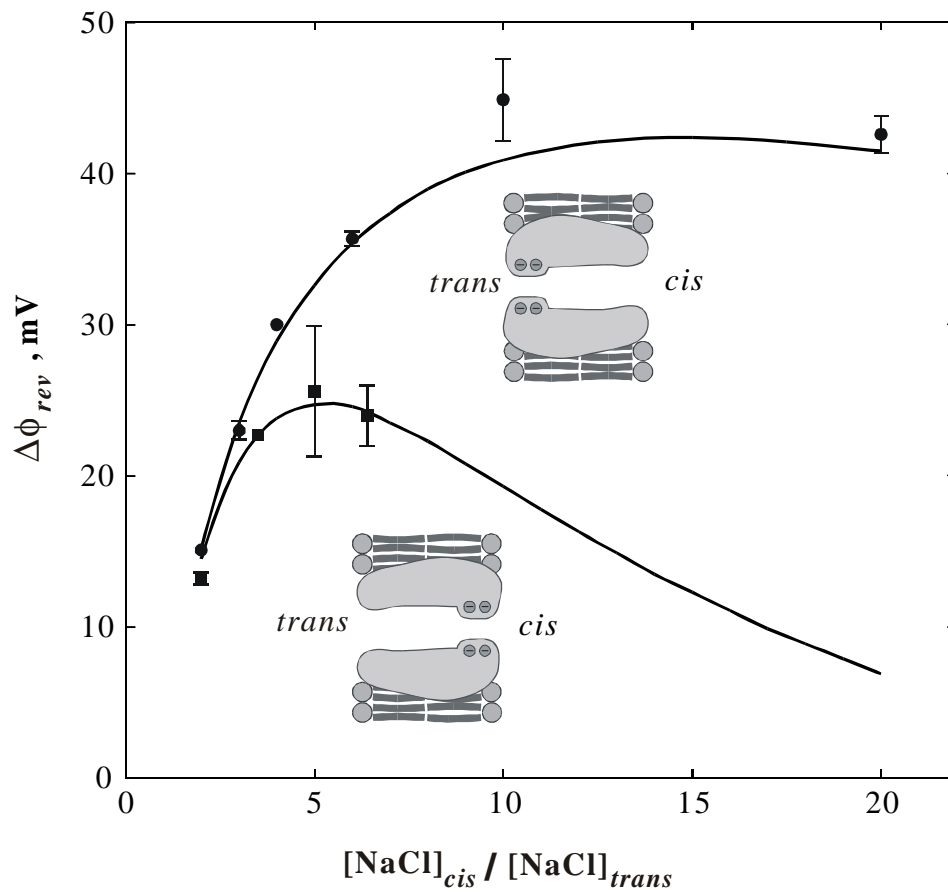
Figure 5.3. Experimental (symbols) and model prediction (solid lines) of the reversal potential as a function of the *cis | trans* concentration ratio for a fixed low electrolyte concentration of 0.10 M. Each symbol represents at least 3 experiments.

data for the lower curve we have encountered problems which will be described and discussed in the next section. Completion of the lower curve will allow us to determine if the theoretical model also applies to this case. This is the region where we anticipate more problems for the model since it involves heavy screening of the charged residues and PNP models tend to overestimate it (Corry et al., 2000).

The reversal potential curves can be explained again by the asymmetric distribution of charged residues. The reversal potential arises from the different ability of the different types of ions to cross the porin. Since the charge residues are negative, the electrostatic repulsion tends to exclude Cl^- ions from the porin making the porin cation selective. To achieve $I = 0$, a positive electric potential is applied to the *trans side* (the compartment of smaller electrolyte concentration). This field hinders the movement of the Na^+ ions and facilitate that of the Cl^- ions making $J_+ = J_-$ and therefore the current null (see Eq. 5).

Reversal potential is a measure of the selectivity of the porin. An overall increase of the electrolyte concentration results in a larger screening of the charged residues. This allows a larger number of Cl^- ions to enter the porin, which causes a decrease in the reversal potential. In the case considered in Fig.5.3, the electrolyte concentration is increased only in the *cis* side while it is kept constant in the *trans* side. We have then two combined effects which act in opposite ways on the reversal potential. On one hand, the increase of the concentration ratio results in a higher net ionic flux and therefore tends to increase the reversal potential. On the other hand, the increased concentration of the electrolyte solution is more effective at screening the charged residues of the filter and thus the porin should becomes less selective and the reversal potential decreases. The

115

behavior of the reversal potential at a given concentration ratio c_{cis}/c_{trans} depends on which of the two effects dominates. In the upper curve of Fig. 5.3 we can see that the first effect dominates for low values of c_{cis}/c_{trans}, the reversal potential increases with the concentration ratio. As c_{cis}/c_{trans} becomes higher, the better screening due to the increase of c_{cis} eventually stops the increase of $\Delta\phi_{rev}$ and flattens the curve. In the lower curve of the same figure, the two competing effects can be seen more clearly. As in the upper curve, for low c_{cis}/c_{trans} it increases with the concentration ratio. It then reaches a maximum around $c_{cis}/c_{trans}=5$, and it decreases when the screening of the filter residues dominates.

The difference between the two curves can be explained by the position of the filter. It was mentioned above that the neutral part of the porin limits the amount of ions that can reach the filter from the solution opposite to it. In both curves, the electrolyte concentration is higher on the *cis* side. In the upper curve, the filter faces the *trans* side. This means that the effect of the increase of c_{cis} in the screening of the filter is limited by the neutral part of the porin. This limitation does not exist in the lower curve where the filter faces the *cis* side. As a result the screening of the filter charged residues is not so effective in the upper curve and the increase of the concentration ratio dominates over a wider interval of c_{cis}/c_{trans}.

Direction of the channel insertion

As theory predicts, for each salt gradient we should expect two different values for the reversal potential depending on the orientation of the channel insertion. When the

selectivity filter faces the high salt solution (*cis* side) the reversal potential should be lower than for the opposite orientation because of more effective screening in high salt. Published results (Song et al., 1999) reported a preferential orientation of PorA/C1 insertion with the selectivity filter on the side opposite to the side of protein addition. However, those results were obtained in the absence of a salt gradient. In the presence of a NaCl gradient the values of the reversal potential which we measured upon insertion of PorA/C1 either from the high or from the low salt side were essentially the same (Fig.5.4).

These results could be explained in two ways. First, contrary to theoretical expectations, the values of the reversal potential, for the two channel orientations, are not significantly different. Second, the salt gradient determines the insertion direction of PorA/C1. To test these hypotheses we devised a special technique of channel insertion. We assumed that channels do not change their orientation after insertion into a membrane. PorA/C1 was initially inserted in the presence of a 2-fold gradient (0.10 M NaCl in the high salt side, 0.050 M NaCl in the low salt side). Then a concentrated NaCl solution was added to the low salt side to reverse the gradient. In the Fig. 5.5 we compare the reversal potential obtained using this new method with those from the previous graph for a 6-fold gradient. Values confirm the conclusion that in the presence of the salt gradient PorA/C1 preferentially inserts in the direction with the selectivity filter facing the low salt side.

We also observed that in contrast to channels oriented with the preferential direction of insertion (i.e. selectivity filter in the low salt side), PorA/C1 channels with
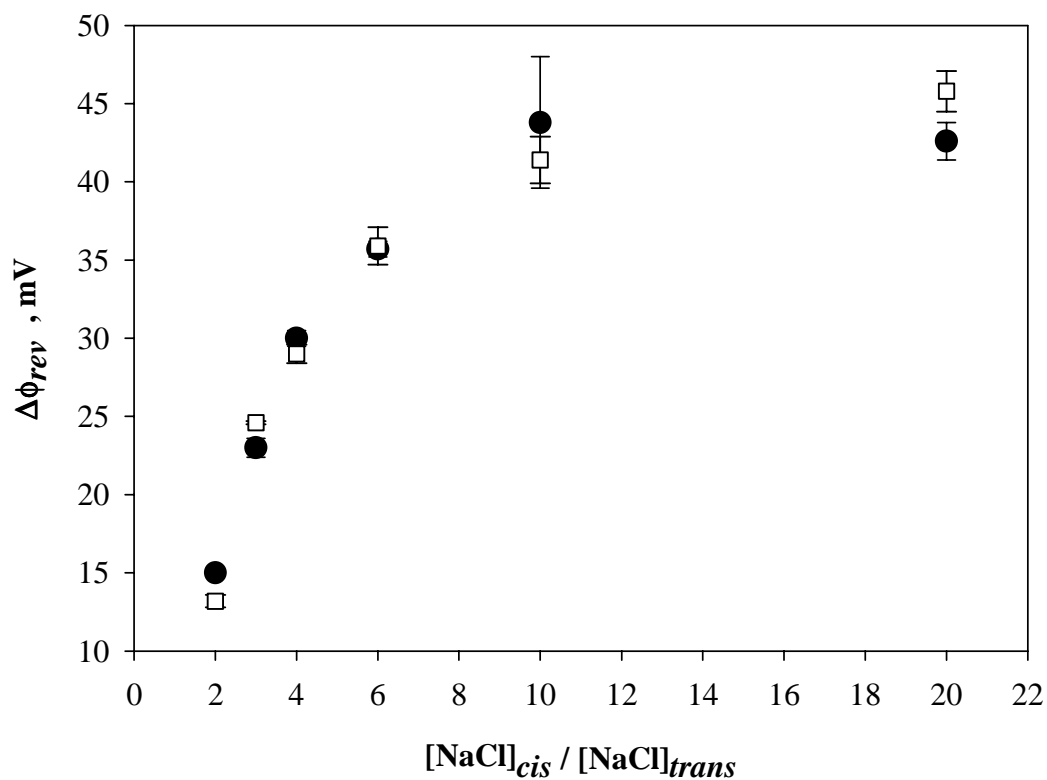
Figure 5.4. Reversal potential as a function of NaCl gradient does not depend on the side

of PorA/C1 addition. PorA/C1 was added to the high salt side (*filled circles*) or to the low

salt side (*open squares*). Each point represents at least 3 experiments.
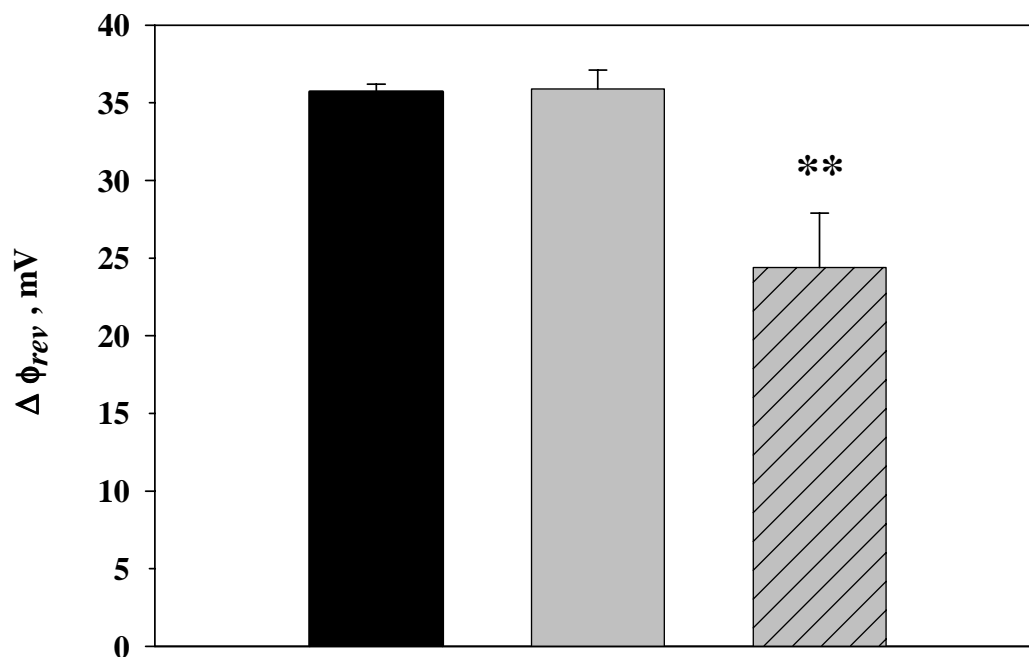
Figure 5.5. Reversal potential of PorA/C1 in the presence of a 6-fold salt gradient. PorA/C1 was added to the high salt side (*black bar,* 4 experiments), to the low salt side (*gray bar,* 3 experiments), or inserted followed by gradient inversion (*striped bar, 3* experiments).

the opposite orientation were not stable. Sometimes a channel of that type underwent conformational changes with time leading to a loss of selectivity and a simultaneous increase in conductance. However, more often the changes in these properties were not correlated. This instability made the measurements of the reversal potential more complicated. Therefore the values for the lower curve in Fig.5.3 were collected immediately after the gradient reversal.

Attempts to control the direction of PorA/C1 insertion by applying an external electrical field in an effort to align the molecule as one would align a dipole, were not successful. Insertion at high voltages resulted in unstable channels with low selectivity. The electrical field apparently distorts the channel folding rather than directing its orientation in phospholipid membranes.

CONCLUSION

A theoretical model is presented to describe the transport properties of the class 1 porin PorA/C1 from *Neisseria meningitidis*. The model is based on a PNP approach in two dimensions and an inferred geometry from homologous porins. It is able to reproduce the experimental results of the current-voltage curve and the reversal potential values. This indicates that the average transport properties are mainly determined by the long-range electrostatic distribution and not by specific ion-porin interactions. In addition, the inferred geometry and the charged residues distribution are validated. The transport limiting factor is the rate at which ions can access the filter. The asymmetry exhibited by the porin is then explained by the different number of charge carriers at the filter entrance and the neutral entrance.

All results obtained so far indicate the suitability of the theoretical model for the explanation of the transport properties of the porin. The instability of the channel under the relatively mild conditions of a salt gradient is a surprising finding that may have biological or biophysical significance.

CHAPTER 6: FUTURE DIRECTIONS

My dissertation work includes two aspects in the study of large ion channels. The first is an investigation of their physiological functions, and the second –research on channel structure. These are closely related since the function of a protein (channel) is strictly determined by its structure. The objects of my study, mitochondrial VDAC and meningococcal PorA/C1, have different origins and may play different roles in cell homeostasis. However, they share similar properties: a large conductance and a high selectivity for certain permeants. A knowledge of their structure and an understanding of the underlying mechanisms that are responsible for their properties should provide us with a better understanding of the main principles of ion permeation through large channels and their selectivity. In this chapter I will describe possible directions in the further study of VDAC and PorA/C1.

VDAC isoforms

As was already mentioned, mitochondrial VDAC is often present as multiple isoforms. The major one, VDAC1, has been intensively studied and its functions as a channel former and regulator of metabolite flux is generally accepted. However, recent publications demonstrate that surprising VDAC functions might be expected from other isoforms. These are not necessarily channel formers. For example, yeast VDAC2 makes virtually no contribution to the permeability of the mitochondrial outer membrane to NADH (Lee et al., 1998), mouse VDAC3 demonstrates a very poor channel-forming activity (Xu et al., 1999) whereas purified mouse VDAC2 exhibits two classes of channels with slightly different properties. At the same time the functions of some

isoforms appear to be quite different from those of VDAC1. Indeed, mouse VDAC2 binds pro-apoptotic factor BAK while VDAC1 does not (Cheng et al., 2003), human VDAC1 and VDAC2 are different in their ability to bind hexokinase (Blachly-Dyson et al., 1993), and, finally, mice lacking a poor channel former VDAC3 demonstrate male sterility (Sampson et al., 2001). The latter should indicate a specialized function of this protein. Our study of the electrophysiological properties of VDAC-like proteins (isoforms) from Drosophila also suggests that VDAC may play a more complex role in the cell than just a channel former. Indeed, recent observations showed that a double knock-out of CG17139 and CG17140, which demonstrate no channel activity and atypical voltage dependency, respectively (Komarov et al., 2004), results in a lethal mouse phenotype (Bill Craigen, personal communication).

D.melanogaster represents a potentially effective genetic model system for detailed research into VDAC function(s) in vivo. Thus, knowledge of the physiological role(s) of VDAC-like proteins is mandatory for future study. In this thesis I have presented the results obtained from in vitro experiments. However, some of the limitations of the approaches I used highlight the need for in vivo experiments.

In the future the D.melanogaster system may provide new insights into the structural organization of VDAC isoforms. It could be used as an effective tool in the study of the functional role(s) of such structural elements as the N-terminal extensions or the long loop regions. Indeed, N-terminal extensions represented by VDAC-like proteins CG17139 and CG17140 were also found in mouse (Xu et al., 1999) and human (Blachly-Dyson et al., 1993) VDAC2 and may be involved in substrate binding.

VDAC and apoptosis

The role of VDAC in the programmed cell death still remains controversial. There are at least three possible scenarios of how VDAC may participate in the initiation of the cytochrome c dependent apoptotic pathway. According to one of those, VDAC may be involved in the formation of the permeability transition pore (PTP) that leads to either the release of Ca^{2+} ions or metabolites from the matrix space (Szabo and Zoratti, 1993; Szabo et al., 1993; Crompton et al., 1998; Marzo et al., 1998) or to osmotic swelling of the matrix followed by rupture of the mitochondrial outer membrane (Halestrap et al., 2002). However, there is evidence that VDAC is not a constituent of PTP in yeast (Gross et al., 2000) as well as a knock-out of mouse VDAC1 does not inhibit PTP formation (Michael Forte, presentation at the 2005 Biophysical Society meeting). The last observation does not exclude the possibility of mouse VDAC2 or VDAC3 participation in the PTP complex. Again, it emphasizes the importance of the study of VDAC isoforms.

Another scenario assumes that the opening of VDAC via interactions with proapoptotic proteins like BAX may lead to the cytochrome c release (Shimizu et al., 2000). However there is strong evidence that closure of VDAC serves as a hallmark of apoptosis (Doran and Halestrap, 2000; Vander Heiden et al., 2000). This latter view still requires some level of interaction between VDAC and anti-apoptotic factors as it was shown for Bcl-X_L, which maintains VDAC in the open conformation. Indeed, VDAC's open state allows for the continued exchange of metabolites such as ATP and ADP between the cytosol and the mitochondrial spaces, whereas apoptosis requires this exchange to decrease or cease. The generation of the mouse VDAC2 mutant permanently

open to metabolites, which was reported in Chapter 4, would be able to resolve this issue. The expression of this mutant in mice can clarify if VDAC in the open conformation inhibits the initiation of apoptosis.

Physiological role of PorA/C1

The preferential direction of insertion exhibited by PorA/C1 may be closely related to its physiological function in bacteria. Previously the "auto-directed" insertion was shown for VDAC (Zizi et al., 1995; Xu and Colombini, 1996,1997). In this case VDAC molecules, which are already in the membrane, determine the orientation of subsequent insertions of VDAC from an aqueous solution. However, the orientation of the first channel insertion is rather spontaneous. Previous study of PorA/C1 (Song et al., 1999) demonstrated that the narrow (selectivity filter) part of the channel preferentially inserted into the planar membrane and thus faced the chamber site opposite to the site of the protein addition. My experiments showed that the orientation of PorA/C1 insertion strongly depends on the direction of the salt gradient. The additional observation that the channel in the opposite orientation is not stable and exhibits weaker selectivity may lead to insights into the role of PorA/C1 in bacterial physiology.

Expression of these properties may be associated with the difference in osmotic pressure on two sides of the bacterial membrane. It is known that PorA/C1 forms heterotrimers with two PorB/C3 channels (Minetti et al., 1997) that are poorly selective and voltage-gated (Lynch et al., 1984; Song et al., 1998c). It may appear that high selectivity of PorA/C1 plays a role only when the extracellular environment has a lower osmotic pressure. In this case the channel with the selectivity filter, facing the

extracellular space, generates a local Donnan potential which keeps PorB/C3 channels in

the closed state. In turn, it prevents leakage of constituents from the periplasmic space.

Under higher osmotic pressure conditions there is no need to preserve the inner solute

composition and therefore PorA/C1 exhibits a weaker selectivity. Testing of this

hypothesis will require *in vivo* studies of the properties of PorA/C1.

REFERENCES

Abrecht, H., E. Goormaghtigh, J.M. Ruysschaert, and F. Homble. 2000. Structure and orientation of two voltage-dependent anion-selective channel isoforms. An attenuated total reflection fourier-transform infrared spectroscopy study. *J. Biol. Chem*. 275: 40992-40999.

Adams, V., L. Griffin, J. Towbin, B. Gelb, K. Worley, and E.R. McCabe. 1991. Porin interaction with hexokinase and glycerol kinase: metabolic microcompartmentation at the outer mitochondrial membrane. *Biochem. Med. Metab. Biol.* 45: 271-291.

Aiello, R., A. Messina, B. Schiffler, R. Benz, G. Tasco, R. Casadio, and V. De Pinto. 2004. Functional characterization of a second porin isoform in Drosophila melanogaster. DmPorin2 forms voltage-independent cation-selective pores. *J. Biol. Chem.* 279:25364-25373.

Alcaraz, A., E.M. Nestorovich, M. Aguilella-Arzo, V.M. Aguilella, and S.M. Bezrukov. 2004. Salting out the ionic selectivity of a wide channel: the asymmetry of OmpF. *Biophys. J.* 87:943-957.

Anflous, K., D.D. Armstrong, and W.J. Craigen. 2001. Altered mitochondrial sensitivity for ADP and maintenance of creatine-stimulated respiration in oxidative striated muscles from VDAC1-deficient mice. *J. Biol. Chem.* 276:1954-1960.

Benz, R., A. Schmid, and G.H.Vos-Scheperkeuter. 1987. Mechanism of sugar transport through the sugar-specific LamB channel of Escherichia coli outer membrane. *J. Membr. Biol.* 100:21-29.

Berezhkovskii, A.M., and S.M. Bezrukov. 2005. Optimizing transport of metabolites through large channels: molecular sieves with and without binding. *Biophys. J.* 88:L17-19.

Bezrukov, S.M., and I. Vodyanoy. 1993. Probing alamethicin channels with water-soluble polymers. Effect on conductance of channel states. *Biophys. J.* 64:16-25.

Blachly-Dyson E., A. Baldini, M. Litt, E.R. McCabe, and M. Forte. 1994. Human genes encoding the voltage-dependent anion channel (VDAC) of the outer mitochondrial membrane: mapping and identification of two new isoforms. *Genomics.* 20: 62-67.

Blachly-Dyson, E., and M. Forte. 2001. VDAC channels. *IUBMB Life.* 52: 113-118.

Blachly-Dyson, E., E.B. Zambronicz, W.H. Yu, V. Adams, E.R. McCabe, J. Adelman, M. Colombini, and M. Forte. 1993. Cloning and functional expression in yeast of two human isoforms of the outer mitochondrial membrane channel, the voltage-dependent anion channel. *J. Biol. Chem.* 268: 1835-1841.

Blachly-Dyson, E., J. Song, W.J. Wolfgang, M. Colombini, and M. Forte. 1997. Multicopy suppressors of phenotypes resulting from the absence of yeast VDAC encode a VDAC-like protein. *Mol. Cell. Biol.* 17: 5727-5738.

Blachly-Dyson, E., S. Peng, M. Colombini, and M. Forte. 1990. Selectivity changes in site-directed mutants of the VDAC ion channel: structural implications. *Science*. 247: 1233-1236.

Blachly-Dyson, E., S.Z. Peng, M.Colombini, and M.Forte. 1989. Probing the structure of the mitochondrial channel, VDAC, by site-directed mutagenesis: a progress report. *J. Bioenerg. Biomembr.* 21: 471-483.

Blount, P., S.I.Sukharev, P.C.Moe, B.Martinac, and C.Kung. 1999. Mechanosensitive channels of bacteria. *Methods Enzymol.* 294:458-482.

Booth, I.R., and P.Louis. 1999. Managing hypoosmotic stress: aquaporins and mechanosensitive channels in Escherichia coli.*Curr. Opin. Microbiol.* 2:166-169.

Cardenas A.E., R.D. Coalson, and M.G. Kurnikova. 2000. Three-dimensional Poisson-Nernst-Planck theory studies: influence of the membrane electrostatics on gramicidin A channel conductance. *Biophys. J.* 79:80-93.

Cheng, E. H.-Y., T. Sheiko, J.K. Fisher, W. J. Craigen, and S.J. Korsmeyer. 2003. VDAC2 Inhibits BAK Activation and Mitochondrial Apoptosis. *Science.* 301:513-517.

Clarke, S. 1976. **A** major polypeptide component of rat liver mitochondria: carbamyl phosphate synthetase. J. Biol. Chem. 251**:** 950 – 961.

Colombini, M. 1979. A candidate for the permeability pathway of the outer mitochondrial membrane. *Nature*. 279:643-645.

Colombini, M. 1980. Structure and mode of action of a voltage dependent anion-selective channel (VDAC) located in the outer mitochondrial membrane. *Ann. N Y Acad. Sci.* 341:552-563.

Colombini, M. 1987. Regulation of the mitochondrial outer membrane channel, VDAC. *J. Bioenerg. Biomembr.* 19:309-320.

Colombini, M. 1989. Voltage gating in the mitochondrial channel, VDAC. *J. Membr. Biol.* 111: 103-111.

Colombini, M., E. Blachly-Dyson, and M. Forte. 1996. VDAC, a channel in the outer mitochondrial membrane. *In* Ion Channels, Vol. 4. T. Narahashi, editor. Plenum press, New York. 169-202.

Corry B., S. Kuyucak, and S.H. Chung. 2000. Test of continuum theories as models of ion channels. II. Poisson-Nernst-Planck theory versus Brownian Dynamics. *Biophys. J.* 78:2364-2381.

Crompton, M., S. Virji, and J.M. Ward. 1998. Cyclophilin-D binds strongly to complexes of the voltage-dependent anion channel and the adenine nucleotide translocase to form the permeability transition pore. *Eur. J. Biochem.* 258:729-735.

Daum, G., P.C. Bohni, and G. Schatz. 1982. Import of proteins into mitochondria. Cytochrome b2 and cytochrome c peroxidase are located in the intermembrane space of yeast mitochondria. *J. Biol. Chem.* 257: 13028-13033.

De Pinto, V., R. Benz, C. Caggese, and F. Palmieri. 1989. Characterization of the mitochondrial porin from Drosophila melanogaster. *Biochim. Biophys. Acta.* 987: 1-7.

Doran, E., and A.P. Halestrap. 2000. Cytochrome c release from isolated rat liver mitochondria can occur independently of outer-membrane rupture: possible role of contact sites. *Biochem. J.* 348:343-350.

Douce, R., J. Bourguignon, R.Brouquisse, and N. Neuburger. 1987. Isolation of plant mitochondria: general principles and criteria of integrity. *Methods Enzymol.* 148:403-412.

Elkeles, A., K.M. Devos, D. Graur, M. Zizi, and A. Breiman. 1995. Multiple cDNAs of wheat voltage-dependent anion channels (VDAC): isolation, differential expression, mapping and evolution. *Plant Mol. Biol.* 29: 109-124.

Fatt, P., and B.L.Ginsborg. 1958. The ionic requirements for the production of action potentials in crustean muscles fibres. *J.Physiol. (London).* 142:516-543.

Freitag, H., R.Benz, and W.Neupert. 1983. Isolation and properties of the porin of the outer mitochondrial membrane from Neurospora crassa. *Methods Enzymol.* 97: 286-294.

Gellerich F.N., Z.A.Khuchua, and A.V.Kuznetsov. 1993. Influence of the mitochondrial outer membrane and the binding of creatine kinase to the mitochondrial inner membrane on the compartmentation of adenine nucleotides in the intermembrane space of rat liver mitochondria. *Biochim.Biophys.Acta.* 1140:327-334.

Gellerich, F.N, and W. Kunz. 1987. Cause and consequences of dynamic compartmentation of adenine nucleotides in the mitochondrial intermembrane space in respect to exchange of energy-rich phosphates between cytosol and mitochondria. *Biomed.Biochim.Acta.* 46:S545-S548.

Gietz D., A. St Jean, R.A. Woods, and R.H. Schiestl. 1992. Improved method for high efficiency transformation of intact yeast cells. *Nucleic Acids Res.* 20: 1425.

Gietz R.D., and A. Sugino. 1988. New yeast-Escherichia coli shuttle vectors constructed with in vitro mutagenized yeast genes lacking six-base pair restriction sites. *Gene.* 74: 527-534.

Gincel, D, H.Zaid, and V.Shoshan-Barmatz. 2001.Calcium binding and translocation by the voltage-dependent anion channel: a possible regulatory mechanism in mitochondrial function. *Biochem. J.* 358:147-155.

Goldman, D.E. 1943. Potential, impedance, and rectification in membranes. *J.Gen.Physiol.* 27:37-60.

Gross, A., K. Pilcher, E. Blachly-Dyson, E. Basso, J. Jockel, M.C. Bassik, S.J. Korsmeyer, and M. Forte. 2000. Biochemical and genetic analysis of the mitochondrial response of yeast to BAX and BCL-X(L). *Mol. Cell Biol*. 20:3125-3136.

Hagiwara, S., and K.I.Naka. 1964. The initiation of spike potential in barnacle muscle fibres under low intracellular Ca^{2+}. *J.Gen.Physiol.* 48:141-161.

Halestrap, A.P., G.P. McStay, and S.J. Clarke. 2002. The permeability transition pore complex: another view. *Biochimie.* 84: 153-166.

Hille B. 2001. Ionic Channels of Excitable Membranes, 3rd Ed. Sinauer Associates Inc., Sunderland, M.A.

Hille B. 1992. Ionic Channels of Excitable Membranes, 2nd Ed. Sinauer Associates Inc., Sunderland, M.A.

Hodgkin, A.L., and A.F. Huxley. 1952.A quantitative description of membrane current and its application to conduction and excitation in nerve. *J.Physiol. (London).* 117:500-544.

Hodgkin, A.L., A.F. Hukley, and B.Katz. 1952. Measurements of current-voltage relations in the membrane of the giant axon of *Loligo. J.Physiol. (London).* 116:424-448.

Hodgkin, A.L., and B.Katz. 1949. The effect of sodium ions on the electrical activity of the giant axon of the squid. *J.Physiol.(London).* 108:37-77.

Holden, M.J., and M. Colombini. 1988. The mitochondrial outer membrane channel, VDAC, is modulated by a soluble protein. *FEBS Lett.* 241: 105-109.

Hollerbach U., D.P. Chen, D.D. Busath, and B. Eisenberg. 2000. Predicting function from structure using the Poisson-Nernst-Planck equations: sodium current in the gramicidin A channel. *Langmuir.* 16:5509-5514.

Hollerbach U., D.P. Chen, D.D. Busath, and B. Eisenberg. 2002. Concentration-dependent shielding of electrostatic potentials inside the gramicidin A. *Langmuir.* 18:3626-3631.

Holmuhamedov, E.L., A. Jahangir, A.Oberlin, A. Komarov, M.Colombini, and A.Terzic. 2004. Potassium channel openers are uncoupling protonophores: implication in cardioprotection. *FEBS.* 568:167-170.

Im W., and B. Roux. 2002. Ion permeation and selectivity of OmpF porin: a theoretical study based on Molecular Dynamics, Brownian Dynamics, and continuum electrodiffusion theory. *J. Mol. Biol.* 322:851-869.

Jeanteur, D., J.H. Lakey, and F. Pattus. 1991. The bacterial porin superfamily: sequence alignment and structure prediction. *Mol Microbiol.* 5:2153-21.

Kaiser, C., S. Michaelis, and A. Mitchell. 1994. *Methods in yeast genetics: a Cold Spring Harbor Laboratory course manual.* Cold Spring Harbor, NY, Cold Spring Harbor Laboratory Press.

Komarov, A.G., B.H.Graham, W.J. Craigen, and M. Colombini. 2004. The physiological properties of a novel family of VDAC-like proteins from Drosophila melanogaster. *Biophys. J.* 86:152-162.

Koumanov A., U. Zachariae, H. Engelhardt, and A. Karshikoff. 2003. Improved 3D continuum calculations of ion flux through membrane channels. *Eur. Biophys. J.* 32:689-702.

Kullman, L, M.Winterhalter, and S.M. Bezrukov. 2002. Transport of maltodextrins through maltoporin: a single-channel study. *Biophys. J.* 82:803-812.

Kurnikova M.G., R.D. Coalson, P. Graf, and A. Nitzan. 1999. A lattice relaxation algorithm for three dimensional Poisson-Nernst-Planck theory with application to ion transport through the gramicidin A channel. *Biophys. J.* 76:642-656.

Kyte, J., and R.F. Doolittle. 1982. A simple method for displaying the hydropathic character of a protein. *J. Mol. Biol.* 157: 105-132.

Laemmli, U.K. 1970. Cleavage of structural proteins during the assembly of the head of Bacteriophage T$_4$. *Nature (London).* 227:680-685.

Lee, A.C., X. Xu, E. Blachly-Dyson, M. Forte, and M. Colombini. 1998. The role of yeast VDAC genes on the permeability of the mitochondrial outer membrane. *J. Membr. Biol.* 161:173-181.

Levitt, D.G. 1985. Strong electrolyte continuum theory solution for equilibrium profiles, diffusion limitation, and conductance in charged ion channels.*Biophys. J.* 48:19-31.

Levitt, D.G. 1989. Continuum model of voltage-dependent gating. Macroscopic conductance, gating current, and single-channel behavior. *Biophys. J.* 55:489-498.

Levitt, D.G. 1991. General continuum theory for multiion channel. I. Theory. *Biophys. J.* 59:271-2777.

Luckey, M, and H.Nikaido. 1980. Specificity of diffusion channels produced by lambda phage receptor protein of Escherichia coli. *Proc. Natl. Acad. Sci. U S A.* 77:167-171.

Lucquin B., and Pironneau O. 1998. Introduction to Scientific Computing. John Wiley & Sons, *West Sussex.*

Lynch, E.C., M.S. Blake, E.C. Gotschlich, and A. Mauro. 1984. Studies of porins: Spontaneously transferred from whole cells and reconstituted from purified proteins of *Neisseria gonorrhoeae* and *Neisseria meningitidis*. Biophys. J. 45:104-107.

MacKinnon, R, S.L.Cohen, A.Kuo, A.Lee, and B.T.Chait. 1998. Structural conservation in prokaryotic and eukaryotic potassium channels. *Science.* 280:106-109.

Mannella, C.A. 1982. Structure of the outer mitochondrial membrane: ordered arrays of porelike subunits in outer-membrane fractions from Neurospora crassa mitochondria. *J. Cell Biol.* 94:680-687.

Mannella, C.A. 1989. Structure of the mitochondrial outer membrane channel derived from electron microscopy of 2D crystals. *J.Bioenerg Biomembr.* 21:427-437.

Mannella, C.A. 1996. Mitochondrial channels revisited. *J.Bioenerg. Biomemb*. 28: 89-91.

Mannella, C.A., and M.Colombini. 1984. Evidence that the crystalline arrays in the outer membrane of Neurospora mitochondria are composed of the voltage-dependent channel protein. *Biochim Biophys Acta.* 774:206-214.

Mannella, C.A., M.Forte, and M.Colombini. 1992. Toward the molecular structure of the mitochondrial channel, VDAC. *J. Bioenerg. Biomembr.* 24:7-19.

Martinac, B., M.Buechner, A.H.Delcour, J.Adler, and C.Kung. 1987. Pressure-sensitive ion channel in Escherichia coli. *Proc. Natl. Acad. Sci. U S A.* 84:2297-2301.

Marzo, I., C.Brenner, N. Zamzami, S.A. Susin, G.Beutner, D.Brdiczka, R. Remy, Z.H. Xie, J.C. Reed, and G. Kroemer. 1998. The permeability transition pore complex: a target for apoptosis regulation by caspases and bcl-2-related proteins. *J. Exp. Med*. 187:1261-1271.

McEnery M.W., A.M. Snowman, R.R. Trifiletti, and S.H. Snyder. 1992. Isolation of the mitochondrial benzodiazepine receptor: association with the voltage-dependent anion channel and the adenine nucleotide carrier. *Proc. Natl. Acad. Sci. USA*. 89: 3170-3174.

Mikhailov, V., M. Mikhailova, K. Degenhardt, M.A.Venkatachalam, E. White, and P. Saikumar. 2003. Association of Bax and Bak homo-oligomers in mitochondria. Bax requirement for Bak reorganization and cytochrome c release. *J. Biol. Chem.* 278:5367-5376.

Minetti, C.A., J.Y. Tai, M.S. Blake, J.K. Pullen, S.M. Liang, and D.P. Remeta. Structural and functional characterization of a recombinant PorB class 2 protein from Neisseria meningitidis. Conformational stability and porin activity. *J. Biol. Chem.* 272:10710-10720.

Montal, M., and P.Mueller. 1972. Formation of bimolecular membranes from lipid monolayers and a study of their electrical properties. *Proc. Natl. Acad. Sci. USA.* 69:3561-3566.

Morais-Cabral, J.H., Y.Zhou, and R.MacKinnon. 2001. Energetic optimization of ion conduction rate by the K+ selectivity filter. *Nature.* 414:37-42.

Neher, E., and B.Sakmann. 1976. Single-channel currents recorded from membrane of denervated frog muscle fibres. *Nature (London).* 260:779-802.

Nestorovich, E.M., C.Danelon, M.Winterhalter, and S.M.Bezrukov. 2002. Designed to penetrate: time-resolved interaction of single antibiotic molecules with bacterial pores. *Proc. Natl. Acad. Sci. U S A.* 99:9789-9794.

Noskov S.Y., W. Im, and B. Roux. 2004. Ion permeation through the α-hemolysin channel: theoretical studies based on Brownian Dynamics and Poisson-Nernst-Planck electrodiffusion theory. *Biophys. J.* 87:2299-2309.

Ohnishi, T., K.Kawaguchi, and B.Hagihara.1966. Preparation and some properties of yeast mitochondria. *J. Biol. Chem.*241:1797-1806.

Oliva, M., V. De Pinto, P. Barsanti, and C. Caggese. 2002. A genetic analysis of the porin gene encoding a voltage-dependent anion channel protein in Drosophila melanogaster. *Mol. Genet. Genomics.* 267: 746-756.

Onsager L. 1926. Zur theory der elektrolyte (1). *Physikalische Zeitschrift.* 27:388-392.

Onsager L. 1927. Zur theory der elektrolyte (2). *Physikalische Zeitschrift.* 28:277-298.

Peng, S., E. Blachly-Dyson, M.Forte, and M.Colombini. 1992. Large scale rearrangement of protein domains is associated with voltage gating of the VDAC channel. *Biophys. J.* 62:123-131.

Rapizzi E., P. Pinton, G. Szabadkai, M.R. Wieckowski, G. Vandecasteele, G. Baird, R.A. Tuft, K.E. Fogarty, and R. Rizzuto. 2002. Recombinant expression of the voltage-dependent anion channel enhances the transfer of Ca2+ microdomains to mitochondria. *J. Cell Biol.* 159: 613-624.

Rostovtseva ,T.K., and S.M.Bezrukov. 1998. ATP transport through a single mitochondrial channel, VDAC, studied by current fluctuation analysis. *Biophys.J.* 74:2365-2373.

Rostovtseva, T., and M.Colombini. 1997. VDAC channels mediate and gate the flow of ATP: implications for the regulation of mitochondrial function. *Biophys. J.* 72:1954-1962.

Rostovtseva, T.K., A. Komarov, S.M. Bezrukov, and M. Colombini. 2002a. Dynamics of nucleotides in VDAC channels: structure-specific noise generation. *Biophys.J.* 82:193-205.

Rostovtseva, T.K., A. Komarov, S.M. Bezrukov, and M. Colombini. 2002b. VDAC channels differentiate between natural metabolites and synthetic molecules. *J. Membr. Biol.* 187:147-156.

Rostovtseva, T.K., and M.Colombini. 1996. ATP flux is controlled by a voltage-gated channel from the mitochondrial outer membrane. *J.Biol.Chem.* 271:28006-28008.

Roux, B, and R.MacKinnon. 1999. The cavity and pore helices in the KcsA K+ channel: electrostatic stabilization of monovalent cations. *Science.* 285:100-102.

Rubin, G.M., L. Hong, P. Brokstein, M. Evans-Holm, E. Frise, M. Stapleton, and D.A. Harvey. 2000. A Drosophila complementary DNA resource. *Science.* 287: 2222-2224.

Ryerse J., E. Blachly-Dyson, M. Forte, and B. Nagel. 1997. Cloning and molecular characterization of a voltage-dependent anion-selective channel (VDAC) from Drosophila melanogaster. *Biochim. Biophys. Acta.* 1327: 204-212.

Sampson M.J., R.S. Lovell, and W.J. Craigen. 1997. The murine voltage-dependent anion channel gene family. Conserved structure and function. *J. Biol. Chem.* 272: 18966-18973.

Sampson, M.J., R.S. Lovell, D.B. Davison, and W.J. Craigen. 1996. A novel mouse mitochondrial voltage-dependent anion channel gene localizes to chromosome 8. *Genomics.* 36: 192-196.

Sampson, M.J., W.K. Decker, A.L. Beaudet, W. Ruitenbeek, D. Armstrong, M.J. Hicks, and W.J.Craigen. 2001. Immotile sperm and infertility in mice lacking mitochondrial voltage-dependent anion channel type 3. *J. Biol. Chem.* 276: 39206-39212.

Schein, S.J., M. Colombini, and A. Finkelstein. 1976. Reconstitution in planar lipid bilayers of a voltage-dependent anion-selective channel obtained from paramecium mitochondria. J.Membr.Biol. 30:99-120.

Schuss Z., B. Nadler, and R.S. Eisenberg. 2001. Derivation of Poisson and Nernst-Planck equations in a bath and channel from a molecular model. *Phys. Rev. E.* 64:036116

Schwarz, G., C. Danelon, and M.Winterhalter. 2003. On translocation through a membrane channel via an internal binding site: kinetics and voltage dependence. *Biophys. J.* 84:2990-2998.

Shimizu, S., T. Ide, T. Yanagida, and Y. Tsujimoto. 2000. Electrophysiological study of a novel large pore formed by BAX and the voltage-dependent anion channel that is permeable to cytochrome c. *J. Biol.Chem.* 275:12321-12325.

Sims S.M., W.I. Higuchi, V. Srinivasan, and K. Peck. 1993. Ionic partition-coefficients and electroosmotic flow in cylindrical pores – comparison of the predictions of the Poisson-Boltzmann equation with experiment. *J. Col. Interface Sci.* 155**:**210-220.

Song J., C.A.S.A. Minetti, M.S. Blake, and M. Colombini. 1999. Meningococcal PorA/C1, a channel that combines high conductance and high selectivity. *Biophys. J.* 76:804-813.

Song, J., C.Midson, E. Blachly-Dyson, M. Forte, and M. Colombini. 1998a. The topology of VDAC as probed by biotin modification. *J. Biol. Chem.* 273:24406-24413.

Song, J., C.Midson, E. Blachly-Dyson, M. Forte, and M. Colombini. 1998b. The sensor regions of VDAC are translocated from within the membrane to the surface during the gating processes. *Biophys. J.* 74: 2926-2944.

Song, J., C.A. Minetti, M.S. Blake, and M. Colombini. 1998c. Successful recovery of the normal electrophysiological properties of PorB (class 3) porin from Neisseria meningitidis after expression in Escherichia coli and renaturation. *Biochim. Biophys. Acta.* 1370:289-298.

Song, J., and M. Colombini. 1996. Indications of a common folding pattern for VDAC channels from all sources. *J. Bioenerg. Biomembr.* 28:153-161.

Sotocassa, G.L, B.Kuylenstierna, L. Ernster, and A.Begstrand. 1967. Separation and enzymatic properties of the inner and outer membranes of rat liver mitochondria. *Methods Enzymol.* 10:448-463.

Spencer, R.H., G.Chang, and D.C.Rees. 1999. 'Feeling the pressure': structural insights into a gated mechanosensitive channel. *Curr. Opin. Struct. Biol.* 9:448-454.

Su, S., and P.J.Russell. 1967. Adenylate kinase from baker's yeast (II. Substrate specificity). *Biochim.Biophys.Acta.* 132:370-378.

Sukharev, S. 2002. Purification of the small mechanosensitive channel of Escherichia coli (MscS): the subunit structure, conduction, and gating characteristics in liposomes. *Biophys J.* 83:290-298.

Szabo, I., and M.Zoratti. 1993. The mitochondrial permeability transition pore may comprise VDAC molecules. I. Binary structure and voltage dependence of the pore. *FEBS Lett.* 330:201-205.

Szabo, I., V. De Pinto, and M. Zoratti. 1993. The mitochondrial permeability transition pore may comprise VDAC molecules. II. The electrophysiological properties of VDAC are compatible with those of the mitochondrial megachannel. *FEBS Lett.* 330:206-210.

Szmelcman, S, and M.Hofnung. 1975. Maltose transport in Escherichia coli K-12: involvement of the bacteriophage lambda receptor. *J. Bacteriol.* 124:112-118.

Teorell, T. 1953. Transport processes and electrical phenomena in ionic membranes. Prog.Biophys.Biophys.Chem. 3:305-369.

The-FlyBase-Consortium. 2003. "The FlyBase database of the Drosophila genome projects and community literature." *Nucleic Acids Res.* 31: 172-175.

Thomas L., E. Blachly-Dyson, M. Colombini, and M. Forte. 1993. Mapping of residues forming the voltage sensor of the voltage-dependent anion-selective channel. *Proc. Natl. Acad. Sci. USA.* 90:5446-5449.

Vander Heiden, M.G., N.S. Chandel, X.X. Li, P.T. Schumacker, M. Colombini, and C.B. Thompson. 2000. Outer mitochondrial membrane permeability can regulate coupled respiration and cell survival. *Proc. Natl. Acad. Sci. U S A.* 97:4666-4671.

Vander Heiden, M.G., X.X. Li, E. Gottleib, R.B. Hill, C.B. Thompson, and M. Colombini. 2001. Bcl-x_L Promotes the Open Configuration of VDAC and Metabolite Passage through the Mitochondrial Outer Membrane. *J. Biol. Chem.* 276: 19414-19419.

Weeber E.J., M. Levy, M.J. Sampson, K. Anflous, D.L. Armstrong, S.E. Brown, J.D. Sweatt, and W.J. Craigen. 2002. The role of mitochondrial porins and the permeability transition pore in learning and synaptic plasticity. *J. Biol. Chem.* 277: 18891-18897.

Wielburski, A., and B.D. Nelson. 1983. Evidence for the sequential assembly of cytochrome oxidase subunits in rat liver mitochondria. *Biochem. J.* 212:829-834.

Xu X., W. Decker, M.J. Sampson, W.J. Craigen, and M. Colombini. 1999. Mouse VDAC isoforms expressed in yeast: channel properties and their roles in mitochondrial outer membrane permeability. *J. Membr. Biol.* 170: 89-102.

Xu, X., and M. Colombini. 1996. Self-catalyzed insertion of proteins into phospholipid membranes. J. Biol. Chem. 271:23675-23682.

Xu, X., and M. Colombini. 1997. Autodirected insertion: preinserted VDAC channels greatly shorten the delay to the insertion of new channels. *Biophys. J.* 72:2129-2136.

Zambrowicz, E.B., and M.Colombini. 1993. Zero-current potentials in a large membrane channel: a simple theory accounts for complex behavior. *Biophys. J.* 65:1093-1100.

Zhou, Y, J.H.Morais-Cabral, A.Kaufman, and R.MacKinnon 2001. Chemistry of ion coordination and hydration revealed by a K+ channel-Fab complex at 2.0 A resolution. *Nature.* 414:43-48.

Zizi, M., L. Thomas, E. Blachly-Dyson, M. Forte, and M. Colombini. 1995. Oriented channel insertion reveals the motion of a transmembrane beta strand during voltage gating of VDAC. *J. Membr. Biol.* 144:121-129.